

Diss. ETH No. 17865

Geostatistical Inference of Hydrogeological Parameters with a Large Number of Unknowns

A dissertation submitted to the
SWISS FEDERAL INSTITUTE OF TECHNOLOGY
ZURICH

for the degree of
Doctor of Science

presented by
WEI LI
M.Sc.

born November 28, 1977
citizen of HeBei, China

accepted on the recommendation of
Prof. Dr. Peter Reichert, examiner
PD Dr.-Ing. Olaf A. Cirpka, co-examiner
Prof. Dr.-Ing. Wolfgang Kinzelbach, co-examiner

2008

Acknowledgments

I would like to thank my supervisor PD Dr.-Ing. Olaf A. Cirpka for his brilliant supervision.

I am also very thankful to Prof. Dr. Peter Reichert and Prof. Dr.-Ing. Wolfgang Kinzelbach for their constructive discussion and suggestions.

I would like to thank my family, girl friend, colleagues, and all the other friends, who support me all the time.

Contents

Abstract	xv
Zusammenfassung	xxi
1 Problem Statement	1
1.1 Hydrogeological Parameters as Spatial Random Fields	1
1.2 Parameter Estimation in Groundwater Modeling	2
1.3 Geostatistical Inverse Models	3
1.4 Selection of Inverse Method	8
1.5 Tasks of Thesis	9
2 Methods	17
2.1 Governing Equations	18
2.1.1 Groundwater Flow Equations	18
2.1.2 Temporal Moments of Drawdown	22
2.1.3 Moment-Generating Equations	23
2.2 Bayes' Theorem	26
2.3 Geostatistical Description of Spatial Random Parameters	27
2.4 Prior Distribution	30

2.5	Structure of Covariance Matrices	31
2.6	Spectral Representation	33
2.6.1	Generation of Autocorrelated Fields	34
2.6.2	Computation of Cross-Covariance Matrices	36
2.6.3	Parameterization with KL Expansion	39
2.7	Formulation of the Quasi-Linear Geostatistical Inverse Approach	44
2.8	Modified LM Algorithm	49
2.9	Estimation of Geostatistical Parameters	50
2.10	Inference with Karhunen-Loève Expansion	53
2.11	Evaluation of Sensitivities	59
3	Performance Tests of Inference with Karhunen-Loève Expansion	63
3.1	Field Setup	64
3.2	Estimation on a Regular Grid	65
3.3	Estimation on an Unstructured Grid	71
3.4	Summary	75
4	Applications to Field Data	77
4.1	Field and Test Descriptions	77
4.1.1	Field Description	77
4.1.2	Description of Pumping Tests	78
4.1.3	Description of Flowmeter Tests	79
4.2	Two-Dimensional Estimation	81
4.2.1	Data Preparation	83
4.2.2	Kriging of Pseudo-Local Values	88

4.2.3	Quasi-Linear Geostatistical Inversion of Temporal Mo- ments	91
4.2.4	Comparison of Estimates	96
4.2.5	Summary	99
4.3	Three-Dimensional Estimation	101
4.3.1	Discharge Ratios as Data of Flowmeter Tests	104
4.3.2	Numerical Implementation and Results	106
4.3.3	Summary	112
5	Conclusions and Outlook	113
5.1	Main Findings	113
5.2	Recommendations	115
5.3	Concluding Remarks	119
5.4	Future Research	119
	Bibliography	131

List of Tables

3.1	Geometric parameters, pumping conditions, and geostatistical parameters of log-transmissivity and log-recharge for all test cases of the inversion with the KL expansion; parameters of discretization for the test case on a regular grid.	66
3.2	Performance results for the reference case and orthonormal residuals (Section 3.2) and estimation on unstructured grids (Section 3.3)	73
4.1	Field and grid information of the two-dimensional application, prior and posterior information of hydraulic parameter fields in Section 4.2.2 and 4.2.3.2, and the results of comparison in Section 4.2.4.	102
4.2	Geometric and geostatistical parameters used in the joint inversion	107

List of Figures

1.1	A schematic illustration of porous media at different scales. . . .	4
1.2	Schematic illustrate of the concept of hydraulic tomography. Circles indicate pumping or monitoring locations.	12
2.1	Transient drawdown in a pumping test as function of time for various regimes of extraction.	24
2.2	One-dimensional illustration of covariance function and semi-variogram of a second-order stationary spatial random variable. σ^2 is the variance and h the separation distance.	29
2.3	Graphic illustration of Toeplitz-like covariance matrices for one-, two- and three-dimensional applications on regular grids. Here, the variance for all cases is unity.	32
2.4	Finite domain Ω' embedded in a large unit cell Ω of a periodic domain. Four unit cells are shown to visualize periodicity. . . .	36
2.5	Finite and periodic function.	37
2.6	Graphic illustration of the procedures in the quasi-linear geostatistical inverse approach of Kitanidis [1995].	45

- 2.7 Graphic illustration of sensitivities of zeroth and first temporal moment of drawdown with respect to hydrogeological parameters. a) is the sensitivity of zeroth temporal moment with respect to log-transmissivity; b) the sensitivity of first temporal moment with respect to log-transmissivity; c) the sensitivity of first temporal moment with respect to log-storativity. The black square indicates the pumping location and the cross is the location of one monitoring well. 61
- 3.1 Polygonal domain used in the example calculations of the geostatistical inference with the KL expansion. 65
- 3.2 Hypothetical test case. a) True distribution of log-conductivity (K in m/s); b) known distribution of log-recharge (N in m^3/s); c) true distribution of hydraulic heads; d) estimated log-conductivity field using 400 KL terms on a rectangular grid; e) associated estimation variance; f) bottom topography. Stars: locations of head measurements; square: location of pumping well. 67
- 3.3 Performance of the Karhunen-Loève expansion. a) Computational effort of the inverse method with the KL expansion (stars) as function of the number of KL terms. Dotted line: effort for the inverse method using the full prior covariance matrix. b) Normalized difference of the estimates, NRMSE, according to Eq. (3.1). c) Normalized difference of the estimation variance, ND, according to Eq. (3.2). d) Normalized difference of the estimates, $NRMSE^0$, according to Eq. (3.3). 70
- 3.4 Estimation variance of the entries of the weight vector ζ using 1600 KL terms, sorted by their eigenvalues. 72
- 4.1 Dimension of the field and well locations of the test site Krauthausen. Crosses indicate the location of wells used for pumping tests and circles for flowmeter tests. 78

-
- 4.2 Typical setup of a flowmeter test and a graphic illustration of the data. (a) is the normalized cumulative discharge profile and (b) is the profile of relative hydraulic conductivity. 80
- 4.3 Interpolated fields of $\ln T$, $\ln S$ and their corresponding standard derivations of estimation using the values of conventional type-curve approach as pseudo-local values. Circles are the well locations of pumping tests. 91
- 4.4 Influence of the measurement error on the inversion results. The horizontal axes are the measurement error used in the inverse procedure. A: estimation of geostatistical parameters with varying correlation length; A1: influence on the estimated correlation length; A2: influence on the value of objective function. B: estimation of geostatistical parameters with fixed correlation length; B1: influence on the estimated prior variance of $\ln T$; B2: influence on the estimated prior variance of $\ln S$ 95
- 4.5 A: the most likely estimate of $\ln T$ from geostatistical inversion of the two-dimensional application; B: corresponding standard deviations of estimation; C: kriged $\ln T$ field based on pseudo-local values. Crosses are the well locations of all available pumping tests. The color scales for the two $\ln T$ fields are identical. 97
- 4.6 $\ln T$ at locations of head measurements. Circles indicate the estimated $\ln T$ values of the geostatistical inverse approach. Error bars correspond to \pm one standard deviation of estimation. Crosses stand for the calculated pseudo-local values of $\ln T$ obtained from the conventional method. 99

-
- 4.7 Results of joint geostatistical inversion of flowmeter and pumping-test data. Sub-figure a) is the estimate of $\log_{10}K$ with joint data of flowmeter and pumping tests; sub-figure b) displays the standard deviation of estimation of $\log_{10}K$ with joint data. Vertical black solid lines and the circles are the locations of the wells in flowmeter tests; and the vertical gray lines and the crosses indicate the positions of the wells used in multiple pumping tests. Contour lines display the corresponding depth-averaged values. . 109
- 4.8 Fields of depth-averaged $\log_{10}K$ with joint data and with draw-down data only. Sub-figure a) shows the depth-averaged values of $\log_{10}K$ with joint data; sub-figure b) depth-averaged $\log_{10}K$ with drawdown data only; sub-figure c) the difference of the two depth-averaged fields. 111

Abstract

Flow and transport models in porous media have become a very important tool in groundwater management. To implement these models, spatial distributions of hydrogeological parameters must be known. Due to scarcity of direct measurements, the parameters are mainly inferred from secondary dependent information such as head or concentration measurements. The inference of hydrogeological parameters from secondary information is referred to as inverse problem of groundwater modeling. Because of consistent assumptions about the spatial variability of porous media, inverse methods within the framework of geostatistics are well suited for estimating the spatial distributions of hydrogeological parameters in heterogeneous aquifers. In geostatistics, the parameter field is regarded as a spatial random variable.

Within the geostatistical inverse approaches, the Quasi-Linear Geostatistical Inverse Approach of Kitanidis [1995] with its modifications appears to be the most efficient, particularly with respect to required CPU time in quantifying the expected value of the parameters and their related estimation uncertainty for the cases with a large number of unknowns. Despite this advantage, a couple of difficulties of applying this inverse approach remain.

The inverse approach requires evaluation of cross-covariance matrices in the inference. Efficient spectral methods of computing these terms [Nowak et al., 2003] require regular structured grids and will fail when the domain is discretized by unstructured grids which may be important for practical applications. Explicitly computing these matrices is prohibitive for cases with a large number of unknowns. In this thesis, I parameterize the parameter field using a

truncated series of base functions efficiently derived from the covariance matrix by spectral methods. The parameterization of a spatial random field using truncated series is the application of the Karhunen-Loève(KL) expansion [Loève, 1977]. The reduced dimension in the parameterization can reduce the computational costs in estimating the parameter field. The base functions are continuous in space and do not distinguish discretization schemes.

I integrate the parameterization with the KL expansion into the inverse approach and implement this integrated inverse approach using structured and unstructured grids in synthetic test cases. I compare the inverse approach with the KL expansion and the inverse approach with the full covariance matrix in which the FFT method of accelerating evaluation of cross-covariance matrices can be applied. The computational effort, estimates, and estimation variances are investigated. Results show that I can obtain a reliable estimate of hydrogeological parameters using a limited number of truncated terms. If a high number of KL terms are needed, the inverse approach with the full covariance matrix outperforms the inverse approach with the KL expansion. However, for smooth covariance functions, particularly with large correlation lengths, a few KL terms are sufficient and the parameterization with the KL expansion becomes more efficient. This work has been published by Li and Cirpka [2006].

Applicability of the inverse approach in analyzing field data is investigated. In this thesis, two applications with different spatial dimensions, a two-dimensional and a three-dimensional inference, are conducted. In the field applications, the measurements of drawdown during pumping tests and discharge profiles of flowmeter tests in fully screened wells at the test site Krauthausen, Germany, are used. For these two estimations, I apply the inverse approach with full covariance matrix on regular grids and accelerate the evaluation of cross-covariance matrices using the FFT method.

In the two-dimensional analysis, I test the feasibility of the inverse approach given measurements of pumping tests in estimating the fields of transmissivity and storativity. To estimate the field of storativity, I have to apply transient data of drawdown. To avoid high correlation of transient data in a drawdown curve, I

apply temporal moments of drawdowns [Li et al., 2005] to extract the most important information of transient curves. The corresponding moment-generating equations are at steady state, which can be solved much more efficiently than the transient flow equations.

For the estimated transmissivity, the inverse approach provides estimates showing more spatial variability than the interpolated field of the values obtained by the conventional type-curve approach. This comes from the consistent assumption of the former approach on the structure of porous media. Structures are obtained in the regions where the pumping tests were conducted and uncertainties of the estimate are decreased in these regions. However, uncertainties are still high for the areas far away from well locations. Considering the estimate of storativity, both approaches obtain a high value of estimated variance, which is believed unrealistic, because the variability of all terms making up the storativity is small in space so that the distribution of storativity is presumed to show small variance. I believe that this is an effect of aliasing. The estimated distribution of transmissivity is smoother than the real field. The unresolved variability at small local scales has a large effect on the simulated first temporal moments, representing the characteristic time of drawdown, than the zeroth temporal moments, representing final drawdown. Given a smooth estimate of transmissivity, the inverse approach attributes the derived variability in first temporal moments to the variability of storativity. In the estimation, I assumed a two-dimensional aquifer. The unresolved vertical variability may also be a particular cause for the unrealistic results. Data quality influences the estimation of parameter fields and geostatistical parameters. When the measurement error is large, I obtain increased values of estimated correlation lengths and decreased values of variances, which smooth the estimated fields of hydrogeological parameters. The two-dimensional study has been published by Li et al. [2007].

I conduct a three-dimensional estimation of hydrogeological parameters at the same site to test the performance of the inverse approach with a large number of unknowns. Due to lack of measurements supporting a three-dimensional estimation of specific storage coefficient, particularly regarding to the vertical

direction, the field of specific storage coefficient is not estimated. In the three-dimensional estimation, I jointly apply the data of pumping and flowmeter tests to obtain the field of hydraulic conductivity. Measurements of pumping tests reflect depth-averaged horizontal features of aquifers, whereas the flowmeter data contain the relative vertical distributions of hydraulic conductivity. I use final drawdown measurements of pumping tests and discharge profiles of the flowmeter tests as my data for the inversion. By considering discharge profiles, I avoid converting the relative hydraulic conductivities to absolute values making the integration of flowmeter data into the analysis of pumping tests consistent.

With about one million of unknowns, the inverse approach used roughly two days CPU time to finish the estimation of hydraulic conductivity on a standard personal computer. The results show that three-dimensional structures are obtained in the vicinity of the wells where flowmeter tests were conducted. In the region where only pumping test data exist, the estimated hydraulic conductivity becomes vertically uniform. The remaining uncertainty of the estimate decreases considerably near the wells for flowmeter tests. The three-dimensional study has been published by Li et al. [2008].

Overall, with the geostatistical inverse approach using a sufficient number of measurements with suitable support volumes, I can obtain reliable estimates of spatial distributions of hydrogeological parameters with reasonable computational effort. On unstructured grids, the inverse approach with the KL expansion [Li and Cirpka, 2006] appears to be the most efficient method. On structured grids, the method using the full covariance matrix can be applied to problems with up to millions of unknowns on a standard personal computer. In both methods, a good spatial distribution of the estimated fields is obtained mainly in the regions where aquifer tests are available. In order to identify all relevant structures in a formation, about one measurement per correlation length is required. However, traditional hydraulic investigation techniques such as pumping and flowmeter tests are costly because they require wells. Efficient data-acquisition techniques based on geophysical monitoring of hydraulic tests such as electrical resistivity tomography and a proper integration of these techniques into ground-

water inverse modeling seem necessary.

Zusammenfassung

Strömungs- und Transportmodelle sind wichtige Werkzeuge in der Bewirtschaftung von Grundwasserressourcen. Zu Ihrer Verwendung muss die räumliche Verteilung hydrogeologischer Parameter, namentlich der Durchlässigkeit und des Speicherkoeffizienten, bekannt sein. Weil direkte Messungen dieser Grössen selten sind, werden sie meistens aus Messungen abhängiger Grössen, wie dem Grundwasserspiegel oder der Konzentration eines gelösten Stoffes, abgeleitet. Die Ermittlung der hydrogeologischen Kenngrössen aus sekundärer Information wird als inverses Problem der Grundwassermodellierung bezeichnet. Inverse Methoden auf der Grundlage einer geostatistischen Beschreibung des Grundwasserleiters sind gut geeignet um die räumliche Verteilung hydrogeologischer Parameter in heterogenen Grundwasserleitern zu ermitteln, weil die geostatistische Charakterisierung eine konsistente Grundlage für die Beschreibung räumlich variabler Grössen darstellt. Konzeptionell beruht die Geostatistik auf der Annahme, dass das Parameterfeld als räumliche Zufallsvariable betrachtet werden kann.

Innerhalb der geostatistischen inversen Methoden ist der quasi-lineare geostatistische Ansatz von Kitanidis [1995] - mit verschiedenen Modifikationen - besonders günstig, vor allen Dingen in Bezug auf die rechnerische Effizienz in der Abschätzung des besten Schätzwertes und der damit verbundenen Schätzunsicherheit. Nichtsdestotrotz verbleiben Schwierigkeiten in der Anwendung der genannten Methode.

Der gewählte inverse Ansatz erfordert die Berechnung von Kreuz-Kovarianzmatrizen, die die Korrelation zwischen allen gemessenen Grössen und allen

diskretisierten Parametern beschreiben. Effiziente spektrale Methoden zur Berechnung dieser Matrizen [Nowak et al., 2003] erfordern die Diskretisierung des Gebietes mittels regelmässiger strukturierter Gitter und können nicht angewendet werden, wenn das Gebiet durch unstrukturierte Gitter diskretisiert wird, wie dies in vielen praktischen Anwendungen der Fall ist. Eine explizite Berechnung der Kreuz-Kovarianz-matrizen ist bei grossskaligen Anwendungen praktisch nicht möglich. In dieser Dissertationsschrift parametrisiere ich das räumlich kontinuierliche Parameterfeld mittels einer abgebrochenen Reihe von Basisfunktionen, die mit spektralen Methoden aus der Auto-Kovarianzfunktion abgeleitet werden können. Die Entwicklung ist als Karhunen-Loève-Entwicklung [Loève, 1977] bekannt. Durch Einbettung des Berechnungsgebietes in eine grössere Einheitszelle eines periodischen Gebietes können schnelle Fouriertransformationmethoden verwendet werden. Ausserdem ist die Form der Basisfunktionen analytisch vorgegeben. Der Abbruch der Entwicklungsreihe nach Berücksichtigung aller dominanten Terme kann zu einer Verringerung des Rechenaufwandes führen. Die Basisfunktionen sind kontinuierliche trigonometrische Funktionen und können auf beliebigen Gittern abgebildet werden.

Ich habe die Parametrisierung des Parameterfeldes mittels der Karhunen-Loève-Entwicklung in den genannten inversen Ansatz integriert und implementierte ein vollständiges inverses Modell für strukturierte und unstrukturierte Gitter. Ich führte Vergleichsrechnungen anhand synthetischer Testbeispiele durch. Im Vergleich zum inversen Ansatz unter Verwendung der vollständigen Kovarianzfunktion ist der Ansatz unter Anwendung der Karhunen-Loève-Entwicklung auf strukturierten Gittern etwas aufwändiger, zumindest wenn viele Karhunen-Loève-Terme berücksichtigt werden müssen. Im Fall glatter Kovarianzfunktionen mit grosser Korrelationslänge kann jedoch die Karhunen-Loève-Entwicklung nach vergleichsweise wenigen Gliedern abgebrochen werden, sodass die Entwicklung rechnerische Vorteile bietet. Auf unstrukturierten Gittern ist mir keine effizientere Methode zur Berechnung von Kreuzkovarianztermen bekannt. Diese Arbeiten wurden von Li and Cirpka [2006] veröffentlicht.

Die vorliegende Dissertationsschrift behandelt inverse Methoden zur Analyse

von Felddaten. Ich zeige zwei Feldanwendungen mit unterschiedlicher Dimensionalität. In diesen Anwendungen werden Pumpversuche und Flowmeter-Daten vom Testfeld Krauthausen des Forschungszentrums Jülich ausgewertet. Die Auswertung der Pumpversuche, die in vollständig verfilterten Brunnen durchgeführt wurden, erfolgte mit einem zweidimensionalen Modell. Bei Berücksichtigung der Flowmeterdaten wechselte ich zu einer dreidimensionalen Betrachtung. Im Testfeld wurden 24 Kleinpumpversuche unter Verwendung von 52 Beobachtungsrohren durchgeführt. Dies führte zu 179 Absenkungskurven. Flowmeter-Messungen lagen für 22 Beobachtungsrohre vor.

In der zweidimensionalen Anwendung versuchte ich aus instationären Pumpversuchsdaten die räumliche Verteilung der Transmissivität und des Speicherkoefizienten zu ermitteln. Da instationäre Daten zeitlich stark korreliert sind, charakterisierte ich die Absenkungskurven mittels ihrer zeitlichen Momente [Li et al., 2005]. Die zugehörigen momentengenerierenden Gleichungen entsprechen stationären Absenkungsgleichungen mit verteiltem Quell-/Senkenterm.

Die Absenkungskurven wurden zum Vergleich mittels des Theiss-Typkurvenverfahrens ausgewertet. Hierbei ergab sich, dass mit dem inversen Verfahren die räumliche Variabilität der Transmissivität besser aufgelöst werden konnte. Das Typkurvenverfahren beruht auf der Annahme eines homogenen Grundwasserleiters, was offensichtlich im Widerspruch zu Daten steht, die für unterschiedliche Kombinationen von Pump- und Beobachtungsbrunnen zu unterschiedlichen Werten führen. Die inverse Methode ermöglicht es, hydraulische Strukturen in der Nähe von Beobachtungsrohren zu identifizieren. In diesen Bereichen wird die Unsicherheit signifikant verringert. In grösserer Entfernung zu den Beobachtungsrohren verbleibt die Unsicherheit jedoch auf hohem Niveau. Die ermittelten räumlichen Felder des Speicherkoefizienten zeigen eine starke räumliche Variabilität. Diese Variabilität erscheint unrealistisch, weil die Kenngrößen, die zum Speicherkoefizienten beitragen (Porosität, Kompressibilität des Wassers und des Porenraums) nur geringfügig schwanken. Ich vermute, dass die unaufgelöste Variabilität der Durchlässigkeit zu einer systematischen Überschätzung der Variabilität des Speicherkoefizienten führt. Die Schätzung der geostatistis-

chen Kenngrößen hängt darüberhinaus stark von der Messgenauigkeit der Absenkung ab. Ein grosser Messfehler führt zu einer grossen geschätzten Korrelationslänge und einer kleinen Varianz und damit zu glatten Feldern der geschätzten hydrogeologischen Parameter. Die zweidimensionale Studie wurde von [Li et al., 2007] veröffentlicht.

Die dreidimensionale Anwendung beruht auf denselben Daten wie das zweidimensionale Beispiel. Zusätzlich verwendete ich die vorliegenden Flowmeterdaten. In dieser Anwendung schätzte ich lediglich die Durchlässigkeitsverteilung ab, weil keine Messungen vorlagen, die auf die dreidimensionale Verteilung des spezifischen Speicherkoeffizienten sensitiv wären. Die Flowmeterdaten geben ein Vertikalprofil der relativen Durchlässigkeit innerhalb des Profiles wieder. In meinem inversen Algorithmus verwende ich direkt die Durchflussprofile der Flowmetertests. Es ist also nicht notwendig, die Flowmeterdaten zunächst in absolute Durchlässigkeiten umzuwandeln. Letzteres wäre am Standort auch nicht möglich, weil tiefenintegrierte direkte Messungen der Durchlässigkeit fehlen.

Das Berechnungsgebiet ist in etwa eine Million Finite Elemente unterteilt. Für jedes Element schätzte ich die Durchlässigkeit ab. Dies erforderte etwa zwei Tage Rechenzeit auf einem Personal Computer. Die ermittelte dreidimensionale Durchlässigkeitsverteilung zeigt eine gute vertikale Auflösung in der Nähe von Beobachtungsrohren, in denen Flowmeter-Versuche durchgeführt wurden. In Gebieten, die von Flowmeter-Brunnen weit entfernt liegen, konnte keine vertikale Differenzierung erreicht werden. Die Schätzvarianz wird in der Nähe der Flowmeter-Brunnen stark reduziert. Die dreidimensionale Studie wurde von Li et al. [2008] veröffentlicht.

Zusammenfassend kann festgestellt werden, dass es möglich ist, mit dem geostatistischen inversen Ansatz zuverlässige Schätzungen zur Verteilung hydrogeologischer Kenngrößen vorzunehmen, sofern eine ausreichende Anzahl an Messungen mit angemessenem Messvolumen vorliegen. Der zugehörige Rechenaufwand ist auch für Probleme mit vielen Unbekannten erträglich. Auf unstrukturierten Gittern erscheint der Ansatz unter Verwendung der Karhunen-Loève-Entwicklung [Li and Cirpka, 2006] am effizientesten. Auf regelmässigen struk-

turierten Gittern können bis zu eine Million Parameter mit der Methode unter Verwendung der vollen Kovarianzmatrix auf einem Personal Computer ermittelt werden. Beide Methoden führen zu einer guten räumlichen Auflösung in der Nähe von Beobachtungspunkten. Um alle hydraulisch relevanten Strukturen im Untergrund zu identifizieren muss etwa ein Beobachtungspunkt je Korrelationslänge vorliegen. Hierin liegt eine der wesentlichen Beschränkungen in der Anwendung hydraulischer Versuche. Die Installation eines Beobachtungsrohres ist aufwändig und kostspielig, sodass an den meisten Feldstandorten keine ausreichende räumliche Auflösung der hydrogeologischen Parameterfelder durch die direkte Auswertung hydraulischer Versuche erreicht werden kann. Als effiziente Alternative zu direkten Beobachtungen könnten geophysikalische Messmethoden für das Monitoring hydraulischer Versuche eingesetzt werden. Allerdings erfordert dies die Entwicklung spezieller Methoden, um diese Messdaten in das inverse Schema für die Ermittlung hydrogeologischer Größen zu integrieren.

Chapter 1

Problem Statement

1.1 Hydrogeological Parameters as Spatial Random Fields

Natural porous media in the subsurface are complex and exhibit significant spatial variability [e.g, Cressie, 1991]. It is common that hydrogeological parameters of the subsurface vary by orders of magnitude over short distances [e.g., Freeze, 1975; Kitanidis, 1991]. On large regional scales, these parameters exhibit distinct well-defined features. However, on a local scale, they strongly vary. Figure 1.1 is a graphic illustration of the variability on different scales.

In the literature, there are several approaches of describing the fields of hydrogeological parameters. The most common approach is zonation [e.g, Carrera and Neuman, 1986a;b;c]. Within a zone, the parameters are assumed uniform. The approach by Yeh and Yoon [1981] describes the parameter fields as the sum of known basic functions with coefficients that need to be calibrated. The zones and deterministic functions are useful in representing large-scale variability. However, they have difficulties in accounting for smaller-scale variability. It is thus expedient to describe the parameters in a probabilistic fashion [e.g., Matheron, 1971; Journel and Huijbregts, 1978; Kitanidis and Vomvoris, 1983; Dagan, 1989; Cressie, 1991]. The basic idea is that we do not know the de-

tailed information of the subsurface but some statistical properties such as mean values, the variance and the correlation of hydraulic parameters at two points as a function of the separation distance. Hence, the theory of geostatistics is applicable [Matheron, 1971; Journel and Huijbregts, 1978]. In this sense, the parameters can be regarded as random space variables. Because of their relative position in space, there exist relations among the random variables.

1.2 Parameter Estimation in Groundwater Modeling

In groundwater management, flow and solute transport models in porous media have become very important tools. These models are applied for predicting flow patterns and distributions of solute transport. For such purposes, hydrogeological parameters such as permeabilities, storativities, and diffusivities must be known. However, the required hydrogeological parameters are difficult to obtain. This difficulty is recognized to be a major impediment to wider use of groundwater models and to their full utilization [e.g., Frind and Pinder, 1973; Kitanidis and Vomvoris, 1983]. The major reasons of the difficulty are the scarcity of available direct measurements of the hydrogeological parameters. Even in the case where one has direct measurements, they reflect conditions at the points of measurement and cannot be considered representative of regional conditions [e.g., Freeze, 1972]. In practice, the information about the hydrogeological parameters is mainly extracted from secondary dependent information such as head, or solute concentration measurements.

The inference of hydrogeological parameters from secondary information is normally accomplished through selecting a set of parameters in such a way that the measurements of heads, solute concentrations, and other variables describing the system can be reproduced by the model. This method has widely been applied as a manual trial-and-error procedure. In the past decades, a large number of systematic and computerized methods have been proposed [e.g., Neuman and

Yakowitz, 1979; Kitanidis and Vomvoris, 1983; Yeh and Yoon, 1981; De Marsily et al., 1984; Yeh, 1986; Carrera and Neuman, 1986a;b;c; Sun, 1994]. The process of automated parameter estimation is referred to as the inverse problem of groundwater modeling. The inverse methods based on concepts of zonation or deterministic functions cannot provide detailed information of the hydrogeological parameters due to the averaging or smoothing processes involved. In contrast, inverse methods within the framework of geostatistics appear more suitable for estimating the spatial distribution of hydraulic parameters in heterogeneous aquifers [e.g., Kitanidis and Vomvoris, 1983].

1.3 Geostatistical Inverse Models

Since the 1980's, a variety of inverse models based on geostatistics have been developed [for reviews see Yeh, 1986; Sun, 1994; Zimmerman et al., 1998].

The goal of these inverse methods is to estimate spatial distributions of hydrogeological parameters. In theory, the spatial domain can be discretized infinitely fine while the number of direct or indirect measurements is finite. That is, without introduction of prior knowledge, the inverse problem is ill posed. In geostatistical inversion, the prior knowledge is introduced by assuming that the parameter fields are auto-correlated spatial variables. Kitanidis [1999] has shown that these so-called Tikhonov methods are formally equivalent to assuming particular generalized covariance functions in geostatistical inversion. The various geostatistical methods differ in the implementation of geostatistical regularization. In the following, I briefly review a few prominent geostatistical inverse approaches focusing on their different parameterization of random spatial fields. However, geostatistical inverse approaches may differ from each other in many other aspects, such as the techniques of searching optimal values, and the way how they precede to obtain expected values of hydrogeological parameters and their related estimation uncertainty.

The Pilot-Point Method of RamaRao et al. [1995] and the method of Sequential

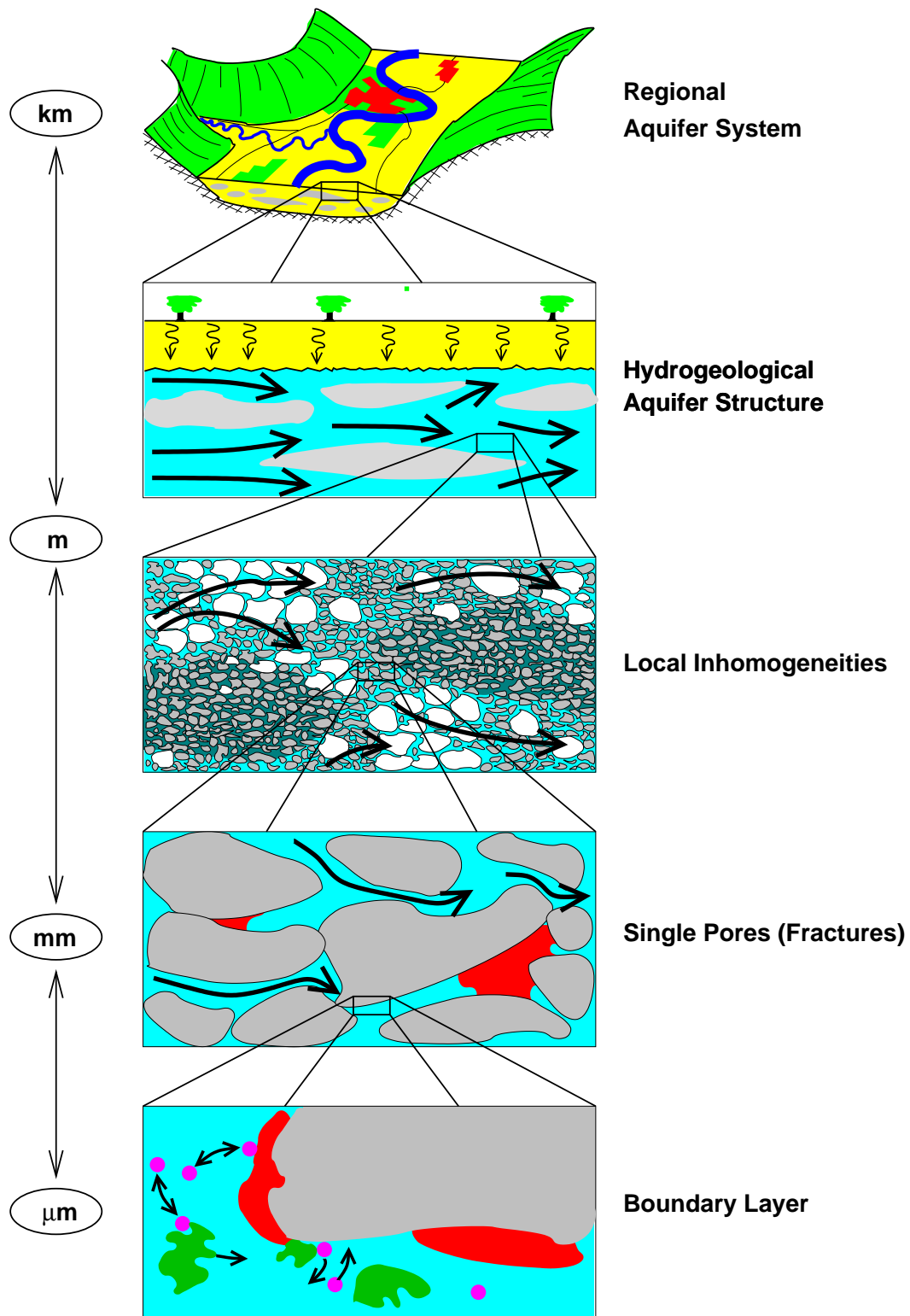


Figure 1.1: A schematic illustration of porous media at different scales.

Self-Calibration of Sahuquillo et al. [1992] replace measurements of dependent quantities by virtual measurements of the independent parameter field itself. From the latter, the full spatial field is obtained by geostatistical interpolation (kriging). In this context, the optimization procedure consists of determining the optimum values of the virtual measurements, in which the number of the variables to be optimized is much smaller than the total number of unknowns of the parameters themselves. Both approaches achieve estimates of hydrogeological parameters by minimizing a least-square objective function. The formulations of these two approaches are mathematically similar. However, they are conceptually different in the way of implementing virtual measurements. The master locations are used to parameterize the perturbations of hydrogeological parameters, and are optimized at once to obtain the field of perturbations. In contrast, pilot points represent the parameters themselves and are located sequentially by a automated searching algorithm. After locating each pilot point, the updated field of hydrogeological parameters is obtained. The Pilot-Point Method of RamaRao et al. [1995] and the method of Sequential Self-Calibration of Gómez-Hernández et al. [1997] involve conditional Monte-Carlo simulations, that is generating many possible outcomes or realizations of the solution. The system response of each realization meets the measurements within the bounds of measurement errors. Realizations fulfilling such conditions are denoted as conditional realizations, because they are conditioned on the measurements. The general properties of the parameter fields are given by the ensemble mean and the corresponding uncertainty fields by the magnitude of variations.

Representer Methods [Benett, 1992; Valstar et al., 2004] parameterize unknown hydrogeological parameters by an expansion with a finite series, which depend on unknown functions called representer. The number of representer are equivalent to the number of measurements, which reduces the computational costs in the parameter estimation. Representer methods consider generalized least-square objective function and explicitly account for model errors, which are assumed to be additive forcing terms in the flow and transport equations. The partial differential equations with the forcing terms will serve as constraints

in the optimization. Minimizing the objective function and considering the constraints lead to Euler-Lagrange equations [Valstar et al., 2004], in which the unknown representers are determined by substituting the unknowns with the finite expansions. The estimate of the parameter fields with full dimension is obtained by substituting the representers into the expansions. If the functional relation between hydrogeological parameters and measurements is linear, the representer methods are almost identical to cokriging-like inverse approaches. In contrast to the Pilot-Point Method of RamaRao et al. [1995] and the method of Sequential Self-Calibration of Sahuquillo et al. [1992], the representer methods [Benett, 1992; Valstar et al., 2004] estimate the expected values and the corresponding uncertainties in a single simulation.

The Successive Sequential Linear Estimator [Yeh et al., 1996; Zhang and Yeh, 1997; Yeh and Liu, 2000] is based on classical cokriging equations, in which a parameter at a given location is computed by a linear combination of direct and indirect measurements. The weights are computed by minimizing the estimation variance subject to constraints (Best Linear Unbiased Estimator, BLUE). Cokriging requires cross-covariance functions that are computed in the Successive Sequential Linear Estimator by linear uncertainty propagation. In the Successive Sequential Linear Estimator, the measurements are introduced sequentially, that is, the unconditional field is conditioned by the first measurement, resulting in a conditional mean and covariance function acting as prior for conditioning on the second measurement, resulting in an updated conditional mean and covariance function, etc.. There are two difficulties of this approach: 1) The prior covariance function from the second measurement onward is non-stationary, losing convenient properties of the stationary covariance function commonly assumed for the unconditional field. 2) Due to linearity, a measurement may be met after conditioning to this particular measurement but no more after conditioning to further measurements. Zhu and Yeh [2005] tried to overcome the latter difficulty by re-adjusting the parameter field to previously used measurements.

The Quasi-Linear Geostatistical Inverse Approach of Kitanidis [1995] and the Maximum a Posteriori Likelihood Method of McLaughlin and Townley [1996]

are conceptually similar to the most of the above mentioned methods in the sense that they rely on linearization of the functional relationship between parameters and measured quantities about the current estimate, and that they maximize the conditional probability density of the parameters using geostatistical prior knowledge. In the Maximum a Posteriori Likelihood Method of McLaughlin and Townley [1996], a system of equations must be solved that is of the order of the number of discretized parameters plus the number of the trend coefficients. Kitanidis [1995] makes use of matrix identities so that the system of equations is only of the order of the number of measurements plus the number of the trend coefficients. The equations used in the Quasi-Linear Geostatistical Inverse Approach of Kitanidis [1995] are identical to the function-estimate form of cokriging using cross-covariance functions obtained by linearization about the estimate itself. This method becomes identical to the Representer Methods [Benett, 1992; Valstar et al., 2004] when the cross-covariance functions are used as representer. In contrast to the Successive Sequential Linear Estimator [Yeh et al., 1996; Zhang and Yeh, 1997; Yeh and Liu, 2000], all measurements are introduced at once so that the prior covariance function remains stationary. Iterations are only needed to update the linearization about the estimate. In addition to most methods mentioned above, the Quasi-Linear Geostatistical Inverse Approach includes a step of estimating the geostatistical parameters, such as variance and correlation lengths, used for the prior covariance function. In the standard version, the Quasi-Linear Geostatistical Inverse Approach results in a smooth estimated parameter field meeting the measurements plus an approximate posterior covariance function. A variant for the generation of conditional realizations exists as well.

The Stochastic Moment Analysis Method by Hernandez et al. [2006] also results in a smooth best estimate. The best estimate itself, however, does not necessarily meet the measurements. Hernandez et al. [2006] account for the effect of the unresolved variability on the mean behavior of the dependent variable, resulting in nonlocal up-scaled equations.

1.4 Selection of Inverse Method

My goal is to estimate hydrogeological parameters in field applications. Such problems are three-dimensional. In numerical models, a three-dimensional discretization can easily lead to millions of unknowns. For such large number of unknowns, a careful selection of computationally efficient approaches becomes extremely relevant. The Pilot-Point Method of RamaRao et al. [1995] and the method of Sequential Self-Calibration of Sahuquillo et al. [1992] require a large number of realizations. The computational effort increases dramatically with the number of conditional realizations and the number of unknowns. This makes any approach based on conditional realizations not applicable for my goal.

The Successive Sequential Linear Estimator [Yeh et al., 1996; Zhang and Yeh, 1997; Yeh and Liu, 2000], the Quasi-Linear Geostatistical Inverse Approach by Kitanidis [1995], the Maximum a Posteriori Likelihood Method of McLaughlin and Townley [1996], and the recent inverse approach with Stochastic Moment Analysis Method by Hernandez et al. [2006] involve cokriging-like techniques. They consider the unknown parameters as a random space function conditioned on given relevant measurements. They need to handle auto-covariances and cross-covariances. For large-scale problems, evaluation of these terms becomes computationally demanding. However, the auto-covariance matrix of a spatial random variable has Toeplitz structure on regular grids when the parameter field is statistically at least intrinsic. This structure can be used to optimize the performance of all required matrix operations using the Fast Fourier Transformation(FFT) method [e.g., Zimmerman, 1998; Nowak et al., 2003]. The methods of the Successive Sequential Linear Estimator [Yeh et al., 1996; Zhang and Yeh, 1997; Yeh and Liu, 2000] and the Stochastic Moment Analysis Method [Hernandez et al., 2006] update the covariance matrices in their iterative procedure. By this, the covariance matrix becomes non-stationary. Consequently, the efficient FFT method cannot be used, making implementation of these two approaches in my thesis not feasible. In contrast to the Successive Sequential Linear Estimator [Yeh et al., 1996; Zhang and Yeh, 1997; Yeh and Liu, 2000], the Quasi-Linear

Geostatistical Inverse Approach [Kitanidis, 1995] and the Maximum a Posteriori Likelihood Method [McLaughlin and Townley, 1996] maintain the structure of the covariance matrix in the estimation. This indicates that the latter two approaches can be sped up by spectral methods. Unlike the Quasi-Linear Geostatistical Inverse Approach [Kitanidis, 1995], the Maximum a Posteriori Likelihood Method [McLaughlin and Townley, 1996] does not take the uncertainty of the trend coefficients into consideration and under-determines the conditional variance. The representer methods [Benett, 1992; Valstar et al., 2004] are not based on Bayes' theorem, the integration of prior information, which may be valuable for stabilizing the inverse procedure, may be difficult. All these considerations made me choose the Quasi-Linear Geostatistical Inverse Approach of Kitanidis [1995] as inverse kernel. For stabilization of the inverse method, I rely on the Levenberg-Marquardt modification of the original Quasi-Linear Geostatistical Inverse Approach introduced by Nowak and Cirpka [2004].

In cases of highly variable parameter fields, it may become inappropriate to estimate a smooth best estimate meeting the original governing equations. Also in these cases, the approximative covariance function obtained by the Quasi-Linear Geostatistical Inverse Approach [Kitanidis, 1995] may become biased. The most rigorous approach for such cases would be the Stochastic Moment Analysis Method of [Hernandez et al., 2006], which unfortunately is computationally very demanding. An alternative would be to apply methods based on generating conditional realizations. Then, the Pilot-Point Method of RamaRao et al. [1995] and the method of Sequential Self-Calibration of Sahuquillo et al. [1992] can be better choices. In the present study, however, I restrict the analysis to cases with only moderate variability, so that the Quasi-Linear Geostatistical Inverse Approach [Kitanidis, 1995] becomes applicable.

1.5 Tasks of Thesis

Despite the advances made in the Quasi-Linear Geostatistical Inverse Approach [Kitanidis, 1995], a couple of difficulties in applying this method remain. To

cope with these difficulties, I suggest a further extension of this inverse approach.

Another objective of this thesis is to examine the applicability of the inverse approach in analyzing field data. Field measurements at test site Krauthausen, Germany [Vanderborght and Vereecken, 2001; Vereecken et al., 1999; 2000] are used. In a two-dimensional application, I test the feasibility of the inverse approach in inferring the fields of transmissivity and storativity. To test the performance of the inverse approach for large-scale problems, I use a resolution of one million of unknowns in estimating the three-dimensional field of hydraulic conductivity at the site.

In the following, I summarize the major contributions of my thesis, discussing background information of the difficulties, the techniques of extension, and specific aspects in field implementations.

- (I) Extending the Quasi-Linear Geostatistical Inverse Approach to unstructured grids.

To solve field problems, one frequently encounters situations where unstructured grids are required, e.g. when the grid is locally refined. The efficient FFT method of computing matrix-matrix products of Nowak et al. [2003] requires grids to be regular. Facing an unstructured grid with a large number of elements, I choose an alternative representation of the spatial parameter fields approximating the fields in reduced dimensions but still producing reliable estimates. For this purpose, I apply the Karhunen-Loève(KL) expansion [Loève, 1977; Ghanem and Spanos, 1991]. In Section 2.6.3, the KL expansion is reviewed in detail.

In continuous domains, an orthonormal representation of autocorrelated, multi-Gaussian field is given by the KL expansion. In the KL expansion, the random spatial variable is parameterized by weighted base functions derived from its covariance function. The base functions are the eigenfunctions of the covariance function times the square-root of the corresponding eigenvalues. Typically, the series of eigenvalues is sorted in a

decreasing order and truncated. The approximation by a truncated series of eigenvalues can potentially reduce the computational cost of estimating the parameter fields, because the number of dominant eigenvalues may be much smaller than the number of grid points of the discretized domain.

A particular annoyance in applying the KL expansion to arbitrary domains lies in the evaluation of the eigenvalues and eigenfunctions. For periodic covariance functions, the eigenfunctions are known to be sinusoidal, and the eigenvalues are proportional to the Fourier coefficients of the covariance function. This simplifies the eigen-decomposition dramatically. For non-periodic covariance functions with stationary increments, the embedding and extracting technique [e.g., Dietrich and Newsam, 1993; Nowak et al., 2003] can be applied. The reproduction of the covariance function using continuous trigonometric functions is independent on the discretization scheme of the spatial random field. Thus, it allows discretizing the domain in arbitrary ways, namely by using unstructured grids.

Since the Quasi-Linear Geostatistical Inverse Approach [Kitanidis, 1995] maintains the covariance matrix intrinsic, a single step of approximating the covariance matrix is needed for all stages of the estimation. In this thesis, I integrate the parameterization with the KL expansion into the Quasi-Linear Geostatistical Inverse Approach [Kitanidis, 1995]. I illustrate the major steps of the integration process in Section 2.10. Detailed aspects, such as the influence of the number of terms after truncation on the estimate, their uncertainties and the computational costs, are investigated in synthetic test cases of Chapter 3.

- (II) Analyzing hydraulic tomography to obtain fields of transmissivity and storativity with transient drawdown data

Pumping tests are common techniques for hydrogeological site investigation. During pumping tests, water is injected or extracted from a production well and changes of water level are monitored in the adjacent observation wells as well as in the production well. Conventional pumping tests are restricted to a single pumping well. Analysis of these tests provides

hydraulic properties over a large influence zone [Butler and Liu, 1993; Gottlieb and Dietrich, 1995]. The obtained transmissivity is a weighted average and does not provide detailed spatial information. To overcome the limitations of conventional pumping tests, hydraulic tomography has been proposed [e.g., Neuman, 1987; Butler and Liu, 1993].

In hydraulic tomography, a series of pumping tests stressing different vertical intervals are performed and the changes of heads or drawdowns are monitored at multiple observation points. Figure 1.2 illustrates the basic concept of hydraulic tomography. By changing the pumping wells and

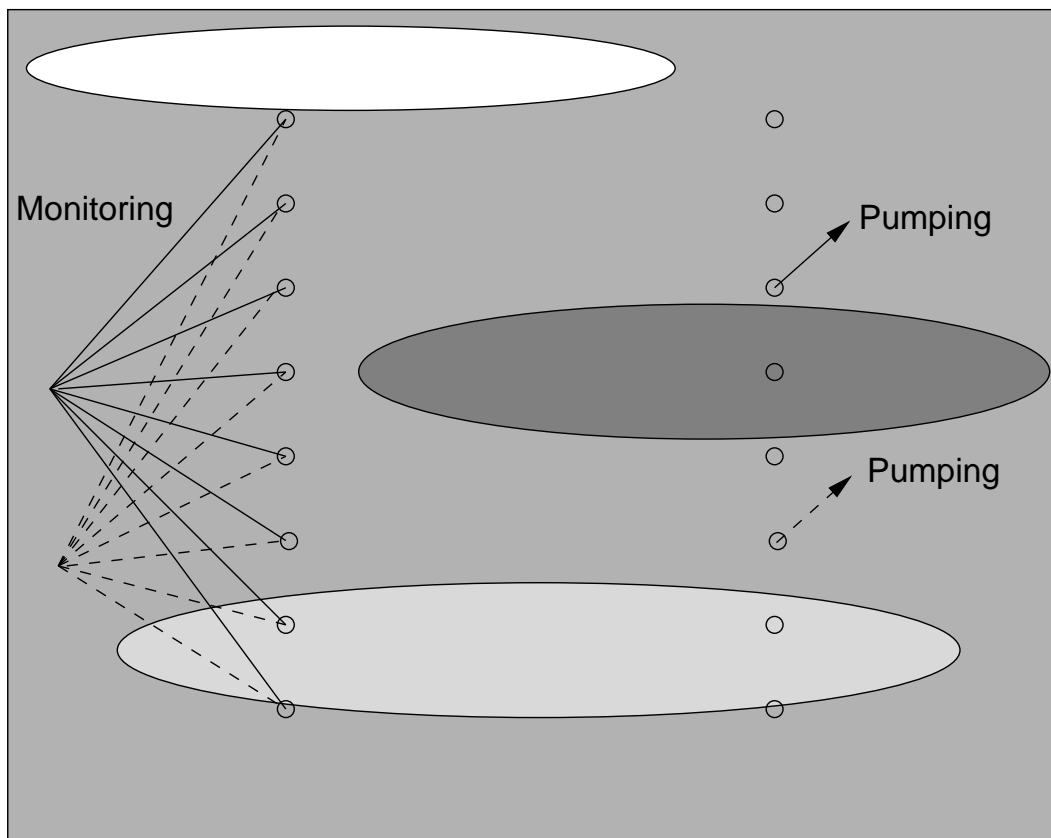


Figure 1.2: Schematic illustrate of the concept of hydraulic tomography. Circles indicate pumping or monitoring locations.

monitoring the response of the heads at other locations, one obtains multiple sets of head data.

Numerical investigations [Bohling, 1993; Gottlieb and Dietrich, 1995; Zhu and Yeh, 2005; 2006]) and sandbox experiments [Yeh and Liu, 2000; Liu et al., 2007] have demonstrated that hydraulic tomography may produce a significantly improved description of the variation of hydraulic parameters. Straface et al. [2007] analyzed field data of hydraulic tomography to estimate transmissivity and storativity. They show that hydraulic tomography can obtain more information than classical aquifer tests using the same well fields.

Transient behavior of drawdown curves in a pumping test is determined by the field of storativity and transmissivity. In contrast, the steady-state values of drawdown of a pumping test are quantified by the field of transmissivity. This indicates that transient data have to be used in order to estimate the field of storativity.

Hendricks Franssen et al. [1999] jointly estimated the fields of transmissivity and storativity with transient hydraulic head data. They used the method of Sequential Self-Calibration of Sahuquillo et al. [1992], which is based on conditional simulation. This method does not rely on cross-covariance matrices between parameters and measurements and is thus less affected by increasing the number of measurements in transient applications than cokriging-like techniques. However, they solved time-demanding transient partial differential groundwater flow equations in each realization. When the number of realizations increases, the computational costs are dramatically rising. Zhu and Yeh [2005] obtained the field of hydraulic conductivity and specific storage coefficients from transient heads. The Successive Sequential Linear Estimator [Yeh et al., 1996; Zhang and Yeh, 1997; Yeh and Liu, 2000] was applied in the latter study. As mentioned previously, this estimator explicitly evaluates the full cross-covariance matrix and is computationally demanding, especially with a large number of unknowns.

Zhu and Yeh [2005] showed that only a few measurement points in time are needed in inverse modeling because the transient heads at a given loca-

tion are strongly correlated in time. The high temporal correlation of transient measurements in a drawdown curve leads to ill-conditioned matrices in the inversion. In addition, it is time-consuming when transient partial differential equations have to be solved in numerical modeling and it becomes highly computationally demanding especially for cases with a large number of unknowns. In my M.Sc. thesis, I have developed the concept of temporal moment of drawdown [Li et al., 2005]. Temporal moments represent the information of transient curves in a condensed form. The major advantage is that the corresponding moment-generating equations are formally equivalent to steady-state flow equations with distributed sources. A transient groundwater equation is replaced by a series of steady-state equations. Solving steady-state flow equations is much more efficient than transient ones.

Concerning storativity, virtual studies have shown strong fluctuations even when a uniform field is applied [Meier et al., 1998]. Because the variability of all terms making up the storativity is small, it is believed that the estimated variability of storativity is biased. The biased results may come from the inconsistent assumption of uniformity of parameter fields. More consistent assumptions on the structures of porous media may help resolve the biased problem.

At the test site Krauthausen, Germany, pumping tests in tomographic format were conducted [Lamertz, 2001]. In Section 4.1, I give a brief description of the test site and the tests conducted. The field data provide a good opportunity to test the feasibility of the Quasi-Linear Geostatistical Inverse Approach in estimating the fields of transmissivity and storativity. With the enhanced data-acquisition technique of hydraulic tomography and more consistent assumptions on the structures of aquifers, I expect to obtain reliable estimates of transmissivity and storativity when applying the inverse approach to field data. In the inverse estimation, I apply the concept of temporal moments of drawdown to extract the condensed information of transient drawdown curves.

A detailed comparison of conventional approaches and the advanced geostatistical inverse approach in analyzing field data is seldom done. In this thesis, I apply both approaches to the transient tomographic drawdown data at the test site Krauthausen (see Section 4.2). The conventional analysis of pumping tests by type-curve methods is based on the assumption of a homogeneous aquifer. Applying these techniques to pumping test data from real heterogeneous aquifers leads to estimates of the hydraulic parameters that depend on the choice of the pumping and observation well positions. In this thesis, I test whether these values may be viewed as pseudo-local values of transmissivity and storativity, which can be interpolated by kriging. I compare such estimates to those obtained by geostatistical inverse modeling, where heterogeneity is assumed in all stages of estimation.

Since the geostatistical parameters have to be estimated from measurements as well, the quality of the measurements determines the results of the estimation. I examine the influence of measurement error on estimating geostatistical parameters of covariance functions in the inversion. In contrast to other synthetic studies, I apply field data in the estimation.

(III) Estimating hydraulic conductivity: A three-dimensional implementation

Estimating three-dimensional fields of hydrogeological parameters is still challenging. In three-dimensional applications with a fine resolution, the number of unknowns can easily be up to millions. For such large number of unknowns, the estimation becomes computationally demanding.

Besides large computational costs, the major difficulty lies in the lack of a sufficient number of measurements with suitable support volumes. Frequently, most available measurements are restricted to particular dimensions and may not be suitable for three-dimensional estimation. A common solution to such problems is to jointly apply data reflecting different aspects of the subsurface.

At the test site, pumping tests and flowmeter tests in fully-screened wells

have been conducted. Flowmeter data contain information about the vertical distribution of hydraulic conductivity, whereas values of drawdown obtained during pumping tests contain information about horizontal variations. This indicates that a three-dimensional field of hydraulic conductivity could be obtained by joint inversion of these two types of data.

In Section 4.3, I attempt to estimate a three-dimensional field of hydraulic conductivity using the measurements of pumping and flowmeter tests. The Quasi-Linear Geostatistical Inverse Approach is applied for this estimation. To test the performance of the inverse approach with a large number of unknowns, I estimate the field of hydraulic conductivity with about one million of unknowns.

Flowmeter data contain only relative values of hydraulic conductivity. To obtain absolute values, the depth-averaged values of hydraulic conductivity at wells need to be known. To achieve these values, one has to rely on other tests such as slug tests or small-scale pumping tests. The conventional analysis of flowmeter tests will be difficult for wells, for which unfortunately extra tests are not available. In some applications, the values of hydraulic conductivity obtained by flowmeter tests are considered as direct measurements of local hydraulic conductivity [e.g., Rehfeldt et al., 1992; Chen et al., 2001]. To my knowledge, the measurements are considered as independent values in the cited studies. The estimates of hydraulic conductivity from flowmeter tests, however, are correlated, which needs to be accounted for in their inference. In my thesis, I use discharge profiles of flowmeter tests as my data. By doing this, I do not need to convert the profiles to absolute hydraulic conductivity. In the Section 4.3.1, I will show that neither the discharge profiles nor the sensitivities of them with respect to hydraulic conductivities depend on the depth-average values of hydraulic conductivity. In my estimation, I fully consider the correlation between the measurements of flowmeter tests. Using the discharge profiles and considering the correlations make the integration of flowmeter data in the joint analysis consistent.

Chapter 2

Methods

In this chapter, I provide the governing equations of groundwater flow and illustrate the tools of estimating hydrogeological parameters given hydraulic measurements.

In Section 2.1, the groundwater flow equations are presented as well as the concept of temporal moments of drawdown and their related moment-generating equations.

In Section 2.2, I summarize Bayes' theorem, which is the base of my inversion methods. Section 2.3 reviews the geostatistical description of spatial random variables, discussing the concepts of stationarity, intrinsic, and covariance functions. Section 2.4 discusses the assumed statistical distributions of the hydrogeological parameters. In Section 2.5, I show the Toeplitz-like structure of covariance matrices on regular grids. The special structure of Toeplitz matrices is directly linked to a possible spectral representation of covariance matrices covered in Section 2.6. The important applications of the spectral representation are discussed in the corresponding subsections of Section 2.6, including generating auto-correlated fields [Dietrich and Newsam, 1993], the spectral method of computing large matrix-matrix products [Nowak et al., 2003], and a functional parameterization of a spatial random field by the Karhunen-Loève expansion (KL) [Li and Cirpka, 2006].

Section 2.7 contains the major formulations of the Quasi-Linear Geostatistical Inverse Approach [Kitanidis, 1995]. Section 2.8 covers the modified Levenberg-Marquardt Algorithm by Nowak and Cirpka [2004] for stabilizing this inverse approach. Geostatistical parameters have to be estimated from measurements as well. In Section 2.9, I discuss the restricted maximum likelihood method [Kitanidis, 1995] of estimating geostatistical parameters. In Section 2.10, I integrate the parameterization by the KL expansion into the Quasi-Linear Geostatistical Inverse Approach [Kitanidis, 1995] making the inverse approach also applicable on unstructured grids with a large number of unknowns. The sensitivities of measurements with respect to hydrogeological parameters are required in the inference. Section 2.11 covers the efficient computation of sensitivity matrices with the adjoint-state method [Sun and Yeh, 1990]. Some typical patterns of sensitivity functions are illustrated.

2.1 Governing Equations

In this section, I present groundwater flow equations and demonstrate how transient data from pumping tests relate to the temporal moments of drawdown in a pumping test with unit-pulse extraction. The latter equations have been published for the first time in Li et al. [2005].

2.1.1 Groundwater Flow Equations

Three-Dimensional Flow

I consider three-dimensional flow in groundwater. The hydraulic heads h [m] meet the following partial differential equation:

$$S_0 \frac{\partial h}{\partial t} - \nabla \cdot (K \nabla h) = W, \quad (2.1)$$

in which the coefficients S_0 [1/m] and K [m/s] are the specific storage coefficient and hydraulic conductivity, respectively, and W [1/s] denotes an internal volumetric source/sink term.

Pumping tests are frequently conducted for characterizing aquifers. With a pumping rate Q [m³/s] at location \mathbf{x}_w [m], the groundwater flow equation becomes:

$$S_0 \frac{\partial h}{\partial t} - \nabla \cdot (K \nabla h) = W - Q \delta(\mathbf{x} - \mathbf{x}_w), \quad (2.2)$$

subject to the initial and boundary conditions:

$$h = h_0 \text{ at } t = t_0, \quad (2.3)$$

$$h = h_{Diri} \text{ on } \Gamma_{Diri} \forall t, \quad (2.4)$$

$$-\mathbf{n} \cdot (K \nabla h) = q_{Neu} \text{ on } \Gamma_{Neu} \forall t, \quad (2.5)$$

where $\delta(\mathbf{x} - \mathbf{x}_w)$ [1/m³] is the Dirac delta function, \mathbf{x}_w [m] is the location of the pumping well, h_0 [m] is the field of hydraulic heads before pumping, t [s] is time, t_0 [s] is the time at which pumping starts, Γ_{Diri} and Γ_{Neu} denote Dirichlet and Neumann boundaries, h_{Diri} [m] stands for the fixed-head values at Dirichlet boundaries, q_{Neu} [m/s] is the normal flux component at Neuman boundaries, and \mathbf{n} [–] is the unit vector normal to the boundaries. Since my studies are mainly about pumping tests, I will focus on groundwater flow equations of pumping tests in the later descriptions.

The field of h_0 [m] before pumping meets the following equation:

$$S_0 \frac{\partial h_0}{\partial t} - \nabla \cdot (K \nabla h_0) = W, \quad (2.6)$$

subject to the boundary conditions:

$$h_0 = h_{Diri} \text{ on } \Gamma_{Diri} \forall t, \quad (2.7)$$

$$-\mathbf{n} \cdot (K \nabla h_0) = q_{Neu} \text{ on } \Gamma_{Neu} \forall t. \quad (2.8)$$

Frequently the hydraulic head h [m] is replaced by drawdown s [m]:

$$s = h_0 - h. \quad (2.9)$$

Under the condition that the only changing boundary condition is that related to pumping, I can subtract Eq. (2.2) from Eq.(2.6), consider the boundary conditions, and obtain the partial differential equation for drawdowns in a pumping test:

$$S_0 \frac{\partial s}{\partial t} - \nabla \cdot (K \nabla s) = Q(t) \delta(\mathbf{x} - \mathbf{x}_w), \quad (2.10)$$

with the initial and boundary conditions:

$$s = 0 \text{ at } t = t_0, \quad (2.11)$$

$$s = 0 \text{ on } \Gamma_{Diri} \forall t, \quad (2.12)$$

$$-\mathbf{n} \cdot (K \nabla s) = 0 \text{ on } \Gamma_{Neu} \forall t. \quad (2.13)$$

In practice, one conducts a pumping test either by extracting water with a rate $Q(t)$ over a finite period of time, or by pumping with a constant rate Q until steady state is reached. Due to the linearity of Eq. (2.10), the drawdown $s_Q(\mathbf{x}, t)$ for an arbitrary pumping regime $Q(t)$ can be computed from the drawdown $s_\delta(\mathbf{x}, t)$ [s/m^2], valid for instantaneous extraction of a unit volume, by convolution:

$$s_Q(\mathbf{x}, t) = \int_0^t s_\delta(\mathbf{x}, t - \tau) Q(\tau) d\tau. \quad (2.14)$$

For the case of continuous extraction, i.e., $Q(t) = Q$, I consider the steady-state drawdown $s_\infty(\mathbf{x}) = Q \int_0^\infty s_\delta(\mathbf{x}, \tau) d\tau$, and the deviation from the steady-state drawdown $\Delta h(\mathbf{x}, t) = s_\infty(\mathbf{x}) - s(\mathbf{x}, t) = Q \int_t^\infty s_\delta(\mathbf{x}, \tau) d\tau$.

Two-Dimensional Flow in Confined Aquifers

For two-dimensional regional applications in confined aquifers, S_0 becomes the depth-integrated storativity $S [-]$ and K transmissivity $T [m^2/s]$. I consider drawdown as my target variable. Then, the depth-integrated groundwater flow equation becomes:

$$S \frac{\partial s}{\partial t} - \nabla \cdot (T \nabla s) = Q \delta(\mathbf{x} - \mathbf{x}_w), \quad (2.15)$$

where $\delta(\mathbf{x} - \mathbf{x}_w) [1/m^2]$ denotes the two-dimensional Dirac function. The corresponding boundary conditions are:

$$s = 0 \text{ at } t = t_0, \quad (2.16)$$

$$s = 0 \text{ on } \Gamma_{Diri} \forall t, \quad (2.17)$$

$$-\mathbf{n} \cdot (T \nabla s) = 0 \text{ on } \Gamma_{Neu} \forall t. \quad (2.18)$$

Two-Dimensional Flow in Unconfined Aquifers

In contrast to confined aquifers, the water thickness in unconfined aquifers depends on the hydraulic head h . I consider that the porosity is much larger than storage coefficients. Thus, the depth-integrated groundwater flow equation for unconfined aquifers becomes:

$$n_e \frac{\partial h}{\partial t} - \nabla \cdot (\bar{K}(h - z_{bot}) \nabla h) = W - Q \delta(\mathbf{x} - \mathbf{x}_w), \quad (2.19)$$

in which $n_e [-]$ is the porosity of the porous media, $\bar{K} [m/s]$ is the depth-averaged hydraulic conductivity, and $z_{bot} [m]$ is the vertical position of the aquifer bottom. The corresponding boundary conditions are:

$$h = h_0 \text{ at } t = t_0, \quad (2.20)$$

$$h = h_{Diri} \text{ on } \Gamma_{Diri} \forall t, \quad (2.21)$$

$$-\mathbf{n} \cdot (K \nabla h) = q_{Neu} \text{ on } \Gamma_{Neu} \forall t. \quad (2.22)$$

2.1.2 Temporal Moments of Drawdown

The transient behavior of the drawdown $s(\mathbf{x}, t)$ can be characterized by its temporal moments. The k -th moment $m_k(s(\mathbf{x})) [ms^{k+1}]$ is defined by:

$$m_k(s(\mathbf{x})) = \int_0^\infty t^k s(\mathbf{x}, t) dt. \quad (2.23)$$

Here, I consider the zeroth moment $m_0(s(\mathbf{x}))$ and the first moment $m_1(s(\mathbf{x}))$. In Li et al. [2005], I have demonstrated that the zeroth and first temporal moments can provide sufficient information about the transient curves of drawdown in estimating hydrogeological parameters. For a unit-pulse extraction, the zeroth moment corresponds to the steady-state drawdown of a corresponding pumping test with continuous extraction, whereas the normalized first moment $m_1(s(\mathbf{x}))/m_0(s(\mathbf{x}))$ is a characteristic time of drawdown.

The moments of the unit-pulse response $s_\delta(\mathbf{x}, t)$ are related to those of the drawdown $s_Q(\mathbf{x}, t)$ due to extraction $Q(t)$ over a time period by:

$$m_0(s_\delta(\mathbf{x})) = \frac{m_0(s_Q(\mathbf{x}))}{m_0(Q)}, \quad (2.24)$$

$$\frac{m_1(s_\delta(\mathbf{x}))}{m_0(s_\delta(\mathbf{x}))} = \frac{m_1(s_Q(\mathbf{x}))}{m_0(s_Q(\mathbf{x}))} - \frac{m_1(Q)}{m_0(Q)}, \quad (2.25)$$

whereas the moments of $s_\delta(\mathbf{x}, t)$ can be computed from quantities of continuous extraction by:

$$m_0(s_\delta(\mathbf{x})) = \frac{s_\infty(\mathbf{x})}{Q}, \quad (2.26)$$

$$\frac{m_1(s_\delta(\mathbf{x}))}{m_0(s_\delta(\mathbf{x}))} = \frac{m_0(\Delta h(\mathbf{x}))}{s_\infty(\mathbf{x})}. \quad (2.27)$$

In Figure 2.1, zeroth moments are marked as shaded areas, and characteristic times m_1/m_0 by vertical lines. For the cases of a pulse-like extraction and an extraction over a time period, the characteristic times are the centers of gravity of the shaded areas.

Due to the identities given above, it is clear that the zeroth and first moments for unit-pulse extraction, $m_0(s_\delta(\mathbf{x}))$ and $m_1(s_\delta(\mathbf{x}))$, can be computed for any type of pumping regime occurring in practical applications.

2.1.3 Moment-Generating Equations

Harvey and Gorelick [1995b] derived moment-generating equations for the transport of sorbing solutes using the Laplace transform of the transport equation. Here, I derive the moment-generating equations for drawdown s_δ due to unit-pulse extraction, without applying the Laplace transformation. In order to compute the k -th moment, I multiply Eq. (2.10) with t^k , integrate over time, apply rules of partial integration to the term with the time derivative, and consider the initial condition, Eq. (2.20). For $Q(t) = \delta(t)$, I arrive at:

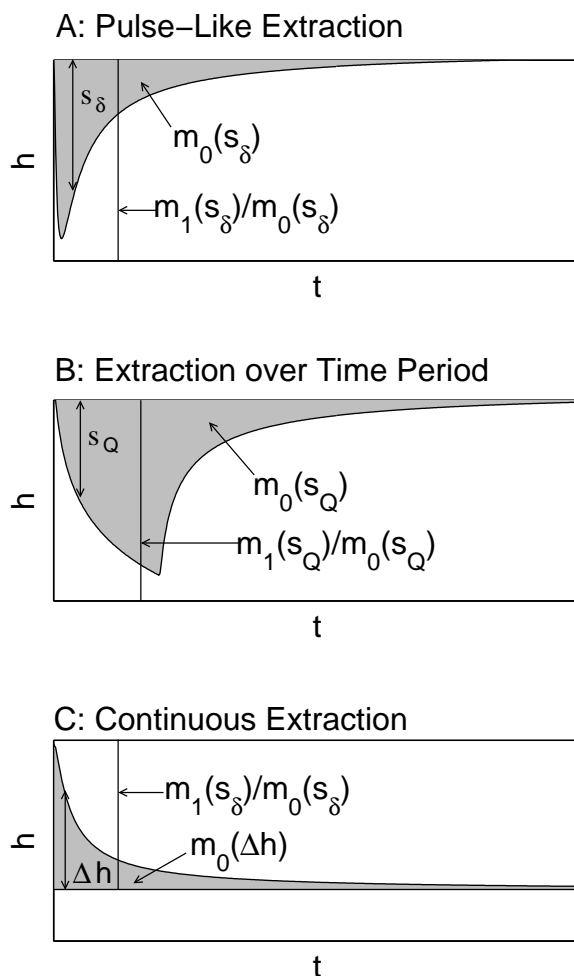


Figure 2.1: Transient drawdown in a pumping test as function of time for various regimes of extraction.

$$-\nabla \cdot (K \nabla m_k) = \delta_{k0} \delta(\mathbf{x} - \mathbf{x}_w) + k S_0 m_{k-1}. \quad (2.28)$$

Here, δ_{k0} is the Kronecker delta, which is unity for $k = 0$ and zero otherwise. The boundary conditions are obtained by multiplying Eqs. (2.12) and (2.13) with t^k and integrating over time:

$$m_k = 0 \text{ on } \Gamma_{Diri} \forall t, \quad (2.29)$$

$$\mathbf{n} \cdot \nabla m_k = 0 \text{ on } \Gamma_{Neu} \forall t. \quad (2.30)$$

The equation generating the zeroth moment $m_0(s_\delta(\mathbf{x}))$, Eq. (2.28) with $k = 0$, is a steady-state groundwater flow equation with an extraction rate of unity at the well location. It does not depend on the specific storage coefficient S_0 . Because I consider the normalized case of a unit pulse, $m_0(s_\delta(\mathbf{x}))$ neither depends on the pumping rate. By contrast, the moment-generating equations for the higher-order moments $m_{k>0}(s_\delta(\mathbf{x}))$, Eq. (2.28) with $k > 0$, are steady-state flow equations with a distributed rather than a point-like source. The distributed source term is proportional to the next lower-order moment $m_{k-1}(s_\delta(\mathbf{x}))$ and the storage coefficient $S_0(\mathbf{x})$. Therefore, the zeroth moment $m_0(s_\delta(\mathbf{x}))$ can be used to infer the distribution of hydraulic conductivity $K(\mathbf{x})$, whereas at least the zeroth and first moments, $m_0(s_\delta(\mathbf{x}))$ and $m_1(s_\delta(\mathbf{x}))$, are needed to jointly estimate the specific storage coefficient $S_0(\mathbf{x})$.

By applying moment-generating equations, I transfer the transient groundwater flow problem into a steady-state framework. In this thesis, I use the two most important and characteristic temporal moments, i.e., the zeroth and first moments, to characterize drawdown curves. For given parameter distributions, they are computed by solving two elliptic equations. In comparison to solving for transient hydraulic heads in multiple time steps, one thus drastically reduces the computational costs.

The concept of temporal moments of concentration has successfully been applied to hydrogeological inverse problems by Harvey and Gorelick [1995a], James et al. [1997], Cirpka and Kitanidis [2000], and Nowak and Cirpka [2006]. In Li et al. [2005], I could demonstrate the applicability to drawdown. In Section 4.2, I show an application to field data, which has been published in Li et al. [2007]. This approach has also been taken up by Zhu and Yeh [2006].

2.2 Bayes' Theorem

Since the derivation of my inverse approach is based on Bayes' theorem [e.g., Mood et al., 1963], I give the major formulations of the theorem in this section. The major reason of choosing Bayes' theorem is that it is the basic law of information processing, describing how additional information improves the statistical characterization of the parameter field [e.g., Rubin, 2003, chapter 2].

Bayes' theorem is based on the definition of conditional probabilities [e.g., Mood et al., 1963]:

$$p(A|B) = \frac{p(A, B)}{p(B)}, \quad (2.31)$$

in which $p(A|B)$ is the probability density for event A to occur, conditioned on the occurrence of event B , $p(A, B)$ denotes the joint probability density of the two events A and B , and $p(B)$ stands for the probability density of event B regardless of event A . An alternative expression of Eq. (2.31) can be obtained by considering $P(A|B)p(B) = p(B|A)p(A)$:

$$p(A|B) = \frac{p(B|A)p(A)}{p(B)}, \quad (2.32)$$

where $p(A)$ is the probability density of event A regardless of event B and $p(B|A)$ is the probability density for event B to occur, conditioned on the occurrence of event A . In Bayesian terminology, $p(A)$ is the prior probability density of A before considering any occurrence and $p(A|B)$ is the posterior probability density of A after accounting for the influence of the additional information from B . In most statistical textbooks, Eq. (2.32) is denoted Bayes' theorem, in other textbooks Eq. (2.31).

2.3 Geostatistical Description of Spatial Random Parameters

Hydrogeological parameters are distributed in space. On a regional scale, these parameters have a relatively regular structure that may be described deterministically [Kitanidis and Vomvoris, 1983]. However, on small local scales these parameter can strongly vary [Kitanidis and Vomvoris, 1983]. Field measurements have shown that hydraulic conductivity can vary over several orders in the same aquifer [e.g., Freeze, 1975]. The large uncertainty about the spatial distribution of hydrogeological parameters has led us to consider a stochastic approach [Matheron, 1971; Journel and Huijbregts, 1978; Kitanidis and Vomvoris, 1983; Dagan, 1989; Cressie, 1991; Gómez-Hernández and Wen, 1998] rather than conventional zonation concept or a deterministic model.

The concept of geostatistics was introduced by Matheron [1971], and has been refined ever since [e.g., Cressie, 1991]. The basic idea is to regard the parameters as autocorrelated spatial random variables. A useful and practical way of characterizing spatial random variables $Y(\mathbf{x})$ is by their first two statistical moments: the expected value $E[Y(\mathbf{x})]$ and the auto-covariance function $R_{Y'Y'}(\mathbf{x}_1, \mathbf{x}_2)$.

$$Y(\mathbf{x}) = Y'(\mathbf{x}) + \sum_i^{n_\beta} X_i(\mathbf{x})\beta_i, \quad (2.33)$$

$$E[Y(\mathbf{x})] = \sum_i^{n_\beta} X_i(\mathbf{x})\beta_i(\mathbf{x}), \quad (2.34)$$

$$R_{Y'Y'}(\mathbf{x}_1, \mathbf{x}_2) = E[Y'(\mathbf{x}_1) \otimes Y'(\mathbf{x}_2)], \quad (2.35)$$

in which $Y(\mathbf{x})$ stands for the random spatial variables, $X_i(\mathbf{x})$ denotes a deterministic base function, $\beta_i(\mathbf{x})$ is the corresponding trend coefficient, n_β is the number of trend coefficients, $Y'(\mathbf{x})$ is the random fluctuation about the deterministic trend, and $R_{Y'Y'}(\mathbf{x}_1, \mathbf{x}_2)$ is the covariance function quantifying the vari-

ability and correlation between points \mathbf{x}_1 and \mathbf{x}_2 . For $R_{Y'Y'}(\mathbf{x}_1, \mathbf{x}_2)$, one usually applies a parametric model, depending on the two locations \mathbf{x}_1 and \mathbf{x}_2 and a set of n_θ geostatistical parameters $\boldsymbol{\theta}$, such as the variance and one or multiple correlation lengths. In the later descriptions, I use the variable $R_{Y'Y'|\boldsymbol{\theta}}(\mathbf{x}_1, \mathbf{x}_2)$ to represent the covariance function $R_{Y'Y'}(\mathbf{x}_1, \mathbf{x}_2)$. By doing this, I explicitly state that the $R_{Y'Y'|\boldsymbol{\theta}}(\mathbf{x}_1, \mathbf{x}_2)$ requires knowledge of geostatistical parameters.

In the framework of second-moment characterization, a random field is called second-order stationary when the expected value of the parameter is constant over the domain and the covariance is a function of the separation distance \mathbf{h} between two points of consideration only, but is independent of the actual locations [e.g., Kitanidis and Vomvoris, 1983]:

$$R_{Y'Y'|\boldsymbol{\theta}}(\mathbf{x}_1, \mathbf{x}_2) = R_{Y'Y'|\boldsymbol{\theta}}(\mathbf{x}_1 - \mathbf{x}_2) = R_{Y'Y'|\boldsymbol{\theta}}(\mathbf{h}). \quad (2.36)$$

The value of the covariance function for a distance of zero is the variance, quantifying the overall magnitude of variability:

$$\sigma_Y^2 = \text{Var}(Y) = R_{Y'Y'|\boldsymbol{\theta}}(\mathbf{0}). \quad (2.37)$$

The applicability of $R_{Y'Y'|\boldsymbol{\theta}}(\mathbf{h})$ requires that the mean value is known. To be more general, an alternative measure is the semi-variogram $\gamma(\mathbf{h})$ defined by:

$$\gamma(\mathbf{h}) = \frac{1}{2} \text{Var} [Y(\mathbf{x} + \mathbf{h}) - Y(\mathbf{x})] = \frac{1}{2} \text{E} \left[(Y(\mathbf{x} + \mathbf{h}) - Y(\mathbf{x}))^2 \right], \quad (2.38)$$

where $\gamma(\mathbf{h})$ again depends on the vector \mathbf{h} and not the actual locations. The formulations of $\gamma(\mathbf{h})$ and $R_{Y'Y'|\boldsymbol{\theta}}(\mathbf{h})$ are similar. However, the latter implicitly excludes cases with infinite variance or media with unknown mean. A distribution characterized by a variogram $\gamma(\mathbf{h})$ is referred to as intrinsic. It can be shown that second-order stationarity implies the intrinsic hypothesis, but the converse is not true. In case of second-order stationarity, the following identity holds:

$$R_{Y'Y'|\theta}(\mathbf{h}) = R_{Y'Y'|\theta}(\mathbf{0}) - \gamma(\mathbf{h}). \quad (2.39)$$

Figure 2.2 shows the relation between the semi-variogram and covariance functions for a second-order stationary spatial field.

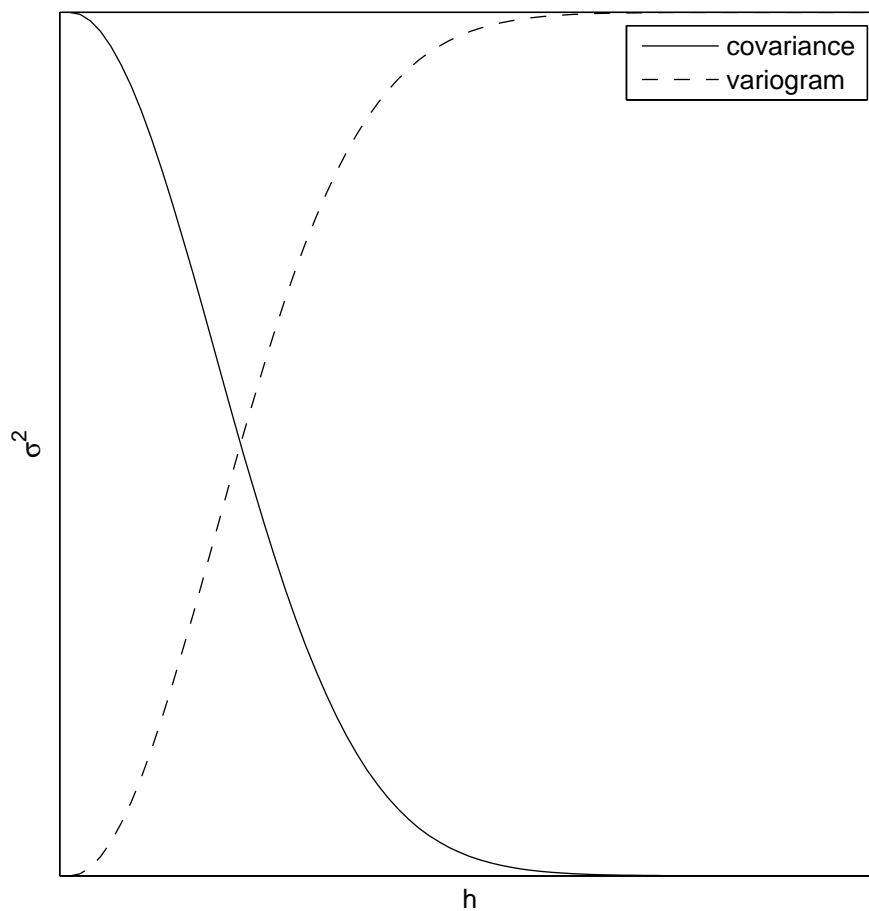


Figure 2.2: One-dimensional illustration of covariance function and semi-variogram of a second-order stationary spatial random variable. σ^2 is the variance and h the separation distance.

2.4 Prior Distribution

The mathematical description of a random variable is its distribution or density function. The common convenient assumption of the distribution is a (multi)Gaussian model. I consider a discretized domain with n discrete values. The expression of $Y(\mathbf{x})$ becomes:

$$\mathbf{Y} = \mathbf{Y}' + \mathbf{X}\boldsymbol{\beta}, \quad (2.40)$$

in which \mathbf{Y} is the $n \times 1$ vector of discrete $Y(\mathbf{x})$ values, n is the number of points where $Y(\mathbf{x})$ is considered, \mathbf{X} is the $n \times n_\beta$ matrix of discretized base functions, $\boldsymbol{\beta}$ is the $n_\beta \times 1$ vector of the trend coefficients, and \mathbf{Y}' is the $n \times 1$ vector of fluctuations of \mathbf{Y} about the trends. The vector \mathbf{Y} can be aggregated when fields of different hydraulic parameters are to be estimated. Then, in (multi)Gaussian models, the fluctuations and the trend coefficients are expressed as:

$$p(\mathbf{Y}'|\boldsymbol{\theta}) \propto \exp\left(-\frac{1}{2}\mathbf{Y}'^T \mathbf{R}_{\mathbf{Y}'\mathbf{Y}'|\boldsymbol{\theta}}^{-1} \mathbf{Y}'\right), \quad (2.41)$$

$$p(\boldsymbol{\beta}) \propto \exp\left(-\frac{1}{2}(\boldsymbol{\beta} - \boldsymbol{\beta}^*)^T \mathbf{R}_{\boldsymbol{\beta}\boldsymbol{\beta}}^{-1}(\boldsymbol{\beta} - \boldsymbol{\beta}^*)\right), \quad (2.42)$$

in which $\mathbf{R}_{\mathbf{Y}'\mathbf{Y}'|\boldsymbol{\theta}}$ is the $n \times n$ discrete covariance matrix given $\boldsymbol{\theta}$, $\boldsymbol{\beta}^*$ is the $n_\beta \times 1$ vector of prior values of the trend coefficients $\boldsymbol{\beta}$, and $\mathbf{R}_{\boldsymbol{\beta}\boldsymbol{\beta}}$ is the $n_\beta \times n_\beta$ prior covariance matrix of $\boldsymbol{\beta}$. $p(\mathbf{Y}'|\boldsymbol{\theta})$ and $p(\boldsymbol{\beta})$ are also known as prior distributions of the hydrogeological parameters before considering any measurements.

By assuming a (multi)Gaussian model, the probability density function is fully characterized by its mean and covariance. [e.g., Kitanidis and Vomvoris, 1983; Gómez-Hernández and Wen, 1998]. Field data have revealed that the probability density functions of hydrogeological parameters are approximately log-normal [Freeze, 1975]. In the latter descriptions, without special notation, \mathbf{Y} refers to log-parameters. (Multi)Gaussian models are practical and widely ap-

plied. However, this does not imply that all hydrogeological parameters show (multi)Gaussian distributions. For example, parameters with channeling structures are non-Gaussian distributed. For such cases, special techniques like multiple point geostatistics [e.g., Strebelle, 2002], have to be applied.

2.5 Structure of Covariance Matrices

In numerical models, the domain is discretized into cells or elements. The second-order stationary hydrogeological parameters become a number n of discrete values. On a regular equispaced grid, the covariance matrix of the parameter field shows symmetric Toeplitz structure. In later sections, I will show that this special structure is linked to a spectral representation. This spectral analysis can be applied to efficiently generate auto-correlated fields given covariance functions [Dietrich and Newsam, 1993] and to accelerate the computation of cross-covariance matrices [Nowak et al., 2003].

A Toeplitz matrix is an $n \times n$ matrix $\mathbf{T}_n = [t_{k,j} \ k, j = 0, 1, \dots, n-1]$ where $t_{k,j} = t_{k-j}$. A symmetric Toeplitz matrix has the form:

$$\mathbf{T}_n = \begin{bmatrix} t_0 & t_1 & \dots & t_{n-1} \\ t_1 & t_0 & \dots & t_{n-2} \\ \vdots & \vdots & \ddots & \vdots \\ t_{n-1} & t_{n-2} & \dots & t_0 \end{bmatrix}, \quad (2.43)$$

in which each descending diagonal from left to right is constant. To construct the $(k+1)$ -th row of the Toeplitz matrix, one shifts the k -th row to the right by one element, and fills the leading empty position with the k -th element of the series $t_1 \dots t_{n-1}$.

Figure 2.3a) is a graphic illustration of the Toeplitz-like covariance matrix for one-dimensional applications, in which the covariance matrix is a simple Toeplitz matrix as shown in Eq. (2.43). The covariance matrix becomes a symmetric level- d block Toeplitz matrix for higher d -dimensional applications, in which

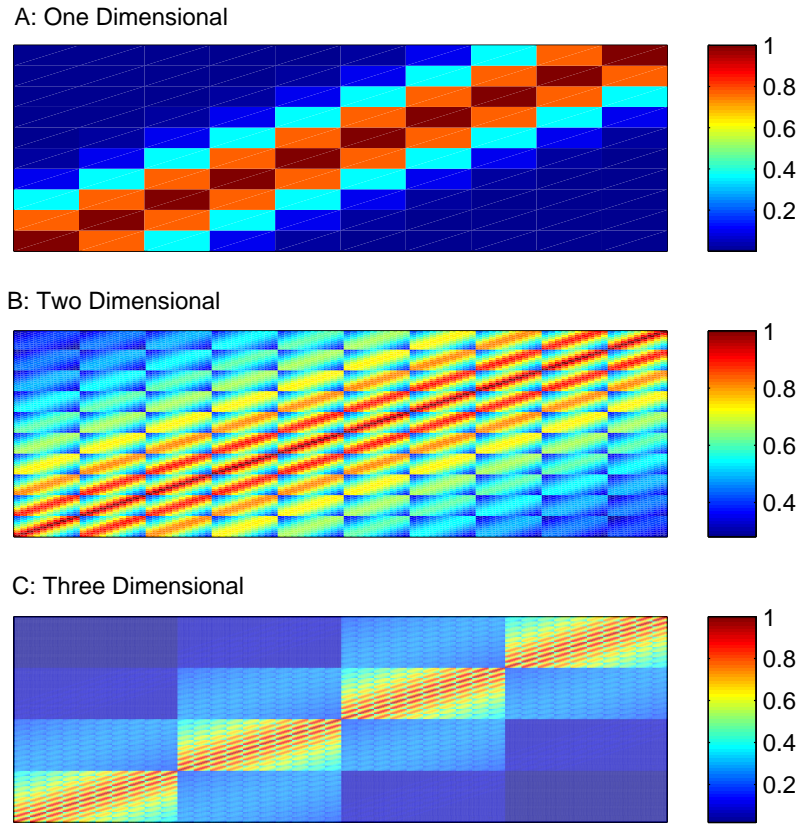


Figure 2.3: Graphic illustration of Toeplitz-like covariance matrices for one-, two- and three-dimensional applications on regular grids. Here, the variance for all cases is unity.

the elements t_i are replaced by \mathbf{T}_i . Figure 2.3b) and 2.3c) show the structures of two- and three-dimensional cases, respectively.

When the covariance function of a random field is periodic, the corresponding covariance matrix becomes circulant. An $n \times n$ circulant matrix has the structure:

$$\mathbf{C} = \begin{bmatrix} c_0 & c_1 & \dots & c_{n-1} \\ c_{n-1} & c_0 & \dots & c_{n-2} \\ \vdots & \vdots & \ddots & \vdots \\ c_1 & c_2 & \dots & c_0 \end{bmatrix}. \quad (2.44)$$

To construct the $k+1$ -th row of the circulant matrix, one shifts the k -th row to the

right by one element, and fills the leading empty position with the last element of the k -th row. In case of a symmetric circulant matrix, c_{n-i} must equal c_i .

2.6 Spectral Methods in Geostatistics

Considering a discrete field of a spatial random variable with n unknowns, the dimension of the auto-covariance matrix of the unknowns is $n \times n$. For a two- or three-dimensional application with a fine resolution, the number of discrete values can easily be up to the order of millions. For a large number of unknowns, storing the covariance matrix and performing matrix operations become computationally prohibitive without supercomputers. However, the special structure of Toeplitz-like matrices can be exploited to reduce the costs of storage and computational effort [e.g., Gray, 1972; Zimmerman, 1998; Barnett, 1990; Dietrich and Newsam, 1993]. This mathematical merit becomes even more convenient if matrices are circulant, because the evaluation of a circulant matrix is directly linked to efficient spectral methods [e.g., Barnett, 1990; Dietrich and Newsam, 1993].

A circulant matrix \mathbf{C} can be decomposed as [e.g., Barnett, 1990, p. 252]:

$$\mathbf{C} = \mathbf{F}^H \mathbf{\Lambda} \mathbf{F}, \quad (2.45)$$

in which \mathbf{F} is the normalized Fourier matrix, \mathbf{F}^H is the Hermitian matrix of \mathbf{F} , and $\mathbf{\Lambda}$ is a diagonal matrix containing eigenvalues of \mathbf{C} . Since a circulant matrix is fully determined by its first column or row, it can be shown that the eigenvalues are defined as the Fourier Transform of the first column of the circulant matrix [e.g., Dietrich and Newsam, 1993], which can be computed by Fast Fourier Transformation(FFT) in $\mathcal{O}(n \log n)$ operations:

$$\boldsymbol{\lambda} = \mathcal{F}(\mathbf{C}_1), \quad (2.46)$$

in which $\boldsymbol{\lambda}$ is an $n \times 1$ vector of eigenvalues, $\mathcal{F}(\cdot)$ stands for the Fourier trans-

form, and C_1 denotes the first column of the circulant matrix C .

It is worth noting that the evaluation of a circulant matrix does not require storing the entire matrix, only the first column or row is needed. This convenient property highly reduces the computational costs in evaluating the relevant matrix operations.

The spectral representation of circulant matrices has become an important tool in generating autocorrelated random spatial fields with known covariance function [Dietrich and Newsam, 1993], and accelerating the computation of cross-covariance matrices [Nowak et al., 2003]. In later sections, I will show that the spectral analysis of covariance functions can help efficiently define a functional parameterization of a spatial random field by the Karhunen-Loève expansion [Loève, 1977; Ghanem and Spanos, 1991]. This parameterization is useful in approximating the spatial random field with a reduced dimension and allows different schemes of discretization.

2.6.1 Generation of Autocorrelated Fields

Autocorrelated fields are realizations of random processes characterized by their mean and covariance functions. Realizations are very useful, for example, to quantify uncertainty of dependent quantifies using Monte Carlo simulations of flow and solute transport problems in groundwater system [e.g., Delhomme, 1979; Dagan, 1982]. In such simulations, a large number of equally likely realizations of the hydrogeological parameters are generated. All realizations share the statistical characterization of spatial variability. The flow and transport equations are numerically solved. The resulting probability distributions of the output variables can be sampled.

When a covariance function is periodic and stationary, Dietrich and Newsam [1993] have shown that realizations of a random field on regular grids can be generated using the Fast Fourier Transformation(FFT):

Algorithm 2.1 Generating realizations via Fast Fourier Transformation

- 1: Define the covariance function C_1 related to a single point in a periodic one- or multi-dimensional domain.
- 2: Compute the (multi-)dimensional FFT of C_1 resulting in \tilde{S} and take element-wise the square root $\sqrt{\tilde{S}}$.
- 3: Generate a d -th order tensor $\mathbf{E} = \mathbf{E}_1 + \mathcal{J}\mathbf{E}_2$ with \mathbf{E}_1 and \mathbf{E}_2 being d -th order tensors of independent real random variable drawn from a Gaussian distribution with mean zero and unit variance. \mathbf{E}_1 and \mathbf{E}_2 have the same dimension with \tilde{S} . \mathcal{J} is the imaginary number.
- 4: Multiply each entry of \mathbf{E} with the corresponding entry of $\sqrt{\tilde{S}}$ yielding a d -th order tensor $\tilde{\mathbf{r}}$.
- 5: Compute the (multi-)dimensional inverse FFT of $\tilde{\mathbf{r}}$ yielding \mathbf{R} .

The real and imaginary part of \mathbf{R} are two independent realizations of the stationary random spatial field with a periodic covariance function. In Algorithm 2.1, d stands for the dimension of the spatial field. That is, in one-dimensional applications, C_1 , \tilde{S} , $\tilde{\mathbf{r}}$, and \mathbf{R} are vectors; in two-dimensional cases, they become matrices, etc.

Under normal circumstances, the covariance matrix is not circulant due to a non-periodic covariance function. For such cases, the embedding and extracting technique can be applied [e.g., Dietrich and Newsam, 1993; Nowak et al., 2003]. Figure 2.4 visualizes the periodic embedding of a spatial variable. The finite domain Ω' is interpreted as a sub-domain of a larger unit cell Ω belonging to an infinite periodic domain. In order to maintain the statistical properties of Ω' in the embedding process, the mean and the covariance function for all separate distances that are observable in Ω' must be identical for Ω . Figure 2.4 shows the random field itself. The corresponding covariance function is symmetric and periodic in all spatial dimensions. Figure 2.5 shows a non-periodic and a periodic covariance function for one-dimensional applications. A periodic covariance function can be obtained in most cases by simply mirroring its corresponding finite covariance function. A detailed graphical description of periodic embedding is given by Dietrich and Newsam [1993] and Nowak et al. [2003].

The generation of realizations is then conducted on the larger periodic domain. With the obtained results, one can extract the entries from the periodic domain to achieve the entries for the finite domain.

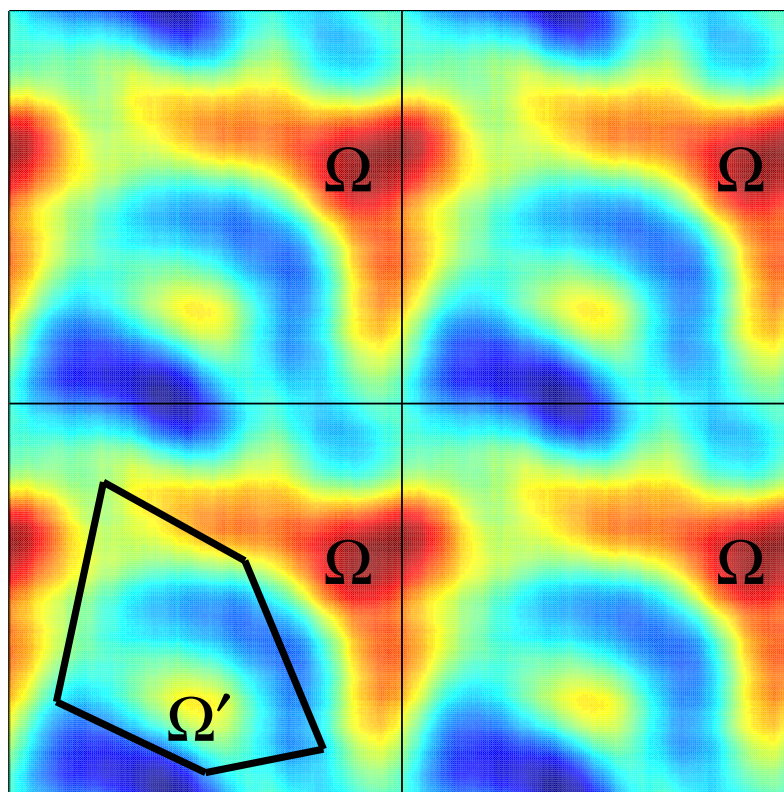


Figure 2.4: Finite domain Ω' embedded in a large unit cell Ω of a periodic domain. Four unit cells are shown to visualize periodicity.

2.6.2 Computation of Cross-Covariance Matrices

The spectral representation of a covariance matrix can also be applied for the computation of cross-covariance matrices [Nowak et al., 2003]. The cross-covariance matrices are required in cokriging-like inverse methods. For large-scale problems, the direct evaluation of these terms is computationally demand-

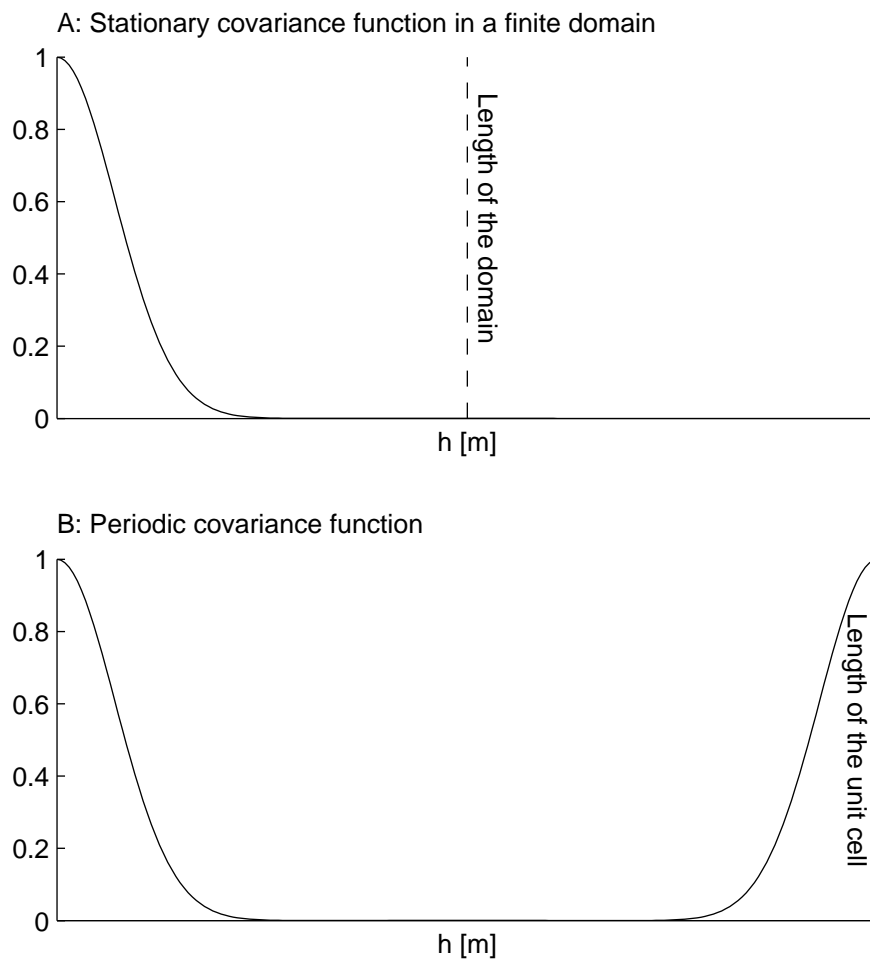


Figure 2.5: Finite and periodic function.

ing. Exploiting the spectral representation of covariance matrices, one can efficiently compute the cross-covariance matrices.

Here, I take the computation of the cross-covariance matrices between hydrogeological parameters $Y(\mathbf{x})$ and hydraulic heads $h(\mathbf{x})$ as an example to illustrate the idea. The cross-covariance of two random variables is commonly defined as:

$$R_{Y'(\mathbf{x}_1)h'(\mathbf{x}_2)} = \mathbb{E} \left[(Y(\mathbf{x}_1) - \bar{Y}(\mathbf{x}_1)) (h(\mathbf{x}_2) - \bar{h}(\mathbf{x}_2)) \right]. \quad (2.47)$$

As approximation, the cross-covariance of dependent variables may be derived from linearization of the functional relationship between the two variables. Tak-

ing second-order stationarity into consideration, one can derive the cross-covariance with the form:

$$\begin{aligned} R_{Y'(\mathbf{x}_1)h'(\mathbf{x}_2)} &= \int R_{Y'(\mathbf{x}_1)Y'(\xi)} \frac{\partial h(\mathbf{x}_2)}{\partial Y(\xi)} d\xi, \\ &= \int R_{Y'Y'}(\mathbf{x}_1 - \xi) \frac{\partial h(\mathbf{x}_2)}{\partial Y(\xi)} d\xi, \end{aligned} \quad (2.48)$$

in which $\frac{\partial h(\mathbf{x}_2)}{\partial Y(\xi)}$ is the sensitivity of the dependent quantity $h(\mathbf{x}_2)$ on $Y(\xi)$. Eq. (2.48) is a convolution type of operation. In the Fourier domain, the convolution becomes a multiplication of the Fourier transforms of the corresponding functions. For some frequently applied models of the covariance function, analytical expressions of their Fourier transformation exist. With the Fourier Transformation of the linearized functional relationship between the heads and the hydrogeological parameters, one can obtain the cross-covariance function by inverse Fourier transformation of the function-multiplication in the Fourier domain.

In a discrete domain with n elements, Eq. (2.48) becomes a matrix-matrix product:

$$\mathbf{R}_{Y'h'} = \mathbf{R}_{Y'Y'} \mathbf{H}^T, \quad (2.49)$$

in which $\mathbf{R}_{Y'h'}$ is the $n \times m$ cross-covariance matrix, $\mathbf{R}_{Y'Y'}$ is the $n \times n$ auto-covariance matrix of Y' , \mathbf{H} is the $m \times n$ sensitivity matrix, and m is the number of dependent states.

According to Dietrich and Newsam [1993] and Nowak et al. [2003], the matrix-vector product of circulant matrix \mathbf{C} with a vector \mathbf{u} can be computed as

$$\begin{aligned} \mathbf{C}\mathbf{u} &= \mathbf{F}^H \mathbf{\Lambda} \mathbf{F}\mathbf{u}, \\ &= \mathcal{F}^{-1} (\mathcal{F}(\mathbf{C}_1) \circ \mathcal{F}(\mathbf{u})), \end{aligned} \quad (2.50)$$

in which \mathcal{F} stands for the Fourier Transform, \mathcal{F}^{-1} is the inverse Fourier Transform, \mathbf{C}_1 is the first column of \mathbf{C} , and \circ denotes element-wise multiplication of two tensors.

When the covariance matrix $\mathbf{R}_{\mathbf{Y}'\mathbf{Y}'}$ is circulant, Eq. (2.50) can directly be applied to the product of $\mathbf{R}_{\mathbf{Y}'\mathbf{Y}'}\mathbf{H}^T$ by considering \mathbf{H} column by column. However, if $\mathbf{R}_{\mathbf{Y}'\mathbf{Y}'}$ is not circulant, one can embed the corresponding covariance function in a bigger periodic domain as illustrated in Section 2.6.1. To make the dimension matching, one has to pad zeros to the columns in \mathbf{H} . The matrix-vector product can be performed on the larger domain. From the obtained result, one extracts the parts corresponding to the original domain [Dietrich and Newsam, 1993; Nowak et al., 2003].

2.6.3 Parameterization of a Spatial Random Field with the Karhunen-Loève Expansion¹

The efficient spectral approach of Nowak et al. [2003] of computing cross-covariance matrices requires the grids to be regular and is no more suitable on unstructured grids as they may result from local refinements. Apparently, computing a full cross-covariance matrix on unstructured grids with a large number of unknowns becomes computationally extremely demanding.

In this section, I exploit a parameterization approximating the parameter field with a reduced dimension. I parameterize the spatial random field by weighted base functions derived from the covariance function. The base functions are eigenfunctions of the covariance function times the square root of the corresponding eigenvalues. This orthonormal representation of auto-correlated random fields with eigenvalues and eigenfunctions is also known as the Karhunen-Loève(KL) expansion [Loève, 1977; Ghanem and Spanos, 1991]. Typically, the series of eigenvalues is sorted in a decreasing order and truncated. In the inversion procedure discussed in Section 2.10, the estimation of the param-

¹The considerations presented in this section have been published in Li et al. [2007].

eter field becomes estimating the weights of the base functions. The cross-covariance matrix between hydrogeological parameters and dependent variables can be approximated by the cross-correlation between the weights of the base functions and the dependent variables. The number of truncated terms is normally much smaller than the number of grid points of the discretized domain. Consequently, the dimension of the cross-covariance matrix between the weights of the base functions and the dependent variables is much smaller than the full cross-covariance matrix without approximation. The approximation by a truncated series of eigenvalues can potentially reduce the computational cost of estimating the parameter field.

The base functions in the parameterization using the KL expansion can be achieved with efficient spectral methods [Li and Cirpka, 2006]. For a periodic covariance function, the eigenvalues are defined by the Fourier transform of the covariance function, and the eigenfunctions are known to be sinusoidal. For a non-periodic covariance function with stationary increment, the embedding and extracting techniques [Dietrich and Newsam, 1993; Nowak et al., 2003] can be implemented (see Section 2.6.1). The reproduction of the covariance functions in continuous trigonometric functions is independent of discretization schemes.

In the following, I briefly illustrate the parameterization using the KL expansion. Considering a discretized form of the continuous random space function $Y'(x)$, I represent $Y'(\mathbf{x})$ as an $n \times 1$ vector \mathbf{Y}' and the covariance function $R_{Y'Y'|\theta}(\mathbf{x}_1, \mathbf{x}_2)$ as an $n \times n$ matrix $\mathbf{R}_{Y'Y'|\theta}$. The expected value of \mathbf{Y}' is a zero vector.

Since the covariance matrix $\mathbf{R}_{Y'Y'}$ is symmetric positive definite, the eigen-decomposition leads to:

$$\mathbf{E}[\mathbf{Y}' \otimes \mathbf{Y}'] = \mathbf{R}_{Y'Y'|\theta} = \mathbf{W}\mathbf{\Lambda}\mathbf{W}^T = \mathbf{W}\mathbf{\Lambda}^{1/2}\mathbf{\Lambda}^{1/2}\mathbf{W}^T, \quad (2.51)$$

in which \mathbf{W} is the $n \times n$ matrix of normalized eigenvectors of $\mathbf{R}_{Y'Y'|\theta}$, $\mathbf{\Lambda}$ is the $n \times n$ diagonal matrix of real nonnegative eigenvalues, and $\mathbf{\Lambda}^{1/2}$ denotes the $n \times n$ diagonal matrix containing the square roots of the eigenvalues. Introducing an $n \times n$ identity matrix \mathbf{I} into the multiplication of matrices does not change

the results. Therefore,

$$\mathbf{E}[\mathbf{Y}' \otimes \mathbf{Y}'] = \mathbf{W}\mathbf{\Lambda}^{1/2}\mathbf{I}\mathbf{\Lambda}^{1/2}\mathbf{W}^T. \quad (2.52)$$

Now I consider an $n \times 1$ vector ζ of uncorrelated standard Gaussian random variables with zero mean and variance of unity:

$$\mathbf{E}[\zeta] = \mathbf{0}, \quad (2.53)$$

$$\mathbf{E}[\zeta \otimes \zeta] = \mathbf{I}, \quad (2.54)$$

$$p(\zeta) \propto \exp\left(-\frac{1}{2}\zeta^T \zeta\right). \quad (2.55)$$

Substituting Eq. (2.54) into Eq. (2.52), I obtain:

$$\mathbf{E}[\mathbf{Y}' \otimes \mathbf{Y}'] = \mathbf{E}\left[(\mathbf{W}\mathbf{\Lambda}^{1/2}\zeta) \otimes (\mathbf{W}\mathbf{\Lambda}^{1/2}\zeta)\right]. \quad (2.56)$$

From the proceeding equation, I can derive:

$$\mathbf{Y}' = \mathbf{W}\mathbf{\Lambda}^{1/2}\zeta, \quad (2.57)$$

in which $\mathbf{W}\mathbf{\Lambda}^{1/2}$ is a deterministic matrix mapping the vector ζ of orthonormal random variables to the vector \mathbf{Y}' of correlated log-conductivity fluctuations

At the limit of an infinitesimally fine resolution, \mathbf{Y}' becomes again the continuous function $Y'(\mathbf{x})$, \mathbf{W} becomes a set of continuous eigenfunctions $w_i(\mathbf{x})$, ζ a set of random variables η_i , and Eq. (2.57) becomes an infinite series:

$$Y'(\mathbf{x}) = \sum_{i=1}^{\infty} \lambda_i^{1/2} w_i(\mathbf{x}) \eta_i. \quad (2.58)$$

The contribution of a particular eigenfunction $w_i(\mathbf{x})$ depends on the size of its eigenvalue λ_i . In the KL expansion, I sort the contributions by λ_i in a descending

order and truncate the series after N terms:

$$Y'(\mathbf{x}) \approx \sum_{i=1}^N \lambda_i^{1/2} w_i(\mathbf{x}) \eta_i = \sum_{i=1}^N f_i(\mathbf{x}) \eta_i, \quad (2.59)$$

with $f_i(\mathbf{x}) = \lambda_i^{1/2} w_i(\mathbf{x})$. N is the total number of dominant eigenvalues. The approximation can potentially reduce the computational effort of estimating $Y'(\mathbf{x})$, because the number N of dominant terms may be much smaller than the typical number n of the elements when $Y'(\mathbf{x})$ is discretized.

In general, eigenvalues and eigenvectors of the covariance function $R_{Y'Y'|\theta}(\mathbf{x}_1, \mathbf{x}_2)$ can be evaluated by solving the Fredholm equation [e.g., Zhang and Lu, 2004]:

$$\int_V R_{Y'Y'|\theta}(\mathbf{x}_1, \mathbf{x}_2) w(\mathbf{x}_1) d\mathbf{x}_1 = \lambda w(\mathbf{x}_2). \quad (2.60)$$

Typically, Eq. (2.60) has to be solved numerically. This algorithm can be computationally demanding because it requires performing a large number of integrations. However, if the random space variable is periodic, the eigenfunctions of the covariance function are known a priori. In the following, $R_p(\mathbf{x})$ denotes the covariance function in a periodic domain. In the two-dimensional case, the eigenfunctions are:

$$\begin{aligned} w_{i,j}^c(\mathbf{x}) &= \begin{cases} \cos \left(\left(\frac{ix_1}{L_1} + \frac{jx_2}{L_2} \right) 2\pi \right) & \text{if } i \neq 0 \text{ or } j \neq 0, \\ 0 & \text{if } i = 0 \text{ and } j = 0, \end{cases} \\ w_{i,j}^s(\mathbf{x}) &= \sin \left(\left(\frac{ix_1}{L_1} + \frac{jx_2}{L_2} \right) 2\pi \right), \end{aligned} \quad (2.61)$$

where $\frac{i}{L_1}, \frac{j}{L_2}$ are the spatial frequencies in the x_1 and x_2 direction, respectively, L_1 and L_2 are the dimensions of the unit cell in each direction, $w_{i,j}^c$ denotes the contributions of cosine-functions and $w_{i,j}^s$ stands for the contribution of sine-functions. Correspondingly, $Y'(\mathbf{x})$ can be expressed as:

$$Y'(x) \approx \sum_{k=1}^{N/2} \lambda_{k \rightarrow i,j} \left(w_{k \rightarrow i,j}(\mathbf{x}) \eta_{k \rightarrow i,j}^c + w_{k \rightarrow i,j}(\mathbf{x}) \eta_{k \rightarrow i,j}^s \right), \quad (2.62)$$

in which the subscript $k \rightarrow i, j$ denotes the index mapping of the k -th dominant eigenvalue to the frequency indices i and j . Thus, $\lambda_{k \rightarrow i,j}$ stands for the k -th dominant eigenvalue, and $w_{k \rightarrow i,j}$ and $\eta_{k \rightarrow i,j}$ are the corresponding eigenfunctions and weights. $\lambda_{i,j}$ is determined from the Fourier series of the periodic covariance function [Dietrich and Newsam, 1993]:

$$\lambda_{i,j} = \begin{cases} 2S_{i,j} & \text{if } j \neq 0, \\ S_{i,j} & \text{if } j = 0. \end{cases} \quad (2.63)$$

with

$$S_{i,j} = \frac{1}{A_p} \int R_p(\mathbf{x}) \exp \left(-2\pi \mathcal{J} \left(\frac{ix_1}{L_1} + \frac{jx_2}{L_2} \right) \right) d\mathbf{x}, \quad (2.64)$$

in which $S_{i,j}$ is the coefficient of the Fourier series of $R_p(\mathbf{x})$ corresponding to indices i and j which range from $-\infty$ to $+\infty$, \mathcal{J} is the imaginary number, and A_p is the area of the unit cell.

$R_p(\mathbf{x})$ is an even symmetric function, which implies that:

$$S_{-i,-j} = S_{i,j}. \quad (2.65)$$

This indicates that there is no need to consider $S_{i,j}$ for negative values of j explicitly. These negative contributions are compensated by the factor of 2 in Eq. (2.63). The proceeding formulations can be easily extended to three dimensions.

In the following, I denote \mathbf{R}_p^{hf} the covariance function of the high frequency terms neglected by the truncation in the KL expansion in a periodic domain. The Fourier coefficients $S_{i,j}$ can be used to compute the covariance matrix \mathbf{R}_p^{hf} :

$$\mathbf{R}_p^{hf} = \sum_{i,j=-\infty}^{+\infty} \delta_{k \leftrightarrow i,j} S_{i,j} \exp \left(2\pi \mathcal{J} \left(\frac{ix_1}{L_1} + \frac{jx_2}{L_2} \right) \right), \quad (2.66)$$

in which $\delta_{k \leftrightarrow i,j}$ is unity when $\lambda_{i,j}$ is not in the set of the N dominant eigenvalues, and zero otherwise.

Random spatial variables which are not periodic can be embedded into periodic ones following the procedure presented in Section 2.6.1 as illustrated in Figure 2.4. In order to compute the eigenvalues, I compute the covariance function for a single point in the embedding domain. The periodic base functions $f_i(x)$ are defined over the entire embedding domain, but I need to evaluate them only in the finite domain Ω' .

The advantage of this approach is twofold. First, the eigenfunctions are analytically defined in the periodic domain; the eigenvalues can efficiently be computed by Fast Fourier Transformation. Second, the approach allows different discretization schemes in the original domain.

2.7 Formulation of the Quasi-Linear Geostatistical Inverse Approach

In this section, I review the major steps of the Quasi-Linear Geostatistical Inverse Approach [Kitanidis, 1995]. This inverse approach applies cokriging-like technique to infer the hydrogeological parameters from measurements. The outcomes of the inverse approach are the most likely estimate of the parameter fields and its corresponding uncertainty.

Here, I assume that the geostatistical parameters are known. Figure 2.6 summarizes the major steps of the inverse approach. In most applications, the geostatistical parameters have to be estimated from measurements as well, which I discuss in the Section 2.9.

The $\ell \times 1$ vector of measurements \mathbf{Z}^m relates to \mathbf{Y} via a function $\mathbf{Z}(\mathbf{Y})$:

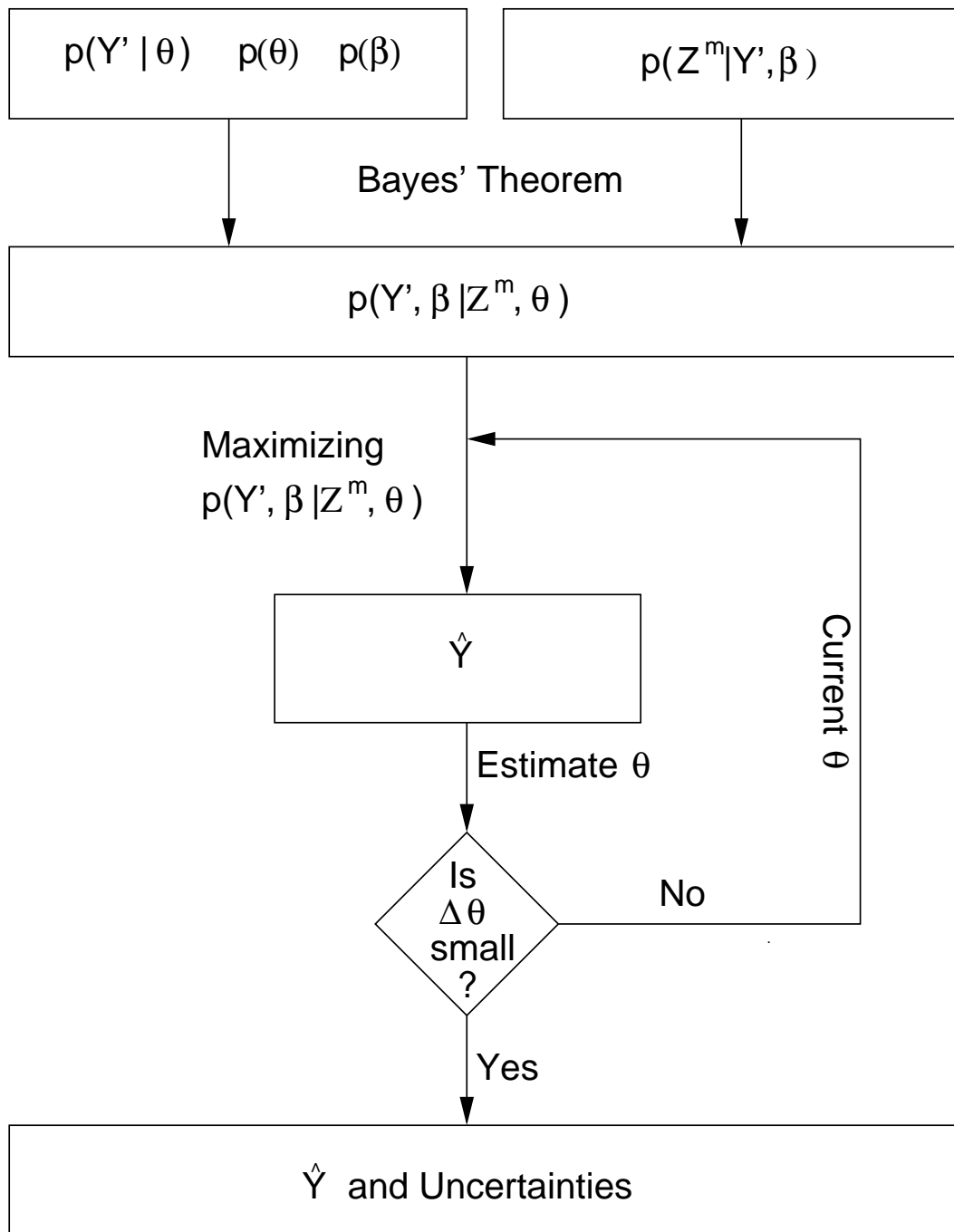


Figure 2.6: Graphic illustration of the procedures in the quasi-linear geostatistical inverse approach of Kitanidis [1995].

$$\mathbf{Z}^m = \mathbf{Z}(\mathbf{Y}) + \mathbf{r}, \quad (2.67)$$

in which ℓ is the number of measurements, and \mathbf{r} is the $\ell \times 1$ vector of measurement errors with zero mean and $\ell \times \ell$ covariance matrix $\mathbf{R}_{\mathbf{ZZ}}$. I consider that the measurements follow a (multi)Gaussian distribution:

$$\begin{aligned} p(\mathbf{Z}^m | \mathbf{Y}) &= p(\mathbf{Z}^m | \mathbf{Y}', \boldsymbol{\beta}) \\ &\propto \exp \left(-\frac{1}{2} (\mathbf{Z}^m - \mathbf{Z}(\mathbf{Y}', \boldsymbol{\beta}))^T \mathbf{R}_{\mathbf{ZZ}}^{-1} (\mathbf{Z}^m - \mathbf{Z}(\mathbf{Y}', \boldsymbol{\beta})) \right), \end{aligned} \quad (2.68)$$

in which $\mathbf{Z}(\cdot)$ is the simulated model output.

Applying Bayes' theorem as discussed in Section 2.2, I obtain the conditional distribution $p(\mathbf{Y}', \boldsymbol{\beta} | \mathbf{Z}^m, \boldsymbol{\theta})$, given the measurements \mathbf{Z}^m and the geostatistical parameters $\boldsymbol{\theta}$:

$$p(\mathbf{Y}', \boldsymbol{\beta} | \mathbf{Z}^m, \boldsymbol{\theta}) = \frac{p(\mathbf{Z}^m | \mathbf{Y}', \boldsymbol{\beta}) p(\mathbf{Y}' | \boldsymbol{\theta}) p(\boldsymbol{\beta})}{p(\mathbf{Z}^m | \boldsymbol{\theta})}, \quad (2.69)$$

in which $p(\mathbf{Z}^m | \boldsymbol{\theta})$ is a scalar constant for a given set of measurements \mathbf{Z}^m that does not depend on \mathbf{Y} . Substituting Eqs. (2.41), (2.42), and (2.68) into Eq. (2.69), I obtain:

$$\begin{aligned} p(\mathbf{Y}', \boldsymbol{\beta} | \mathbf{Z}^m, \boldsymbol{\theta}) \propto \exp \left(-\frac{1}{2} \mathbf{Y}'^T \mathbf{R}_{\mathbf{Y}'\mathbf{Y}'|\boldsymbol{\theta}}^{-1} \mathbf{Y}' - \frac{1}{2} (\boldsymbol{\beta} - \boldsymbol{\beta}^*)^T \mathbf{R}_{\boldsymbol{\beta}\boldsymbol{\beta}}^{-1} (\boldsymbol{\beta} - \boldsymbol{\beta}^*) \right. \\ \left. - \frac{1}{2} (\mathbf{Z}^m - \mathbf{Z}(\mathbf{Y}', \boldsymbol{\beta}))^T \mathbf{R}_{\mathbf{ZZ}}^{-1} (\mathbf{Z}^m - \mathbf{Z}(\mathbf{Y}', \boldsymbol{\beta})) \right). \end{aligned}$$

In the Quasi-Linear Geostatistical Inverse Approach [Kitanidis, 1995], the parameter fields are identified by maximizing the conditional probability density $p(\mathbf{Y}', \boldsymbol{\beta} | \mathbf{Z}^m, \boldsymbol{\theta})$ or minimizing the value of doubled negative logarithm:

$$L(\mathbf{Y}', \boldsymbol{\beta} | \mathbf{Z}^m, \boldsymbol{\theta}) = \mathbf{Y}'^T \mathbf{R}_{\mathbf{Y}'\mathbf{Y}'|\boldsymbol{\theta}}^{-1} \mathbf{Y}' + (\boldsymbol{\beta} - \boldsymbol{\beta}^*)^T \mathbf{R}_{\boldsymbol{\beta}\boldsymbol{\beta}}^{-1} (\boldsymbol{\beta} - \boldsymbol{\beta}^*) + (\mathbf{Z}^m - \mathbf{Z}(\mathbf{Y}', \boldsymbol{\beta}))^T \mathbf{R}_{\mathbf{Z}\mathbf{Z}}^{-1} (\mathbf{Z}^m - \mathbf{Z}(\mathbf{Y}', \boldsymbol{\beta})) + \text{const.}, \quad (2.70)$$

where *const.* includes all terms that do not depend on \mathbf{Y} .

For most applications, the functional relationship $\mathbf{Z}(\mathbf{Y})$ between the measurements \mathbf{Z}^m and the parameter \mathbf{Y} is nonlinear. For such cases, one may apply a successive linearization about the last estimate $\hat{\mathbf{Y}}_k$:

$$\mathbf{Z}^m - \mathbf{Z}(\mathbf{Y}) \approx \mathbf{Z}^m - \mathbf{Z}(\hat{\mathbf{Y}}_k) + \mathbf{H}_k (\mathbf{Y} - \hat{\mathbf{Y}}_k), \quad (2.71)$$

in which k stands for the iteration step and \mathbf{H}_k is the $\ell \times n$ sensitivity matrix of the measurements with respect to the logarithms of hydraulic parameters about the last estimate $\hat{\mathbf{Y}}_k$:

$$\mathbf{H}_k = \left. \frac{\partial \mathbf{Z}}{\partial \mathbf{Y}^T} \right|_{\mathbf{Y}=\hat{\mathbf{Y}}_k}. \quad (2.72)$$

Now I introduce an $\ell \times 1$ vector \mathbf{Z}^0 of "corrected measurements":

$$\mathbf{Z}^0 = \mathbf{Z}^m - \mathbf{Z}(\hat{\mathbf{Y}}_k) + \mathbf{H}_k \hat{\mathbf{Y}}_k. \quad (2.73)$$

Then the objective function of Eq. (2.70) becomes:

$$L(\mathbf{Y}', \boldsymbol{\beta} | \mathbf{Z}^m, \boldsymbol{\theta}) = \mathbf{Y}'^T \mathbf{R}_{\mathbf{Y}'\mathbf{Y}'|\boldsymbol{\theta}}^{-1} \mathbf{Y}' + (\boldsymbol{\beta} - \boldsymbol{\beta}^*)^T \mathbf{R}_{\boldsymbol{\beta}\boldsymbol{\beta}}^{-1} (\boldsymbol{\beta} - \boldsymbol{\beta}^*) + (\mathbf{Z}^0 - \mathbf{H}_k \mathbf{Y}_k)^T \mathbf{R}_{\mathbf{Z}\mathbf{Z}}^{-1} (\mathbf{Z}^0 - \mathbf{H}_k \mathbf{Y}_k) + \text{const.} \quad (2.74)$$

After some reformulation, it can be shown that $\hat{\mathbf{Y}}$, the most likely estimate of \mathbf{Y} , is iteratively identified by solving the following equations until defined criteria of convergence are reached [Kitanidis, 1995] :

$$\hat{\mathbf{Y}}_{k+1} = \mathbf{X}\hat{\boldsymbol{\beta}}_{k+1} + \mathbf{R}_{\mathbf{Y}'\mathbf{Y}'}\mathbf{H}_k^T\hat{\boldsymbol{\xi}}_{k+1}, \quad (2.75)$$

in which $\hat{\boldsymbol{\beta}}_{k+1}$ and $\hat{\boldsymbol{\xi}}_{k+1}$ are computed by:

$$\begin{bmatrix} \mathbf{H}_k\mathbf{R}_{\mathbf{Y}'\mathbf{Y}'}\mathbf{H}_k^T + \mathbf{R}_{\mathbf{Z}\mathbf{Z}} & \mathbf{H}_k\mathbf{X} \\ \mathbf{X}^T\mathbf{H}_k^T & -\mathbf{R}_{\beta\beta}^{-1} \end{bmatrix} \begin{bmatrix} \hat{\boldsymbol{\xi}}_{k+1} \\ \hat{\boldsymbol{\beta}}_{k+1} \end{bmatrix} = \begin{bmatrix} \mathbf{Z}^m - \mathbf{Z}(\mathbf{Y}_k) + \mathbf{H}_k\mathbf{Y}_k \\ -\mathbf{R}_{\beta\beta}^{-1}\boldsymbol{\beta}^* \end{bmatrix}. \quad (2.76)$$

The lower bound of the conditional covariance matrix $\mathbf{R}_{\mathbf{Y}\mathbf{Y}|\mathbf{Z}}$ of the parameter \mathbf{Y} is defined as:

$$\begin{aligned} \mathbf{R}_{\mathbf{Y}\mathbf{Y}|\mathbf{Z}} &\geq \mathbf{R}_{\mathbf{Y}'\mathbf{Y}'} \\ &- \begin{bmatrix} \mathbf{H}\mathbf{R}_{\mathbf{Y}'\mathbf{Y}'} \\ \mathbf{X}^T \end{bmatrix}^T \begin{bmatrix} \mathbf{R}_{\mathbf{Z}\mathbf{Z}} + \mathbf{H}\mathbf{R}_{\mathbf{Y}'\mathbf{Y}'}\mathbf{H}^T & \mathbf{H}\mathbf{X} \\ \mathbf{X}^T\mathbf{H}^T & -\mathbf{R}_{\beta\beta}^{-1} \end{bmatrix}^{-1} \begin{bmatrix} \mathbf{H}\mathbf{R}_{\mathbf{Y}'\mathbf{Y}'} \\ \mathbf{X}^T \end{bmatrix}. \end{aligned} \quad (2.77)$$

Because \mathbf{Z}^0 and \mathbf{H}_k depend on the current estimate, an iterative approach is needed in which \mathbf{Z}^0 and \mathbf{H}_k are updated in each iteration [Kitanidis, 1995]. On regular structured grids, I can accelerate the multiplication of the cross-covariance $\mathbf{H}\mathbf{R}_{\mathbf{Y}'\mathbf{Y}'}\mathbf{H}^T$ using the spectral method of Nowak [2004] as discussed in Section 2.6.2. When the functional relation between the measurements and the hydrogeological parameters is linear, a single estimation step is sufficient and the estimation of the conditional covariance using Eq. (2.77) becomes exact.

2.8 Modified Levenberg-Marquardt Algorithm for the Quasi-Linear Geostatistical Inverse Approach

Since the Quasi-Linear Geostatistical Inverse Approach of Kitanidis [1995] is based on the Gauss-Newton technique [e.g., Press et al., 1992, chapter 9], overshooting of the parameters from one iteration to the next may occur for highly nonlinear cases. I stabilize this approach by the modified Levenberg-Marquardt method of Nowak and Cirpka [2004], which suppresses oscillations by modifying the diagonal entries of the left-hand side matrix in Eq. (2.76). In this modified algorithm, the right hand-side of Eq. (2.76) is split into an innovative and a projecting part:

$$\begin{bmatrix} \mathbf{Z}^m - \mathbf{Z}(\mathbf{Y}_k) + \mathbf{H}_k \mathbf{Y}_k \\ -\mathbf{R}_{\beta\beta}^{-1} \boldsymbol{\beta}^* \end{bmatrix} = \underbrace{\begin{bmatrix} \mathbf{Z}^m - \mathbf{Z}(\mathbf{Y}_k) \\ -\mathbf{R}_{\beta\beta}^{-1} (\boldsymbol{\beta}^* - \hat{\boldsymbol{\beta}}_k) \end{bmatrix}}_{\text{innovative}} + \underbrace{\begin{bmatrix} \mathbf{H}_k \mathbf{Y}_k \\ -\mathbf{R}_{\beta\beta}^{-1} \hat{\boldsymbol{\beta}}_k \end{bmatrix}}_{\text{projecting}}. \quad (2.78)$$

The current estimate of the parameter field is now defined as:

$$\hat{\mathbf{Y}}_{k+1} = \mathbf{X}(\hat{\boldsymbol{\beta}}_{pr} + \hat{\boldsymbol{\beta}}_{in}) + \mathbf{R}_{\mathbf{Y}'\mathbf{Y}'} \mathbf{H}_k^T (\hat{\boldsymbol{\xi}}_{pr} + \hat{\boldsymbol{\xi}}_{in}), \quad (2.79)$$

in which the subindex *pr* stands for the projecting part and *in* is the innovative contribution.

Introducing a Levenberg-Marquardt parameter μ , one computes the values of $\hat{\boldsymbol{\beta}}_{pr}$, $\hat{\boldsymbol{\beta}}_{in}$, $\hat{\boldsymbol{\xi}}_{in}$, and $\hat{\boldsymbol{\xi}}_{pr}$ by:

$$\begin{bmatrix} \mathbf{H}_k \mathbf{R}_{\mathbf{Y}'\mathbf{Y}'|\boldsymbol{\theta}} \mathbf{H}_k^T + \mu \mathbf{R}_{\mathbf{Z}\mathbf{Z}} & \mathbf{H}_k \mathbf{X} \\ \mathbf{X}^T \mathbf{H}_k^T & -(1 + \mu) \mathbf{R}_{\beta\beta}^{-1} \end{bmatrix} \begin{bmatrix} \hat{\boldsymbol{\xi}}_{in} \\ \hat{\boldsymbol{\beta}}_{in} \end{bmatrix} = \begin{bmatrix} \mathbf{Z}^m - \mathbf{Z}(\mathbf{Y}_k) \\ -\mathbf{R}_{\beta\beta}^{-1} (\boldsymbol{\beta}^* - \hat{\boldsymbol{\beta}}_k) \end{bmatrix}$$

$$\begin{bmatrix} \mathbf{H}_k \mathbf{R}_{\mathbf{Y}'\mathbf{Y}'|\boldsymbol{\theta}} \mathbf{H}_k^T - \tau \mathbf{R}_{\mathbf{Z}\mathbf{Z}} & \mathbf{H}_k \mathbf{X} \\ \mathbf{X}^T \mathbf{H}_k^T & -(1 + \mu) \mathbf{R}_{\beta\beta}^{-1} \end{bmatrix} \begin{bmatrix} \hat{\boldsymbol{\xi}}_{pr} \\ \hat{\boldsymbol{\beta}}_{pr} \end{bmatrix} = \begin{bmatrix} \mathbf{H}_k \mathbf{Y}_k \\ -(1 + \mu) \mathbf{R}_{\beta\beta}^{-1} \hat{\boldsymbol{\beta}}_k \end{bmatrix}$$

where $\tau = 1 - (1 + \mu)^{-\gamma}$ and γ is a fine-tune variable.

The modified algorithm is implemented as the following in algorithm 2.2. Define an initial guess $\mathbf{Y}_0 = \mathbf{X}\boldsymbol{\beta}^*$ and an initial value for $\mu > 0$:

Algorithm 2.2 Implementation of the modified Levenberg-Marquardt algorithm

- 1: Compute \mathbf{H}_k unless the change of the parameter fields is negligible.
 - 2: Solve the Eq. (2.79).
 - 3: Compute the value of the objective function (Eq. (2.74)).
 - 4: If the values of Eq. (2.74) does not improve, increase μ and repeat computing Eq. (2.79), and the value of the objective function.
 - 5: Otherwise, decrease the value of μ and continue.
 - 6: Increase k by one and repeat until defined convergence criteria are met.
-

By introducing the projecting and innovative parts, one can separately control these two parts. Through decreasing \mathbf{R}_{ZZ} in the projecting part, deterioration is suppressed ensuring a good reproduction of the simulated measurements in the projecting part; by increasing \mathbf{R}_{ZZ} in innovative part, one can prevent overshooting in this part. Nowak and Cirpka [2004] have shown that the Levenberg-Marquardt parameter μ controls the step size. The innovative part becomes zeros when μ approaches ∞ and the projecting part is identical to the previous estimate. By choosing a proper $\gamma > 0$, the computation can be fine-tuned; for large values of γ , the algorithm becomes more aggressive in suppressing the deterioration of the projecting part.

2.9 Estimation of Geostatistical Parameters

In the previous description of the Quasi-Linear Geostatistical Inverse Approach [Kitanidis, 1995], I have assumed that the geostatistical parameters of the covariance function are known. In many applications, these parameters have to be estimated from measurements as well. The most prominent approaches include variogram-fitting and optimization of the geostatistical parameters [e.g., Kitani-

dis, 1995]. Variogram-fitting requires direct measurements of the hydraulic parameters with different separation distances. In contrast, the optimization technique by Kitanidis [1995], the restricted maximum likelihood method, can utilize both direct measurements and secondary data. This makes the restricted maximum likelihood method more preferable than the variogram-fitting technique, because most data available belong to secondary information.

The restricted maximum likelihood method of Kitanidis [1995] optimizes the set of geostatistical parameters $\boldsymbol{\theta}$ by maximizing the conditional probability density $p(\boldsymbol{\theta}|\mathbf{Z}^m)$ of the geostatistical parameters $\boldsymbol{\theta}$ given measurements \mathbf{Z}^m . In the framework of Bayes' theorem, $p(\boldsymbol{\theta}|\mathbf{Z}^m)$ is given by:

$$p(\boldsymbol{\theta}|\mathbf{Z}^m) = \frac{p(\mathbf{Z}^m|\boldsymbol{\theta})p(\boldsymbol{\theta})}{p(\mathbf{Z}^m)} = \frac{p(\mathbf{Z}^m|\mathbf{Y}', \boldsymbol{\beta})p(\mathbf{Y}'|\boldsymbol{\theta})p(\boldsymbol{\beta})p(\boldsymbol{\theta})}{p(\mathbf{Y}', \boldsymbol{\beta}|\mathbf{Z}^m, \boldsymbol{\theta})p(\mathbf{Z}^m)}, \quad (2.80)$$

in which $p(\mathbf{Z}^m)$ is a scalar, which does not depend on $\boldsymbol{\theta}$.

I assume that the prior probability density function $p(\boldsymbol{\theta})$ of $\boldsymbol{\theta}$ is multi-Gaussian:

$$p(\boldsymbol{\theta}) = \frac{1}{\sqrt{(2\pi)^{n_\theta} \det(\mathbf{R}_{\theta\theta})}} \exp\left(-\frac{1}{2}(\boldsymbol{\theta} - \boldsymbol{\theta}^*)^T \mathbf{R}_{\theta\theta}^{-1}(\boldsymbol{\theta} - \boldsymbol{\theta}^*)\right), \quad (2.81)$$

in which $\boldsymbol{\theta}^*$ is the $n_\theta \times 1$ vector of the prior mean of $\boldsymbol{\theta}$, and $\mathbf{R}_{\theta\theta}$ is the $n_\theta \times n_\theta$ prior covariance matrix. Assuming that linearization about the most likely value of \mathbf{Y} is permissible, it can be shown that $p(\boldsymbol{\theta}|\mathbf{Z}^m)$ is identical to [Kitanidis, 1995]:

$$p(\boldsymbol{\theta}|\mathbf{Z}^m) = \sqrt{\frac{\det(\boldsymbol{\Xi})}{\det(\mathbf{R}_{\theta\theta})}} \cdot \exp\left(-\frac{1}{2}(\mathbf{Z}^0 - \mathbf{H}\mathbf{X}\boldsymbol{\beta}^*)^T \boldsymbol{\Xi}(\mathbf{Z}^0 - \mathbf{H}\mathbf{X}\boldsymbol{\beta}^*) - \frac{1}{2}(\boldsymbol{\theta} - \boldsymbol{\theta}^*)^T \mathbf{R}_{\theta\theta}^{-1}(\boldsymbol{\theta} - \boldsymbol{\theta}^*)\right), \quad (2.82)$$

where $\boldsymbol{\Xi}$ is defined as:

$$\begin{aligned} \Xi &= (\Sigma + \mathbf{H}\mathbf{X}\mathbf{R}_{\beta\beta}\mathbf{X}^T\mathbf{H}^T)^{-1} = \\ \Sigma^{-1} - \Sigma^{-1}\mathbf{H}\mathbf{X}(\mathbf{R}_{\beta\beta}^{-1} + \mathbf{X}^T\mathbf{H}^T\Sigma^{-1}\mathbf{H}\mathbf{X})^{-1}\mathbf{X}^T\mathbf{H}^T\Sigma^{-1}, \end{aligned} \quad (2.83)$$

with

$$\Sigma = \mathbf{R}_{ZZ} + \mathbf{H}\mathbf{R}_{Y'Y'|\theta}\mathbf{H}^T. \quad (2.84)$$

The optimal set of $\boldsymbol{\theta}$ maximizes $p(\boldsymbol{\theta}|\mathbf{Z}^m)$ or minimizes the value of its doubled negative logarithm $L(\boldsymbol{\theta}|\mathbf{Z}^m)$:

$$\begin{aligned} L(\boldsymbol{\theta}|\mathbf{Z}^m) &= -\ln(\det(\Xi)) + (\mathbf{Z}^0 - \mathbf{H}\mathbf{X}\boldsymbol{\beta}^*)^T\Xi(\mathbf{Z}^0 - \mathbf{H}\mathbf{X}\boldsymbol{\beta}^*) \\ &\quad + (\boldsymbol{\theta} - \boldsymbol{\theta}^*)^T\mathbf{R}_{\theta\theta}^{-1}(\boldsymbol{\theta} - \boldsymbol{\theta}^*) + \text{const.}, \end{aligned} \quad (2.85)$$

where all terms that do not depend on $\boldsymbol{\theta}$ are included in the constant. In case of diffuse prior knowledge about $\boldsymbol{\theta}$, the third term in Eq. (2.85) disappears. Finally, the conditional covariance matrix of $\boldsymbol{\theta}$ is approximated by:

$$\mathbf{R}_{\theta\theta|\mathbf{Z}} \approx \left(\mathbf{E} \left[\frac{\partial^2 L(\boldsymbol{\theta}|\mathbf{Z}^m)}{\partial \boldsymbol{\theta} \otimes \partial \boldsymbol{\theta}} \right] \right)^{-1}, \quad (2.86)$$

which is determined at the most likely value.

Because of the underlying non-linearity of the functional relation between the measurements and hydrogeological parameters, the estimate of geostatistical parameters depends on the estimate of the hydrogeological parameters. Thus, an iterative procedure is needed in which the hydrogeological parameters and the geostatistical parameters are estimated in an alternating manner [Kitanidis, 1995]. Figure 1.1 illustrates the alternating procedure of parameter estimation. Since conditional realizations are not needed, the restricted maximum likelihood method is computationally efficient, which makes this approach attractive. However, due to linearization and ignorance of high-order terms, this approach

works well only for cases with a small variance, and it may produce biased results when the variance is high.

2.10 Inference with Karhunen-Loève Expansion

The procedure outlined in this section has been published in Li and Cirpka [2006].

In the simulation of field applications, it may become necessary to use an irregular geometry of the domain or to refine the grid in areas of particular interest. For such cases, the efficient spectral method for computing cross-covariance matrices [Nowak et al., 2003] will fail. In Section 2.6.3, I have shown the parameterization of a spatial random field by the Karhunen-Loève (KL) expansion [Loève, 1977], which uses a reduced dimension and can be discretized by any fashion. In the following, I integrate the parameterization with the KL expansion into the Quasi-Linear Geostatistical Inverse Approach [Kitanidis, 1995], making the inverse approach also applicable to unstructured grids with a large number of unknowns.

In the framework of the KL expansion [Loève, 1977], the fluctuations $Y'(\mathbf{x})$ can be approximated as (see Section 2.6.3):

$$Y'(\mathbf{x}) = \sum_{i=1}^N f_i(\mathbf{x})\eta_i, \quad (2.87)$$

where $f_i(\mathbf{x})$ is the i -th continuous base function, N is the total dominant number of eigenvalues, and η_i is a weight drawn from a standard normal distribution. The weights η_i of all contributions are uncorrelated.

In a discretized domain with n values \mathbf{Y}' , the KL approximation of \mathbf{Y}' is:

$$\mathbf{Y}' = \mathbf{F}\boldsymbol{\zeta} + \mathbf{Y}'_{hf} \approx \mathbf{F}\boldsymbol{\zeta}, \quad (2.88)$$

in which \mathbf{F} is the $n \times N$ matrix of the selected discretized base functions $f_i(\mathbf{x})$, $\boldsymbol{\zeta}$ is the $N \times 1$ random vector of the truncated contributions η_i , and \mathbf{Y}'_{hf} is the $n \times 1$ vector of high frequency terms that have been neglected by the truncation of the KL expansion. The distribution of \mathbf{Y}'_{hf} is Gaussian with zero mean and covariance $\mathbf{R}_{\mathbf{Y}'_{hf}|\boldsymbol{\theta}}^{hf}$:

$$\mathbb{E}[\mathbf{Y}'_{hf}(\mathbf{x})] = \mathbf{0}, \quad (2.89)$$

$$\mathbb{E}[\mathbf{Y}'_{hf}(\mathbf{x} + \mathbf{h})\mathbf{Y}'_{hf}(\mathbf{x})] = \mathbf{R}_{\mathbf{Y}'_{hf}|\boldsymbol{\theta}}^{hf}(\mathbf{h}). \quad (2.90)$$

The distribution of $\boldsymbol{\zeta}$ is Gaussian with zero mean and identity covariance matrix:

$$p(\boldsymbol{\zeta}) \propto \exp\left(-\frac{1}{2}\boldsymbol{\zeta}^T\boldsymbol{\zeta}\right). \quad (2.91)$$

Correspondingly, \mathbf{Y} , the discretized form of $Y(\mathbf{x})$, is approximated by the following sum of matrix-vector products involving the trend parameters $\boldsymbol{\beta}$ and the random parameter vector $\boldsymbol{\zeta}$:

$$\mathbf{Y} \approx \mathbf{X}\boldsymbol{\beta} + \mathbf{F}\boldsymbol{\zeta}. \quad (2.92)$$

I can rewrite Eq. (2.92) in a more condensed form:

$$\mathbf{Y} \approx \mathbf{X}_e\mathbf{b}, \quad (2.93)$$

with

$$\mathbf{X}_e = \begin{bmatrix} \mathbf{X} & \mathbf{F} \end{bmatrix}, \quad (2.94)$$

$$\mathbf{b} = \begin{bmatrix} \boldsymbol{\beta} \\ \boldsymbol{\zeta} \end{bmatrix}. \quad (2.95)$$

As β and ζ are uncorrelated parameters, the covariance matrix of \mathbf{b} becomes:

$$\mathbf{R}_{\mathbf{bb}} = \begin{bmatrix} \mathbf{R}_{\beta\beta} & \mathbf{0} \\ \mathbf{0} & \mathbf{I} \end{bmatrix}, \quad (2.96)$$

where \mathbf{I} is an $N \times N$ identity matrix. The inverse of $\mathbf{R}_{\mathbf{bb}}$ is:

$$\mathbf{R}_{\mathbf{bb}}^{-1} = \begin{bmatrix} \mathbf{R}_{\beta\beta}^{-1} & \mathbf{0} \\ \mathbf{0} & \mathbf{I} \end{bmatrix}. \quad (2.97)$$

In the limiting case that the prior knowledge about the trend coefficients β is diffuse, $\mathbf{R}_{\beta\beta}^{-1}$ is a zero matrix. The $n \times (n_\beta + N)$ matrix \mathbf{X}_e can be interpreted as extended set of discretized base functions for which prior knowledge about the coefficients exists.

Now the measurements \mathbf{Z}^m relates to \mathbf{Y} via a function $\mathbf{Z}(\mathbf{b})$:

$$\mathbf{Z}^m = \mathbf{Z}(\mathbf{b}) + \mathbf{r}. \quad (2.98)$$

The conditional distribution $p(\mathbf{Y}', \beta | \mathbf{Z}^m, \boldsymbol{\theta})$ of the parameters \mathbf{Y} , given the measurements \mathbf{Z}^m and geostatistical parameters $\boldsymbol{\theta}$, can be expressed by the conditional distribution of $p(\mathbf{b} | \mathbf{Z}^m, \boldsymbol{\theta})$ of the parameters \mathbf{b} . I consider that the prior distribution of the parameter vector \mathbf{b} is multi-Gaussian:

$$p(\mathbf{b} | \boldsymbol{\theta}) = \frac{1}{\sqrt{(2\pi)^{n_\beta + N} \det(\mathbf{R}_{\mathbf{bb}})}} \exp\left(-\frac{1}{2}(\mathbf{b} - \mathbf{b}^*)^T \mathbf{R}_{\mathbf{bb}}^{-1}(\mathbf{b} - \mathbf{b}^*)\right), \quad (2.99)$$

Applying Bayes' theorem, I obtain the posterior distribution of \mathbf{b} by:

$$p(\mathbf{b}|\mathbf{Z}^m, \boldsymbol{\theta}) = \frac{1}{\sqrt{(2\pi)^{\ell+n_\beta+N} \det(\mathbf{R}_{\mathbf{ZZ}}) \det(\mathbf{R}_{\mathbf{bb}})}} \cdot \exp\left(-\frac{1}{2}(\mathbf{Z}^m - \mathbf{Z}(\mathbf{b}))^T \mathbf{R}_{\mathbf{ZZ}}^{-1}(\mathbf{Z}^m - \mathbf{Z}(\mathbf{b})) - \frac{1}{2}(\mathbf{b} - \mathbf{b}^*)^T \mathbf{R}_{\mathbf{bb}}^{-1}(\mathbf{b} - \mathbf{b}^*)\right).$$

The expression in the exponential leads to the negative doubled conditional log-probability density function $L(\mathbf{b}|\mathbf{Z}^m, \boldsymbol{\theta})$ of the parameters given the measurements:

$$L(\mathbf{b}|\mathbf{Z}^m, \boldsymbol{\theta}) = (\mathbf{Z}^m - \mathbf{Z}(\mathbf{b}))^T \mathbf{R}_{\mathbf{ZZ}}^{-1}(\mathbf{Z}^m - \mathbf{Z}(\mathbf{b})) + (\mathbf{b} - \mathbf{b}^*)^T \mathbf{R}_{\mathbf{bb}}^{-1}(\mathbf{b} - \mathbf{b}^*) + \text{const.} \quad (2.100)$$

The best estimate of \mathbf{b} is the most likely value, which minimizes $L(\mathbf{b}|\mathbf{Z}^m, \boldsymbol{\theta})$.

Finding the minimum of $L(\mathbf{b}|\mathbf{Z}^m, \boldsymbol{\theta})$ essentially is a quadratic optimization problem, affected by the non-linearity of $\mathbf{Z}(\mathbf{b})$, for which several solution strategies exist. The most prominent ones in the current context are the conjugate gradient method [Hestenes and Stiefel, 1952] and the Gauss-Newton method [e.g., Press et al., 1992, chapter 9], both with several modifications. Here I apply the Gauss-Newton method, because it provides not only the best estimate, but also an approximation of the conditional covariance matrix. The Gauss-Newton method is based on successive linearization about the last estimate $\hat{\mathbf{b}}_k$:

$$\mathbf{Z}(\mathbf{b}) \approx \mathbf{Z}(\hat{\mathbf{b}}_k) + \mathbf{J}_k(\mathbf{b} - \hat{\mathbf{b}}_k), \quad (2.101)$$

in which \mathbf{J}_k is the Jacobian matrix derived about the last estimate $\hat{\mathbf{b}}_k$:

$$\mathbf{J}_k = \left. \frac{\partial \mathbf{Z}}{\partial \mathbf{b}^T} \right|_{\mathbf{b}=\hat{\mathbf{b}}_k}. \quad (2.102)$$

The Jacobian matrix \mathbf{J} can be approximated by:

$$\mathbf{J}_k = \frac{\partial \mathbf{Z}}{\partial \mathbf{b}^T} \approx \frac{\partial \mathbf{Z}}{\partial \mathbf{Y}^T} \frac{\partial \mathbf{Y}}{\partial \mathbf{b}^T} = \mathbf{H} \mathbf{X}_e, \quad (2.103)$$

in which $\partial \mathbf{Z} / \partial \mathbf{Y}^T$ is the sensitivity matrix \mathbf{H} of model outcomes at measurement locations with respect to log-conductivity. The matrix \mathbf{H} can efficiently be computed via the adjoint-state method [Sun and Yeh, 1990].

The residual $\mathbf{Z}^m - \mathbf{Z}(\mathbf{b})$ becomes:

$$\begin{aligned} \mathbf{Z}^m - \mathbf{Z}(\mathbf{b}) &\approx \mathbf{Z}^m - \mathbf{Z}(\hat{\mathbf{b}}_k) + \mathbf{J}_k \hat{\mathbf{b}}_k - \mathbf{J}_k \mathbf{b}, \\ &= \mathbf{Z}^0 - \mathbf{J}_k \mathbf{b}, \end{aligned} \quad (2.104)$$

with the modified measurement vector \mathbf{Z}^0 :

$$\mathbf{Z}^0 = \mathbf{Z}^m - \mathbf{Z}(\hat{\mathbf{b}}_k) + \mathbf{J}_k \hat{\mathbf{b}}_k. \quad (2.105)$$

Then, the corresponding objective function of Eq. (2.100) becomes:

$$\begin{aligned} L(\mathbf{b} | \mathbf{Z}^m, \boldsymbol{\theta}) &= (\mathbf{Z}^0 - \mathbf{J}_k \mathbf{b})^T \mathbf{R}_{\mathbf{ZZ}}^{-1} (\mathbf{Z}^0 - \mathbf{J}_k \mathbf{b}) \\ &\quad + (\mathbf{b} - \mathbf{b}^*)^T \mathbf{R}_{\mathbf{bb}}^{-1} (\mathbf{b} - \mathbf{b}^*) + \text{const.} \end{aligned} \quad (2.106)$$

The minimum of $L(\mathbf{b} | \mathbf{Z}^m, \boldsymbol{\theta})$ is found by setting the partial derivatives of the proceeding objective function with respect to the unknown parameters to a zero vector:

$$\frac{\partial L(\mathbf{b} | \mathbf{Z}^m, \boldsymbol{\theta})}{\partial \mathbf{b}} = \mathbf{J}_k^T \mathbf{R}_{\mathbf{ZZ}}^{-1} (\mathbf{Z}^0 - \mathbf{J}_k \mathbf{b}) - \mathbf{R}_{\mathbf{bb}}^{-1} (\mathbf{b} - \mathbf{b}^*) = \mathbf{0}, \quad (2.107)$$

which leads to an iterative procedure. Based on the k -th iteration, I compute the Jacobian matrix \mathbf{J}_k and the modified measurement vector \mathbf{Z}_k^0 . Then \mathbf{b} is updated by solving:

$$(\mathbf{J}_k^T \mathbf{R}_{ZZ}^{-1} \mathbf{J}_k + \mathbf{R}_{bb}^{-1}) \hat{\mathbf{b}}_{k+1} = \mathbf{J}_k^T \mathbf{R}_{ZZ}^{-1} \mathbf{Z}_k^0 + \mathbf{R}_{bb}^{-1} \mathbf{b}^*. \quad (2.108)$$

I repeat the procedure until a convergence criterion is met.

With the final estimate of the extended set of trend coefficients $\hat{\mathbf{b}}$, I can obtain the most likely estimate $\hat{\mathbf{Y}}$ of the original parameter field:

$$\hat{\mathbf{Y}} = \mathbf{X}_e \hat{\mathbf{b}}. \quad (2.109)$$

A lower bound of the conditional covariance matrix is given by:

$$\mathbf{R}_{\mathbf{Y}\mathbf{Y}|\mathbf{Z}} \geq \mathbf{X}_e \mathbf{R}_{bb|\mathbf{Z}} \mathbf{X}_e^T + \mathbf{R}_{\mathbf{Y}'\mathbf{Y}'}^{hf}, \quad (2.110)$$

in which $\mathbf{R}_{bb|\mathbf{Z}}$ is the $(p + N) \times (p + N)$ conditional covariance matrix of the estimated parameters \mathbf{b} :

$$\mathbf{R}_{bb|\mathbf{Z}} = (\mathbf{J}_k^T \mathbf{R}_{ZZ}^{-1} \mathbf{J}_k + \mathbf{R}_{bb}^{-1})^{-1}. \quad (2.111)$$

The Gauss-Newton method performs best when the functional relation between the unknown parameters and dependent quantities is almost linear. In the limit of a linear system, the optimum is found by a single iteration. In highly non-linear cases, the Gauss-Newton method may converge only when the initial estimate is very close to the optimal set of parameters. To stabilize the method, I can apply the Levenberg-Marquardt method [Levenberg, 1944; Marquardt, 1963; Carrera and Neuman, 1986a;b;c; Nowak and Cirpka, 2004], which suppresses oscillations by amplifying the diagonal entries of the left-hand side matrix in Eq. (2.108).

Here, I have summarized only the procedure of integrating the KL expansion into the Quasi-Linear Geostatistical Inverse Approach [Kitanidis, 1995]. Similarly, the corresponding estimation of geostatistical parameters can also be performed in the framework of the KL expansion. Since the formulations are very close to the one I demonstrated in Section 2.9. I do not repeat the procedure.

For detailed steps, see Li and Cirpka [2006].

2.11 Evaluation of Sensitivities

In the quasi-linear geostatistical approach of inverse modeling, I repeatedly need to evaluate the sensitivity matrix \mathbf{H} , i.e., the matrix of partial derivatives of all measured quantities with respect to all parameters. A multi-dimensional domain may be discretized into $\mathcal{O}(n) \approx 10^4 - 10^6$ elements. Thus, the computational effort of direct numerical differentiation would be prohibitive. A more efficient approach of computing sensitivities is the continuous adjoint-state method, derived by Sun and Yeh [1990].

Analyzing pumping tests is one of my focuses. For illustrating the major steps of the adjoint-state method [Sun and Yeh, 1990], I take a two-dimensional case of estimating transmissivity $T(\mathbf{x})$ and storativity $S(\mathbf{x})$ given measurements of zeroth and first temporal moments of drawdown, $m_0(s_\delta(\mathbf{x}))$ and $m_1(s_\delta(\mathbf{x}))$ as an example. The procedure in three-dimensional applications is identical to the following two-dimensional one. However, the corresponding hydrogeological parameters become hydraulic conductivities K and specific storage coefficients S_0 .

I consider a particular step in the iteration procedure with the current estimates of $\hat{T}(\mathbf{x})$ and $\hat{S}(\mathbf{x})$. First, I solve for the current estimates of the zeroth and the first temporal moments, $\hat{m}_0(s_\delta(\mathbf{x}))$ and $\hat{m}_1(s_\delta(\mathbf{x}))$. Subsequently, I solve for a set of adjoint-state equations for each measurement. In the following, \mathbf{x}_ℓ denotes the measurement location, $k \in [0, 1]$ is the index for the type of measurement, whereas ψ_1 and ψ_0 are the adjoint states of the first and zeroth moment, meeting the adjoint-state equations:

$$-\nabla \cdot (\hat{T} \nabla \psi_1) = \delta_{k1} \delta(\mathbf{x} - \mathbf{x}_\ell), \quad (2.112)$$

$$-\nabla \cdot (\hat{T} \nabla \psi_0) = \delta_{k0} \delta(\mathbf{x} - \mathbf{x}_\ell) + \hat{S} \psi_1, \quad (2.113)$$

subject to the boundary conditions:

$$\psi_i = 0 \text{ on } \Gamma_{Diri}, \quad (2.114)$$

$$\mathbf{n} \cdot \nabla \psi_i = 0 \text{ on } \Gamma_{Neu}, \quad (2.115)$$

for both $i = 0$ and $i = 1$.

Subsequently, the sensitivity densities of the k -th moment measured at \mathbf{x}_ℓ with respect to the log-transmissivity $\ln T(\mathbf{x})$ and log-storativity $\ln S(\mathbf{x})$ at location \mathbf{x} are computed by:

$$\frac{\partial m_k(\mathbf{x}_\ell)}{\partial \ln T(\mathbf{x})} = -\nabla \psi_0(\mathbf{x}) \cdot (\hat{T}(\mathbf{x}) \nabla \hat{m}_0(\mathbf{x})) - \nabla \psi_1(\mathbf{x}) \cdot (\hat{T}(\mathbf{x}) \nabla \hat{m}_1(\mathbf{x})), \quad (2.116)$$

$$\frac{\partial m_1(\mathbf{x}_\ell)}{\partial \ln S(\mathbf{x})} = \psi_1(\mathbf{x}) \hat{S}(\mathbf{x}) \hat{m}_0(\mathbf{x}). \quad (2.117)$$

Figure 2.7 shows some typical patterns of the sensitivity of zeroth and first temporal moments.

Since I consider the parameters to be uniform within elements, the sensitivity densities in Eqs. (2.116 & 2.117) need to be integrated over the volume of the respective element. In summary, I arrive at the following procedure for the computation of sensitivities in algorithm 2.3:

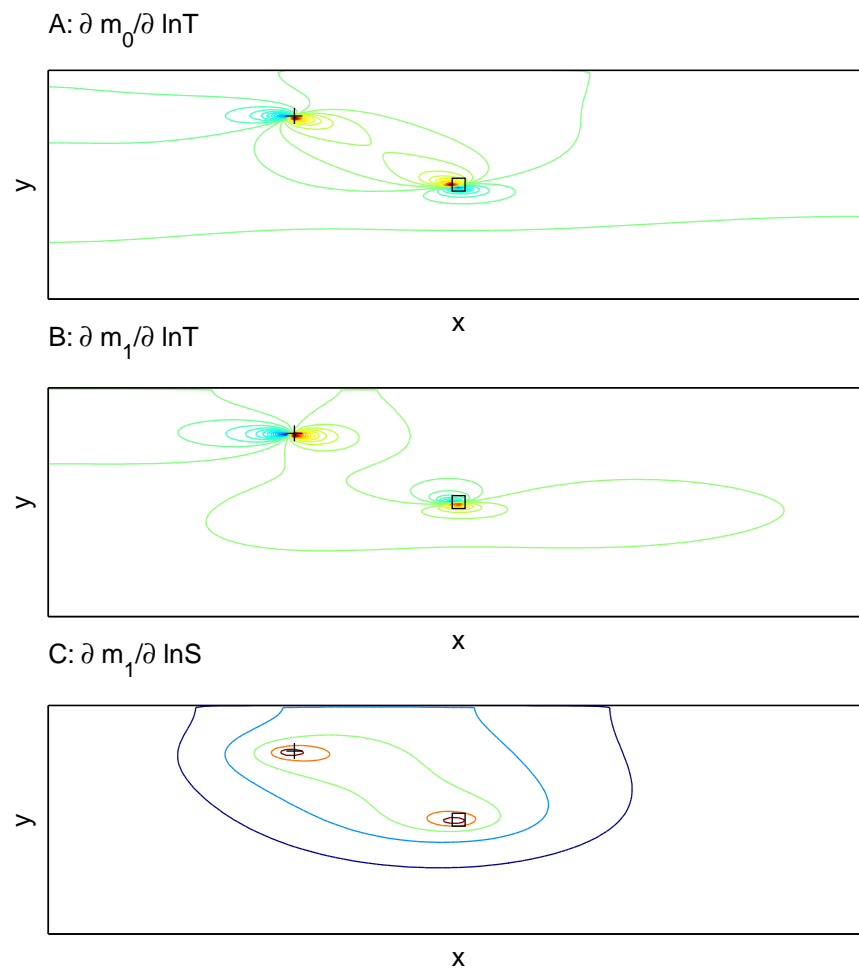


Figure 2.7: Graphic illustration of sensitivities of zeroth and first temporal moment of drawdown with respect to hydrogeological parameters. a) is the sensitivity of zeroth temporal moment with respect to log-transmissivity; b) the sensitivity of first temporal moment with respect to log-transmissivity; c) the sensitivity of first temporal moment with respect to log-storativity. The black square indicates the pumping location and the cross is the location of one monitoring well.

Algorithm 2.3 Computation of sensitivities using adjoint-state method

- 1: In case of a measurement of the zeroth temporal moment or steady-state drawdown, ψ_1 is zero throughout the domain. A single adjoint *pde* of ψ_0 , Eq. (2.113), needs to be solved. This equation is identical to a steady-state groundwater flow equation with a point-like extraction at the observation point. A measurement of $m_0(s_\delta(\mathbf{x}))$ is insensitive to storativity, whereas its sensitivity with respect to log-transmissivity can be computed for each element by integrating Eq. (2.116) over the element.
 - 2: In case of a measurement of the first temporal moment, both adjoint-state variables, ψ_1 and ψ_0 , must be computed. First, one solves for ψ_1 by Eq. (2.112), which is a steady-state groundwater flow equation with a point-like extraction at the observation point. Subsequently, one solves for ψ_0 by Eq. (2.113). This is a steady-state groundwater flow equation with a distributed source term. The sensitivities with respect to log-transmissivity and log-storativity can be computed for each element by integrating Eqs. (2.116 & 2.117) over the element.
-

Chapter 3

Performance Tests of Inference with Karhunen-Loève Expansion

In Section 2.6.3 of Chapter 2, I have shown that the parameterization by the Karhunen-Loève(KL) expansion [Loève, 1977; Ghanem and Spanos, 1991] uses a reduced dimension and has the potential to make the parameter estimation efficient. Since the parameterization does not distinguish grids, both structured and unstructured grids can be applied. In section 2.10, I have integrated the parameterization of a random spatial field with the KL expansion into the Quasi-Linear Geostatistical Inverse Approach [Kitanidis, 1995].

In this chapter, I test the performance of the Quasi-Linear Geostatistical Inverse Approach with the KL expansion¹. I perform several case studies using synthetic data. Here, the hydraulic conductivity is estimated in a two-dimensional unconfined aquifer. I choose an irregular domain with known recharge as the study site.

First, I implement the inverse approach on a regular grid. Computational efforts, estimates and the corresponding estimation variances are compared between the

¹This work has been published by Li and Cirpka [2006]

inverse method using the KL expansion and that relying on the full prior covariance matrix. Subsequently, I apply the inverse method with the KL expansion to a domain discretized by an unstructured grid. The difference of the estimations on structured and unstructured grids are compared.

3.1 Field Setup

As indicated by Figure 3.1, the domain has a polygonal, non-rectangular shape. Table 3.1 lists all parameters of the test cases. Fixed-head boundary conditions are assumed on the bottom of the field, whereas no-flow conditions are attributed to all other sides of the polygon.

I generate fields of log-conductivity $Y = \ln(K)$ and log-recharge $Z = \ln(W)$ using the spectral method by Dietrich and Newsam [1993]) as described in Section 2.6.1. I use the isotropic non-separable exponential covariance function for the fluctuations of both $\ln(K)$ and $\ln(W)$, together with a uniform, but uncertain mean. The values of the geostatistical parameters are given in Table 3.1. Here, β_Y^* and β_Z^* are the uncertain prior mean values for $\ln(K)$ and $\ln(W)$, respectively, whereas $\sigma_{\beta_Y}^2$ and $\sigma_{\beta_Z}^2$ quantify the uncertainties of β_Y and β_Z . The terms σ_Y^2 and σ_Z^2 stand for the variances of the $\ln(K)$ and $\ln(W)$ fluctuations about their mean values. λ refers to the correlation length. For the topography of the aquifer bottom, I use a parabolic function with its minimum around the center of the domain.

Figures 3.2a, 3.2b, and 3.2f show the fields of the generated hydrogeological parameters and the bottom topography, respectively. The locations of 15 measurement points are marked by stars. The pumping well is indicated by a square.

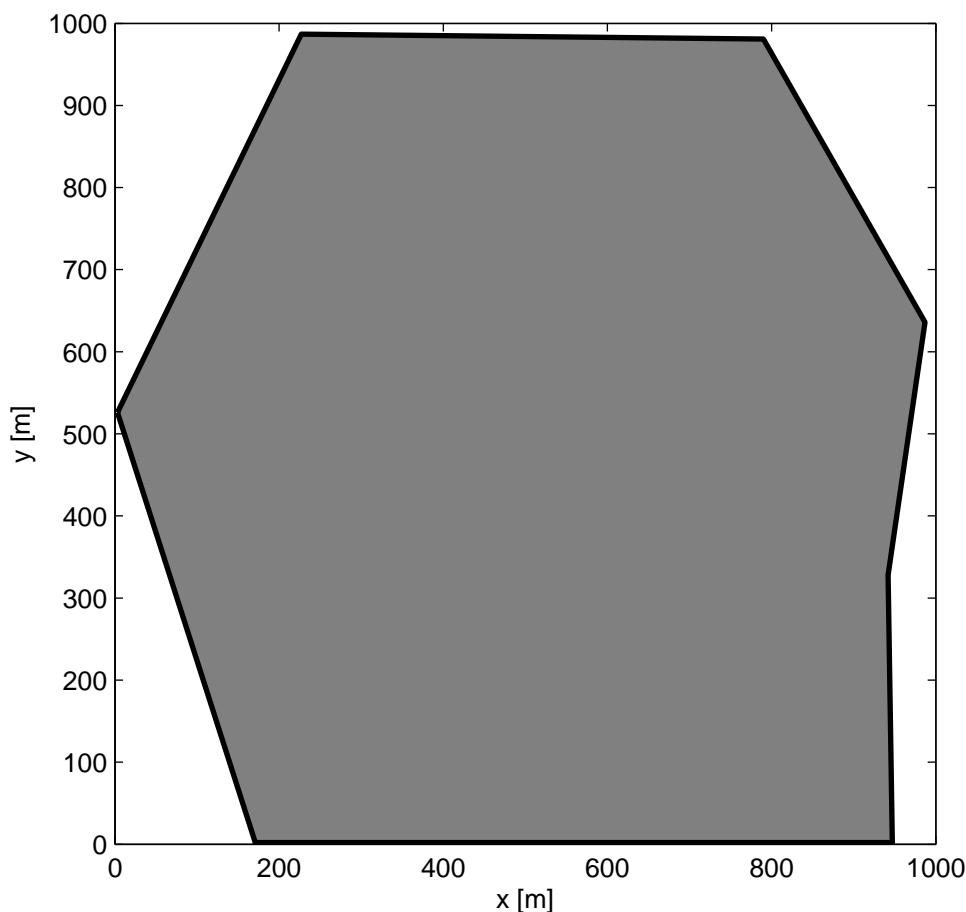


Figure 3.1: Polygonal domain used in the example calculations of the geostatistical inference with the KL expansion.

3.2 Estimation on a Regular Grid

In this section, I evaluate the performance of the inverse method with the KL expansion on a regular grid. Computational efforts, estimates, and the corresponding estimation variances are compared to the geostatistical inverse method using the full prior covariance matrix.

I discretize the virtual rectangular embedding domain by a regular grid and extract the elements falling into the non-rectangular study domain. The number of nodes and elements of the regularly discretized field are given in Table 3.1

Based on the true hydraulic parameters and bottom topography, I solve the

Table 3.1: Geometric parameters, pumping conditions, and geostatistical parameters of log-transmissivity and log-recharge for all test cases of the inversion with the KL expansion; parameters of discretization for the test case on a regular grid.

Geometric Parameters		
L_1	Embedding domain length	1000m
L_2	Embedding domain width	1000m
Pumping Conditions		
Q	Pumping Rate	$4 \times 10^{-3} m^3/s$
$x_{1,w}$	Well Coordinate	600m
$x_{2,w}$	Well Coordinate	600m
Geostatistical Parameters		
σ_Y^2	Prior variance of $\ln(K)$ [K in m/s]	1
	Actual variance of $\ln(K)$	0.76
σ_Z^2	Prior variance of $\ln(N)$ [N in m^3/m^2]	1
	Actual variance of $\ln(N)$	0.70
β_Y^*	Prior mean value of $\ln(K)$ [K in m/s]	-6
β_Z^*	Prior mean value of $\ln(N)$ [N in m^3/m^2]	-20
$\sigma_{\beta_Y}^2$	Prior variance of β_Y^*	1
$\sigma_{\beta_Z}^2$	Prior variance of β_Z^*	1
λ^Y	Correlation length for $\ln(T)$	200m
λ^Z	Correlation length for $\ln(N)$	200m
Measurement Error		
σ_s^2	Variance of drawdown measurement	$25 \times 10^{-6} m^2$
Regular Discretization		
Δx_1	Grid spacing in x_1	6.67m
Δx_2	Grid spacing in x_2	6.67m
	Number of nodes in the domain	18612
	Number of elements in the domain	18315

steady-state equation Eq. 2.19 (the transient term disappears) using the Finite Element Method with bilinear elements. Figure 3.2c displays the true hydraulic heads. Measurements of the heads are taken at the locations marked by stars

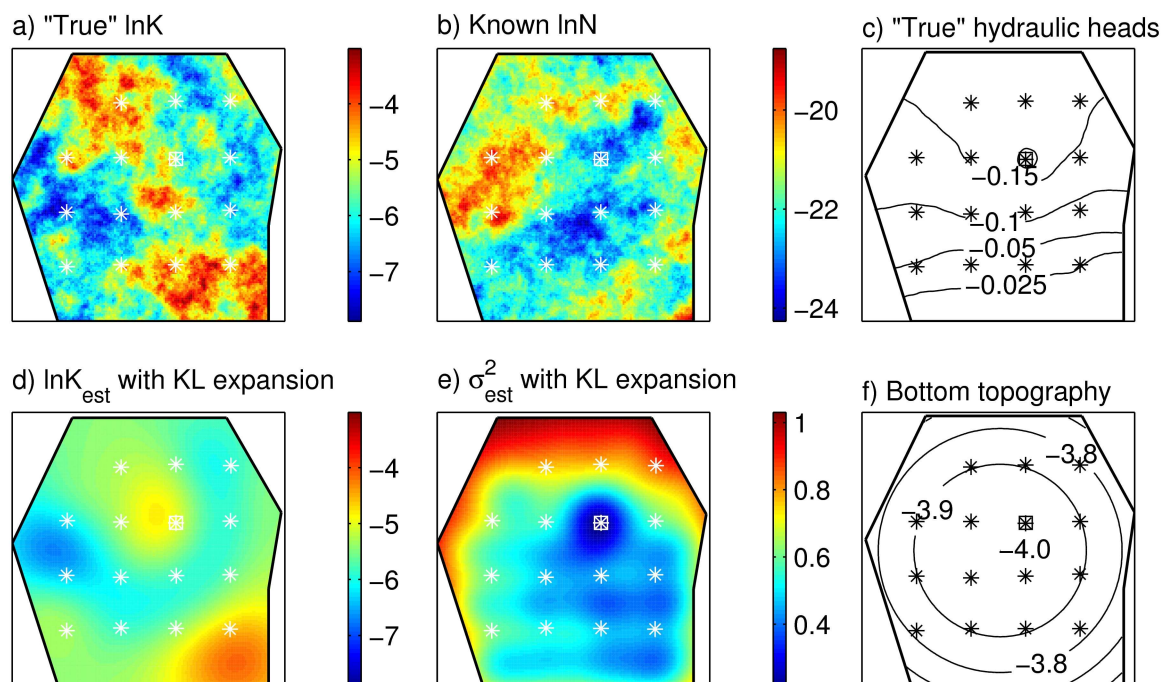


Figure 3.2: Hypothetical test case. a) True distribution of log-conductivity (K in m/s); b) known distribution of log-recharge (N in m^3/s); c) true distribution of hydraulic heads; d) estimated log-conductivity field using 400 KL terms on a rectangular grid; e) associated estimation variance; f) bottom topography. Stars: locations of head measurements; square: location of pumping well.

in Figure 3.2. Artificial uncorrelated measurement errors with zero mean and a standard deviation of $5mm$ are added to the recorded values. This measurement error corresponds to 1.7% of the range of head values in the domain.

With the artificially generated measurement vector \mathbf{Z}^m , I infer the distribution of $\ln(K)$ using the two inverse methods. The continuous adjoint-state method [Sun and Yeh, 1990] was applied for the calculation of sensitivities. The recharge field is assumed to be known. To stabilize my inverse approaches, I use the modified Levenberg-Marquardt algorithm of Nowak and Cirpka [2004]. The estimates using the inverse method with the KL expansion depend on the number of KL terms, whereas the method considering the full prior covariance matrix employs the whole prior information. Thus, I assume that the estimate using the method with the full prior covariance matrix is more accurate, and the latter estimation

will serve as the reference case for later comparisons. Figures 3.2d and 3.2e display an example of the estimate and estimation variance obtained by the inverse method with the KL expansion using 400 KL terms. Since the estimate and estimation variance of the inverse method with the full prior covariance matrix are very similar to the ones of the inverse method with the KL expansion, I do not show separate plots for each inverse method used.

Figure 3.3a shows the computational effort of the reference case and the computational costs of the method with the KL expansion using different numbers of KL terms. The CPU time is normalized by the number of nodes. The normalized CPU time of the reference case is included in Table 3.2. The horizontal line in Figure 3.3a is the computational effort of the reference case, and the stars indicate the computational costs of the estimation using the KL expansion. As is quite obvious, the method with the full prior covariance matrix outperforms the method with the KL expansion for almost any number of KL terms. Both methods are based on periodic embedding of the covariance function. Because the domain is regularly discretized, the matrix multiplications involving the full prior covariance matrix in the first approach can be done in the spectral domain using FFT for the transformation [Nowak et al., 2003]. These techniques are extremely efficient as they make optimal use of the structural properties of the covariance matrix. The method using the KL expansion is more general and exploits periodic properties only in the evaluation of the eigenvalues. For the chosen exponential covariance function, which requires a high number of KL terms, it is slightly less competitive on a structured grid than the reference method. Using the KL expansion, in general, the computational effort increases with increasing number of KL terms. The dimensions of the matrix \mathbf{F} and vector ζ expand when more KL terms are added. Therefore, more time is needed for matrix evaluations. However, when the number of KL terms is not sufficient to catch the major features of the covariance function, the computational cost can also be high, because more iteration steps are needed in the estimation procedure.

To quantify the deviation between the estimates using the inverse method with

the KL expansion and the estimate of the reference case, I compute the normalized root mean square error (NRMSE) defined as:

$$\text{NRMSE} = \sqrt{\frac{1}{n} \sum_{i=1}^n \frac{(p_i^{full} - p_i^{KL})^2}{\sigma_i^2}}, \quad (3.1)$$

where p_i is the log-conductivity in element i , the index *full* stands for the estimate of the method with full prior covariance matrix, the index *KL* denotes the estimate of the method with the KL expansion, and σ_i^2 is the prior variance. Both inverse methods quantify the uncertainty of the estimates also by the estimation variances. To evaluate the difference between the estimation variances of the different methods, I introduce a normalized difference (ND):

$$\text{ND} = \frac{1}{n} \sum_{i=1}^n \frac{|\sigma_{c,full,i}^2 - (\sigma_{c,KL,i}^2 + \sigma_{hf,i}^2)|}{\sigma_i^2}, \quad (3.2)$$

in which $\sigma_{c,full}^2$ and $\sigma_{c,KL}^2$ are the estimation variances of the reference case and the method with the KL expansion, respectively, σ_{hf}^2 stands for the high-frequency uncertainty introduced by the truncation, σ_i^2 is the prior variance, and $|\cdot|$ stands for the absolute value. Figures 3.3b and 3.3c graphically illustrate NRMSE and ND as function of the number of KL terms. Both the differences of the estimated fields and the estimation variances indicate that one can obtain a good estimate using a limited number of KL terms. In my example, about 400 KL terms are sufficient.

Since I know the true hydraulic conductivity field in our particular application, I can quantify the deviation of the estimates from reality by another normalized root mean square error (NRMSE⁰):

$$\text{NRMSE}^0 = \sqrt{\frac{1}{n} \sum_{i=1}^n \frac{(p_i^{true} - p_i^{est})^2}{\sigma_i^2}}, \quad (3.3)$$

where the index *true* denotes the true hydraulic conductivity, and *est* refers to

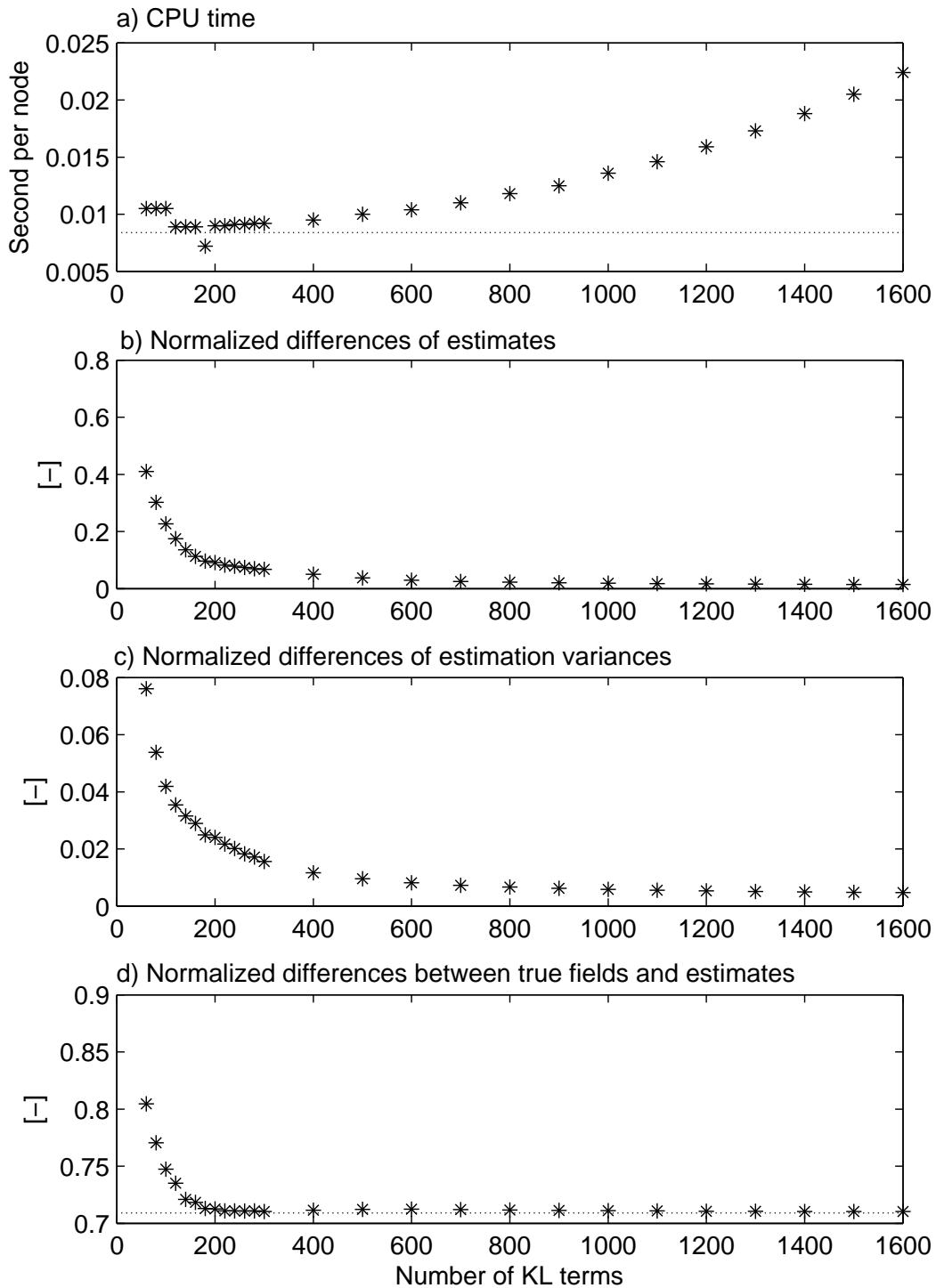


Figure 3.3: Performance of the Karhunen-Loève expansion. a) Computational effort of the inverse method with the KL expansion (stars) as function of the number of KL terms. Dotted line: effort for the inverse method using the full prior covariance matrix. b) Normalized difference of the estimates, NRMSE, according to Eq. (3.1). c) Normalized difference of the estimation variance, ND, according to Eq. (3.2). d) Normalized difference of the estimates, NRMSE^0 , according to Eq. (3.3).

the estimates. Table 3.2 contains NRMSR^0 of the reference case. Figure 3.3d shows NRMSE^0 of the reference case and the method with the KL expansion using different numbers of KL terms. The horizontal line in this sub-figure is the difference between the true field and the estimate of the reference case, and the stars show that differences between the true parameters and the estimates with the KL expansion.

Figure 3.4 shows the estimation variance of the elements of the parameter vector ζ for the case in which 1600 KL terms are used. The entries of ζ are sorted by the size of the eigenvalues. The prior variance of each entry of ζ is unity. Figure 3.4 shows the remaining uncertainty after conditioning of ζ on the measurements. The figure shows that the reduction of uncertainty is not significant for KL terms contributing to the covariance function only to a minor extent, which is expressed by a high KL index. This indicates that increasing the number of KL terms, after a certain level is reached, will not help improving the quality of the estimate. In my example, truncating the series after about 400 KL terms will not introduce significant error. In addition, the computational costs at these stages are comparable to the computational efforts of the reference case.

The validity of the estimate can statistically be tested by considering the orthonormal residuals [Kitanidis, 1995]. The sum of the squared orthonormal residuals should follow the χ^2 distribution. All relevant parameters and results are included in Table 3.2. The mean value of the orthonormal residuals is almost zero, which is the expected value. For the given degree of freedom, 15, the sum of the squared orthonormal residuals, 18.11, corresponds to a χ^2 -probability of 74%, which lies well in the 95% confidence interval. This indicates that the model agrees with the data.

3.3 Estimation on an Unstructured Grid

In this section, I use an unstructured grid with triangular elements when I estimate the hydraulic parameters using the Quasi-Linear Geostatistical Inverse Ap-

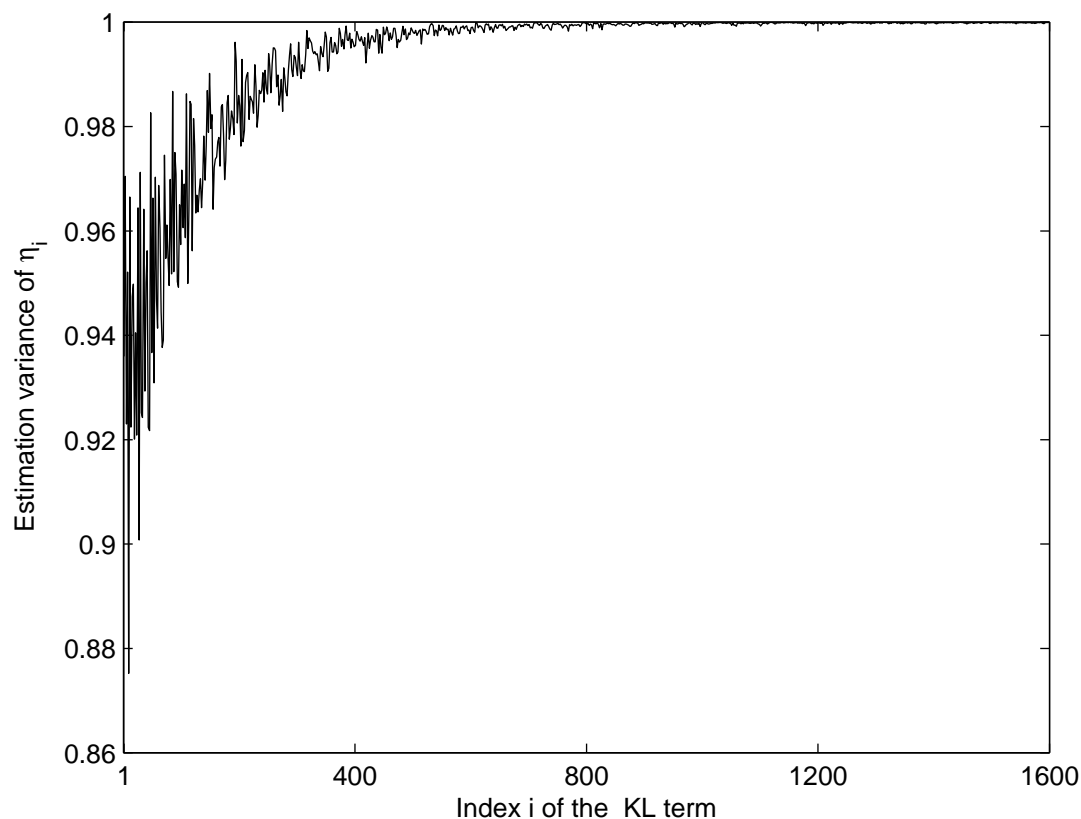


Figure 3.4: Estimation variance of the entries of the weight vector ζ using 1600 KL terms, sorted by their eigenvalues.

proach [Kitanidis, 1995] with the KL expansion. The parameterization does not distinguish between different discretization schemes. This implies that I should obtain essentially the same estimate on the triangular grid as on the structured grid if the number of KL terms is identical.

I use the same polygonal field, locations of monitoring and pumping wells, and pumping rate as defined in Section 3.1. For the generation of the triangular grid, the pde toolbox of Matlab is used. The actual number of nodes and elements are listed in Table 3.2. Except for a slight geometric mismatch, the true $\ln(K)$ and $\ln(N)$ and the topography of the aquifer bottom are identical to those used in Section 3.2.

Table 3.2: Performance results for the reference case and orthonormal residuals (Section 3.2) and estimation on unstructured grids (Section 3.3)

Section 3.2: Performance Results of the Reference Case	
CPU time per node	0.0084
NRMSE ⁰ of the reference case according to Eq. (3.3)	0.7090
Section 3.2: Orthonormal Residuals (Regular Grid)	
Degree of freedom	15
Mean value of the orthonormal residuals	-0.001
Cumulative probability (χ^2 distribution)	0.74
Sum of squares of the orthonormal residuals	18.11
Section 3.3: Estimation on Unstructured Grids	
Number of nodes	14209
Number of elements	28069
NRMSE* according to Eq. (3.4)	0.12
ND* according to Eq. (3.5)	0.0046
CPU time per node	0.0290
CPU time per element	0.0147

I solve the true hydraulic fields using the Finite Element Method with linear shape functions. The measurements are taken by the same procedure as in Section 3.2. With the artificial measurements, I infer the log-conductivity distribution via the inverse method with the KL expansion accelerated by the continuous adjoint-state method [Sun and Yeh, 1990] and stabilized by the Levenberg-Marquardt algorithm of Nowak and Cirpka [2004]. In this estimation, 400 KL terms are used.

To make the estimates of different discretization schemes more comparable, I map the results obtained on the triangular grid onto the rectangular grid used in subsection 3.2. Then I compare the mapped results with the estimate on the rectangular grid. To quantify the differences, I define a normalized root mean square error NRMSE*:

$$\text{NRMSE}^* = \sqrt{\frac{1}{n} \sum_{i=1}^n \frac{(p_i^{\text{mapped}} - p_i^{\text{rec}})^2}{\sigma_{c,i}^{2,\text{mapped}}}}, \quad (3.4)$$

where n is the number of elements of the rectangular grid, p_i^{mapped} denotes the estimate of the triangular grid mapped onto the rectangular one, p_i^{rec} is the estimate on the rectangular grid, and $\sigma_{c,i}^{2,\text{mapped}}$ stands for the mapped estimation variance computed for the triangular grid. For the difference of the estimation variances, I introduce a normalized difference ND^* with respect to the prior variance:

$$\text{ND}^* = \frac{1}{n} \sum_{i=1}^n \frac{|\sigma_{c,i}^{2,\text{mapped}} - \sigma_{c,i}^{2,\text{rec}}|}{\sigma_i^2}, \quad (3.5)$$

in which $\sigma_{c,i}^{2,\text{rec}}$ is the estimation variance on the rectangular grid, and σ_i^2 denotes the prior variance. Here p_i^{rec} and $\sigma_{c,i}^{\text{rec}}$ are the results of estimation with 400 KL terms on the rectangular grid. The resulting NRMSE^* and ND^* are given in Table 3.2. These two numbers include the error introduced by the mapping. Both normalized differences indicate that the estimate on the triangular grid is very close to the estimate on the rectangular grid.

Table 3.2 contains the computational effort for the inverse method on the unstructured grid. The computational costs per node are roughly three times the computational costs of the test case with 400 KL terms on the regular grid. For rectangular grids, I have efficient methods to set up the system of equations. For unstructured grids, by contrast, I have to perform this task element by element. Therefore, the setup will cost more CPU time. Moreover, although the number of nodes of the unstructured grid is close to the number of nodes on the regular grid, the number of elements is about 1.5 times higher. For storing and multiplication of matrices involving element-related properties, such as \mathbf{F} , I expect that the computational time will increase by this factor.

3.4 Summary

I have successfully applied the Quasi-Linear Geostatistical Inverse Approach for the identification of the spatial log conductivity distribution from measurements of heads using the Karhunen-Loève expansion (KL) as parameterization of the log conductivity fluctuations.

In previous studies on uncertainty propagation using the KL expansion [Ghanem, 1998; Zhang and Lu, 2004], a rather smaller number of KL terms were used. In our inverse modeling study, between 200 and 400 terms were needed to achieve estimates that are of similar quality to those obtained by using the full prior covariance matrix. Since the inverse approach with the KL expansion does not distinguish grids, the results on the unstructured grid are very close to the ones on the structured grid. In my case study, the inverse method applying the KL expansion has been outperformed slightly by the method using the full prior covariance function in conjunction with spectral methods for the computation of cross-covariance matrices [Nowak et al., 2003]. This is because of a high number of KL terms. A particular reason for this high number is that I have chosen an exponential covariance function to describe the spatial correlation of log conductivity. This function expresses variations on all scales and its Fourier transform is known to decay only slowly with increasing frequency. For smoother covariance functions, particularly with large correlation lengths, the parameterization by the KL expansion will be more efficient. For such cases, fewer eigenvalues are dominating and the KL expansion can be truncated after fewer terms. For unstructured grids, inverse modeling based on the parameterization by the KL expansion appears to be the most efficient approach.

The KL expansion requires that the log-conductivity field is (multi)Gaussian. Also, the spectral derivation of the base functions demands a stationary covariance function, or at least a non-stationary function that can be traced back to a stationary counterpart [Cirpka and Nowak, 2004].

Extending the inverse approach to three dimensions is straightforward. The KL expansion is applicable in three dimensions and periodic embedding can be used

as well. Then, the three-dimensional groundwater-flow equation rather than the two-dimensional equation is used.

Chapter 4

Applications to Field Data

In this Chapter, I implement the Quasi-Linear Geostatistical Inverse Approach [Kitanidis, 1995] to field data. I conduct both a two-dimensional and a three-dimensional inference. Field data obtained at the test site Krauthausen, Germany [Vanderborcht and Vereecken, 2001; Vereecken et al., 1999; 2000] are used.

Section 4.1 covers the descriptions of the test field and the tests at Krauthausen, Germany. The two- and three-dimensional inferences of the hydrogeological parameters are included in Section 4.2 and 4.3, respectively.

4.1 Field and Test Descriptions

This section describes the test field and the tests at Krauthausen, Germany: First, I will give a brief description of the test site at Krauthausen. Then, the small-scale pumping tests and flowmeter tests at the test site will be described.

4.1.1 Field Description

The Krauthausen test site is located in the southern part of the Lower Rhine Embayment, Germany [Vanderborcht and Vereecken, 2001; Vereecken et al., 1999; 2000]. It has an extension of $200\text{ m} \times 70\text{ m}$. All studies at the test site have

focused on the uppermost aquifer with a thickness of approximately 10 m . This aquifer is part of a flood plain, consisting mainly of gravel and sand sediments. The site is equipped with 73 monitoring wells (approximately 5 cm in diameter) and a single well with approximately 17.5 cm diameter used as pumping well in a large-scale pumping test. Figure 4.1 shows a plan view of the test site and the location of the wells.

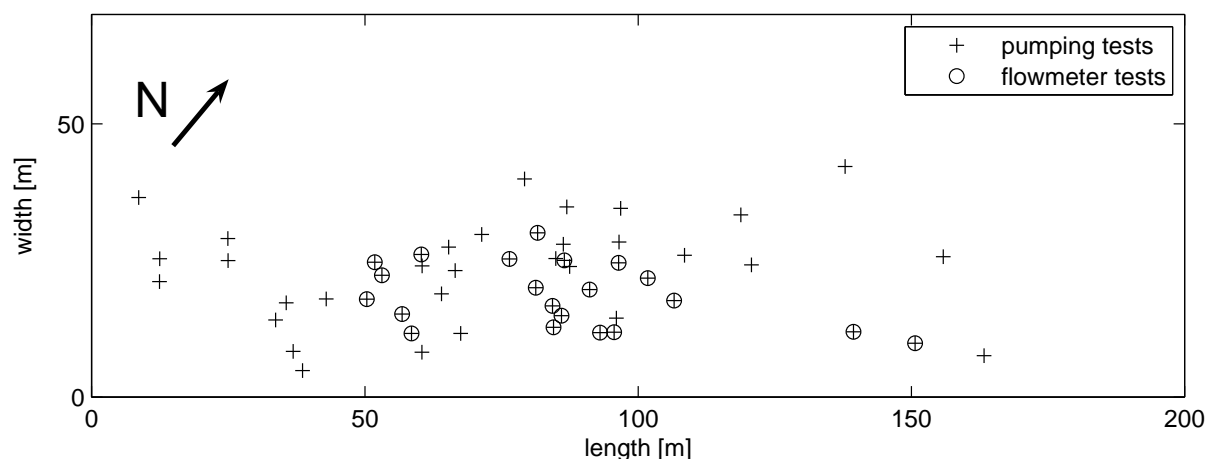


Figure 4.1: Dimension of the field and well locations of the test site Krauthausen. Crosses indicate the location of wells used for pumping tests and circles for flowmeter tests.

4.1.2 Description of Pumping Tests

From March to August 2000, a series of small-scale pumping tests with a discharge rate of $2\text{ m}^3/h$ were conducted at 29 different pumping wells at the test site [Lamertz, 2001]. For each pumping test, approximately 10 wells adjacent to the production wells were used as observation wells. Well locations are marked by crosses in Figure 4.1. The distances of pumping and observation wells range from 1.63 m to 130.91 m . Both the pumping and observation wells were equipped with automatic loggers of hydraulic head with a resolution of 1 mm to measure and store the head changes at time intervals of 10 seconds. The pumping continued for 2 hours.

The small-scale pumping tests were performed in a two-dimensional hydraulic tomographic format. Although this two-dimensional setup is different from the three-dimensional description in Figure 1.2 as suggested by Neuman [1987], Butler and Liu [1993] and Gottlieb and Dietrich [1995], the two-dimensional hydraulic tomography still follows the same philosophy, namely, one stresses an aquifer at different locations and in the meantime observes the response of the aquifer at adjacent wells. By doing this, one obtains a series of measurements reflecting features of the aquifer at different locations.

The drawdowns during the small-scale pumping tests were considerably smaller than the thickness of the aquifer. In addition, I analyze the values of storativity for each pumping test using Theis' [1936] method, resulting in values ranging from 2.5×10^{-4} to 0.017, which indicates confined conditions. Hence, it is permissible to analyze the pumping tests under confined conditions.

4.1.3 Description of Flowmeter Tests

To facilitate later descriptions, I briefly illustrate the setup of a flowmeter test in Figure 4.2. Here, b [m] refers to the aquifer saturated thickness; z_0 [m] stands for the reference level of the borehole bottom; and h [m] the height above the bottom. Extraction of water with a rate Q_p [m^3/s] is conducted until steady state is reached. Then, the vertical flow rate $Q(h)$ [m^3/s] within the borehole is measured by the flowmeter as a function of depth. The cumulative flow $Q(h)$ at height $z_0 + h$ can be expressed as:

$$Q(h) = \sum_i \Delta Q_i, \quad (4.1)$$

in which ΔQ_i [m^3/s] is the induced flow at increment i within the total range of z_0 to $z_0 + h$. The relation between the horizontal hydraulic conductivity K_i and the induced flow ΔQ_i without ambient flow in a borehole can be quantified by Javandel and Witherspoon [1969]:

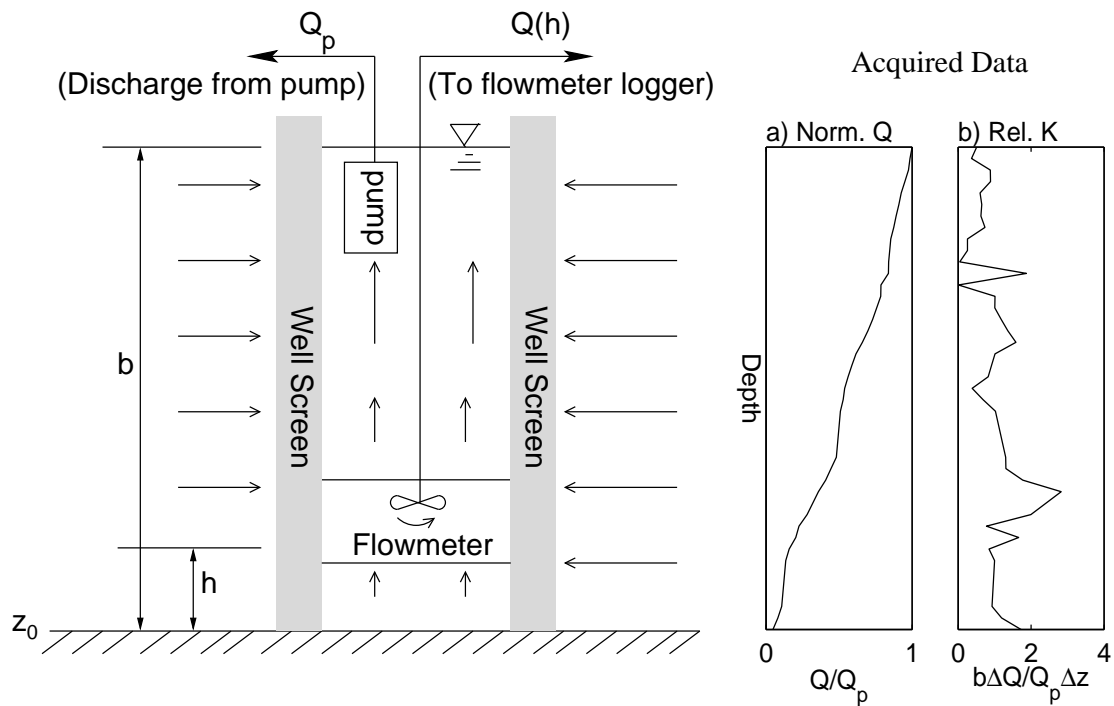


Figure 4.2: Typical setup of a flowmeter test and a graphic illustration of the data. (a) is the normalized cumulative discharge profile and (b) is the profile of relative hydraulic conductivity.

$$\eta_i = \frac{K_i}{\bar{K}} = \frac{\Delta Q_i b}{Q_p \Delta z_i}, \quad (4.2)$$

with

$$\bar{K} = \frac{\sum(K_i \Delta z_i)}{b}, \quad (4.3)$$

where K_i is the hydraulic conductivity of the i -th increment in the direct vicinity of the borehole, \bar{K} is the depth-averaged value of hydraulic conductivity over the depth of the borehole, and Δz_i is the thickness of the i -th measurement increment. I graphically illustrate the profiles of normalized discharges $Q(h)$ and the relative hydraulic conductivities in Figures 4.2a and 4.2b.

In August 1994, flowmeter tests were conducted in 21 suitable wells [Möller, 2003]. The circles in Figure 4.1 indicate the well locations. In the field, a

pumping rate Q_p of $1.5 \text{ m}^3/h$ was applied. A flowmeter was used to measure and record the flow rate Q_i in the wells as a function of depth. The vertical resolution of the measurements was 10 cm .

4.2 Two-Dimensional Estimation

In this section, I test the feasibility of the Quasi-Linear Geostatistical Inverse Approach [Kitanidis, 1995] in estimating the fields of transmissivity and storativity where consistent assumptions about the spatial variability of the subsurface are used².

When applying Jacob's method to transient drawdown data, Meier et al. [1998] have shown that the estimate of storativity in a heterogeneous aquifer strongly fluctuates even when a uniform field of storativity is applied in the true forward simulation. Because the variability of all terms making up the storativity is small, it is believed that the estimated variability of storativity is biased. The biased results may come from the inconsistent assumption of uniformity of parameter fields. In this section, I examine the estimate of storativities with field data in the framework of geostatistics where more consistent assumptions are applied.

Here, I apply the transient drawdown data of tomographic pumping tests at the test site Krauthausen, Germany [Vanderborcht and Vereecken, 2001; Vereecken et al., 1999; 2000]. Since the pumping tests were conducted in fully screened wells, the measurements contain only depth-averaged properties of aquifers. Correspondingly, the outcomes of the estimation, the most likely estimates and their related uncertainties, are also depth-averaged.

The estimation of storativities requires transient drawdown data. Considering full transient drawdown curves in geostatistical inversing is still computationally challenging. However, temporal moments of drawdown by Li et al. [2005] condense transient curves and their related moment-generating equations are

²This two-dimensional estimation has been published by Li et al. [2007]

steady state. Taking temporal moments rather than full drawdown curves drastically reduces the computational effort in the inference. For the two-dimensional estimation, I use the two most important temporal moments of drawdown, the zeroth and first temporal moments, as my data.

I compare the inversed results with the kriged field of the values obtained by the conventional type-curve method. The conventional analysis of pumping tests consists of fitting analytical solution of the flow equation to the measured time curves of drawdown [Theis, 1936]. The estimated transmissivity and storativity values represent apparent parameters, because of the mismatch between real formation and underlying assumptions of analytical solutions. By repeating the curve-fitting technique for all series of pumping tests at different locations, I obtain a set of values of transmissivity and storativity. Then, I interpolate these local values, producing a continuous image of the hydrogeological parameters. Through the comparison, I identify whether these values obtained by conventional methods may be viewed as pseudo-local values of transmissivity and storativity.

As mentioned in Section 2.9, geostatistical parameters of covariance functions such as the variance and the correlation lengths have to be estimated from measurements as well. The quality of measurements influences the corresponding estimates. I examine the influence of measurement errors on estimating geostatistical parameters.

I precede this section as follows: First, I explain the process of data preparation in which the analysis by the type-curve approach and the computation of temporal moments will be presented. Next, I discuss the numerical implementation and results of the estimation. I compare the kriged fields with the ones from geostatistical inversion. Then, I discuss the influence of measurement error on the estimation of geostatistical parameters.

4.2.1 Data Preparation

In this section, I discuss the procedures of data preparation for the conventional type-curve method and the geostatistical inverse approach. Here, the two-dimensional groundwater flow equation Eq. (2.15) under confined conditions and the corresponding boundary conditions are used to describe to distribution of drawdown.

4.2.1.1 Analysis by Theis' Approach

I use Theis' [1936] approach to estimate the log-transmissivity($\ln T$) and log-storativity($\ln S$) from each transient drawdown curve of the small-scale pumping tests. I obtain the optimal values of $\ln T$ and $\ln S$ by minimizing the following objective function \mathcal{L} :

$$\mathcal{L} = \frac{(\mathbf{s} - \mathbf{s}_e)^T (\mathbf{s} - \mathbf{s}_e)}{\sigma_s^2}, \quad (4.4)$$

where \mathbf{s} is the measured drawdown, σ_s is the epistemic error of drawdown, and \mathbf{s}_e is the model output defined by:

$$\mathbf{s}_e(r, t) = \frac{Q(t)}{4\pi T} \text{Ei} \left(\frac{r^2 S}{4Tt} \right), \quad (4.5)$$

in which r is the distance between the production and monitoring wells and $\text{Ei}(\cdot)$ is the exponential integral function.

The epistemic error σ_s^2 of drawdown is assumed uncorrelated and identical for all measurements. σ_s^2 includes random and systematic contributions. In most circumstances, σ_s^2 is not known and need to be estimated. If σ_s^2 reflects the real uncertainty of the drawdown measurements, the value of \mathcal{L} should statistically follow a χ^2 distribution with n_f degree of freedom, where n_f is the number of observations minus the number of estimated parameters. The proper value of σ_s^2 is determined by enforcing \mathcal{L} to meet its expected value.

The estimation covariance matrix \mathbf{Q}_c of the estimated $\ln T$ and $\ln S$ is approximated by the inverse Hessian matrix at the optimal set of the parameters \mathbf{U} :

$$\mathbf{Q}_c = \begin{bmatrix} \sigma_{\ln T}^2 & C_{\ln T \ln S} \\ C_{\ln T \ln S} & \sigma_{\ln S}^2 \end{bmatrix} \approx \left(\frac{\partial^2 \mathcal{L}}{\partial \mathbf{U} \otimes \partial \mathbf{U}} \right)^{-1}, \quad (4.6)$$

where \mathbf{U} is the vector containing the two variables $\ln T$ and $\ln S$, $\sigma_{\ln T}^2$ and $\sigma_{\ln S}^2$ are the estimation variances of the parameter of $\ln T$ and $\ln S$, respectively, and $C_{\ln T \ln S}$ denotes the cross-covariance between $\ln T$ and $\ln S$.

I obtain a pair of $\ln T$ and $\ln S$ values for each drawdown curve. At a location which has been used either as observation point or pumping well in multiple pumping tests, I compute a weighted average from all parameters obtained at this location, resulting in a single pair of $\ln T$ and $\ln S$ values:

$$w_i = \frac{1}{\sqrt{\sigma_{\ln T, i} \times \sigma_{\ln S, i}}}, \text{ for } i = 1 \cdots n_\ell, \quad (4.7)$$

$$\tilde{U}_{\ln T} = \frac{1}{\sum_{i=1}^{\ell} w_i} \sum_{i=1}^{\ell} w_i U_{\ln T, i}, \quad (4.8)$$

$$\tilde{U}_{\ln S} = \frac{1}{\sum_{i=1}^{\ell} w_i} \sum_{i=1}^{\ell} w_i U_{\ln S, i}, \quad (4.9)$$

where w_i is the weight, n_ℓ is the number of pairs of $\ln T$ and $\ln S$ at this location, and $\tilde{U}_{\ln T}$ and $\tilde{U}_{\ln S}$ is the weighted average of $U_{\ln T}$ and $U_{\ln S}$ of the estimated $\ln T$ and $\ln S$, respectively. I consider these weighted averages as pseudo-local measurements in kriging.

The associated measurement error is comprised of the weighted average of the parameter uncertainty in fitting Theis' solution to the single drawdown curves and the variability of the parameter estimates among the different tests:

$$\tilde{\sigma}_{\ln T}^2 = \frac{n_\ell}{\sum_{i=1}^{n_\ell} w_i} + \frac{1}{\sum_{i=1}^{n_\ell} w_i - 1} \sum_{i=1}^{n_\ell} w_i (U_{\ln T, i} - \bar{U}_{\ln T})^2, \quad (4.10)$$

$$\tilde{\sigma}_{\ln S}^2 = \frac{n_\ell}{\sum_{i=1}^{n_\ell} w_i} + \frac{1}{\sum_{i=1}^{n_\ell} w_i - 1} \sum_{i=1}^{n_\ell} w_i (U_{\ln S, i} - \bar{U}_{\ln S})^2, \quad (4.11)$$

$$\begin{aligned} \tilde{C}_{\ln T \ln S} &= \frac{n_\ell}{\sum_{i=1}^{n_\ell} \frac{1}{C_{\ln T \ln S, i}}} + \frac{1}{\sum_{i=1}^{n_\ell} w_i - 1} \\ &\cdot \sum_{i=1}^{n_\ell} w_i (U_{\ln T, i} - \bar{U}_{\ln T}) (U_{\ln S, i} - \bar{U}_{\ln S}), \end{aligned} \quad (4.12)$$

where $\tilde{\sigma}_{\ln T}^2$ and $\tilde{\sigma}_{\ln S}^2$ are the weighted estimation variances of the estimated parameter $\ln T$ and $\ln S$, respectively, $\bar{U}_{\ln T}$ is the arithmetic mean of the estimated $\ln T$ at this location, $\bar{U}_{\ln S}$ stands for the arithmetic mean of the estimated $\ln S$, and $\tilde{C}_{\ln T \ln S}$ is the weighted cross-covariance between $\ln T$ and $\ln S$. In most cases, the latter contribution dominates the computed measurement error. $\tilde{\sigma}_{\ln T}^2$, $\tilde{\sigma}_{\ln S}^2$ and $\tilde{C}_{\ln T \ln S}$ compose the term \mathbf{R}_{ZZ} of Eq. (2.74):

$$\mathbf{R}_{ZZ} = \begin{bmatrix} \tilde{\sigma}_{\ln T, 1}^2 & \mathbf{0} & \mathbf{0} & \tilde{C}_{\ln T \ln S, 1} & \mathbf{0} & \mathbf{0} \\ \mathbf{0} & \ddots & \mathbf{0} & \mathbf{0} & \ddots & \mathbf{0} \\ \mathbf{0} & \mathbf{0} & \tilde{\sigma}_{\ln T, m}^2 & \mathbf{0} & \mathbf{0} & \tilde{C}_{\ln T \ln S, m} \\ \tilde{C}_{\ln T \ln S, 1} & \mathbf{0} & \mathbf{0} & \tilde{\sigma}_{\ln S, 1}^2 & \mathbf{0} & \mathbf{0} \\ \mathbf{0} & \ddots & \mathbf{0} & \mathbf{0} & \ddots & \mathbf{0} \\ \mathbf{0} & \mathbf{0} & \tilde{C}_{\ln T \ln S, m} & \mathbf{0} & \mathbf{0} & \tilde{\sigma}_{\ln S, m}^2 \end{bmatrix}, \quad (4.13)$$

in which m is the number of the measurement locations.

4.2.1.2 Computation of Temporal Moments

As has been shown in Section 2.1, the temporal moments of drawdown for a unit-pulse extraction can be derived from measurements of drawdown observed during continuous pumping. Because the head measurements fluctuated, I obtain more stable estimates of the moments by fitting a parametric function to the observations. The maxentropic semi-infinite distribution for given zeroth and first temporal moments is the exponential one [Gibbs, 1902]. Like Bakker et al. [2007], I use the latter expression to parameterize the drawdown for pulse-like extraction. This results in the following expression for continuous pumping:

$$s_e = Qm_0 \left(1 - \exp \left(-\frac{m_0}{m_1} t \right) \right), \quad (4.14)$$

where m_0 and m_1 denote the zeroth and first temporal moments for pulse-like extraction, respectively. The optimal pair of temporal moments are determined by minimizing the weighted difference between the observed and simulated drawdown curves. The corresponding objective function is similar to Eq. (4.4). The estimation covariance matrix of m_0 and m_1 is given by the inverse Hessian matrix of the objective function at the optimal point.

At late times, when the exponential part in Eq. (4.14) approaches zero, the difference between s and s_e is dominated by the difference between s and Qm_0 . Qm_0 is equivalent to the final drawdown. Statistically, Qm_0 is determined by averaging the measured values of drawdown at late times. According to the statistical formulation, the uncertainty of the estimated final drawdown is defined as the ratio between the squared measurement error of drawdown and the number of the measured drawdown data used. The uncertainty decreases with increasing number of measurement points. However, this uncertainty of the final drawdown does not reflect the real measuring process, for which an accuracy beyond the resolution of the device is impossible. To account for such non-random effects, I add an additional measurement error σ_{s_Δ} to the estimated uncertainty of the final drawdown. This additional measurement error of final drawdown propagates to the estimation variances of the zeroth and first temporal moments

and the cross-variance between the estimated m_0 and m_1 :

$$\tilde{\sigma}_{m_0}^2 = \sigma_{m_0}^2 + \left(\frac{\sigma_{s\Delta}}{Q} \right)^2, \quad (4.15)$$

$$\tilde{\sigma}_{m_1}^2 = \sigma_{m_1}^2 + \left(\frac{m_1}{m_0} \right)^2 \cdot \left(\frac{\sigma_{s\Delta}}{Q} \right)^2, \quad (4.16)$$

$$\tilde{C}_{m_0m_1} = C_{m_0m_1} + \frac{m_1}{m_0} \cdot \left(\frac{\sigma_{s\Delta}}{Q} \right)^2, \quad (4.17)$$

where $\tilde{\sigma}_{m_0}^2$ and $\tilde{\sigma}_{m_1}^2$ are the total uncertainties of the determined m_0 and m_1 values, respectively, and $\tilde{C}_{m_0m_1}$ is the cross-variance between m_0 and m_1 . $\sigma_{m_0}^2$, $\sigma_{m_1}^2$, and $C_{m_0m_1}$ are computed from the inverse Hessian matrix of the objective function at the optimal point. In most cases, the contribution of $\sigma_{s\Delta}$ dominates the total uncertainties. $\tilde{\sigma}_{m_0}^2$, $\tilde{\sigma}_{m_1}^2$ and $\tilde{C}_{m_0m_1}$ are the terms in \mathbf{R}_{ZZ} of Eq. (2.74):

$\mathbf{R}_{ZZ} =$

$$\begin{bmatrix} \tilde{\sigma}_{m_0,1}^2 & \mathbf{0} & \mathbf{0} & \tilde{C}_{m_0m_1,1} & \mathbf{0} & \mathbf{0} \\ \mathbf{0} & \ddots & \mathbf{0} & \mathbf{0} & \ddots & \mathbf{0} \\ \mathbf{0} & \mathbf{0} & \tilde{\sigma}_{m_0,n_m}^2 & \mathbf{0} & \mathbf{0} & \tilde{C}_{m_0m_1,n_m} \\ \tilde{C}_{m_0m_1,1} & \mathbf{0} & \mathbf{0} & \tilde{\sigma}_{m_1,1}^2 & \mathbf{0} & \mathbf{0} \\ \mathbf{0} & \ddots & \mathbf{0} & \mathbf{0} & \ddots & \mathbf{0} \\ \mathbf{0} & \mathbf{0} & \tilde{C}_{m_0m_1,n_m} & \mathbf{0} & \mathbf{0} & \tilde{\sigma}_{m_1,n_m}^2 \end{bmatrix}, \quad (4.18)$$

in which n_m is the number of moment pairs.

The error $\sigma_{s\Delta}$ is not necessary for the previous approach where Theis' method is used to estimate $\ln T$ and $\ln S$, because Theis' approach does not rely on measurements of final drawdown.

4.2.2 Kriging of Pseudo-Local Values

Using the pseudo-local values of $\ln T$ and $\ln S$ obtained from type-curve analysis, I can estimate the geostatistical parameters of the covariance functions following the restricted maximum likelihood method of Kitanidis [1995] as described in Section 2.9. The field dimension and resolution are listed in Table 4.1. Here, a structured regular grid is applied.

Here, I assume diffuse prior knowledge of the geostatistical parameters. The prior knowledge of the trend coefficients β is given in Table 4.1. To avoid negative values in the estimates of $\hat{\sigma}_{\ln T}^2$, $\hat{\sigma}_{\ln S}^2$, and λ , I estimate the logarithms of these parameters. Correspondingly, the uncertainties of these parameters are quantified by the factor of variation (FV), which is the exponential of the standard deviation of the log-parameter. Concerning $\hat{C}_{\ln T \ln S}$, I estimate its related correlation coefficient $r_{\ln T \ln S}$:

$$r_{\ln T \ln S} = \frac{\hat{C}_{\ln T \ln S}}{\sigma_{\ln T} \sigma_{\ln S}}. \quad (4.19)$$

To guarantee that $r_{\ln T \ln S}$ remains within the range between -1 and 1 , I apply the error function as transformation between an auxiliary variable μ , ranging between $-\infty$ and ∞ , and $r_{\ln T \ln S}$, and estimate μ :

$$r_{\ln T \ln S} = \text{erf}(\mu). \quad (4.20)$$

Applying the restricted maximum likelihood method, I obtain the geostatistical parameters and their corresponding uncertainties, which are listed in Table 4.1.

With the estimated geostatistical parameters, I estimate $\ln T$ and $\ln S$ on a regular grid. In interpolation by kriging, I consider local measurements of $\ln T$ and $\ln S$. The functional relation $\mathbf{Z}(\mathbf{Y})$ between the measurements and parameters \mathbf{Y} becomes linear and can be expressed as:

$$\mathbf{Z}(\mathbf{Y}) = \mathbf{H}\mathbf{Y}, \quad (4.21)$$

where \mathbf{H} is a $2n_\ell \times 2n$ extraction matrix with a single unit element per line. Then, the objective function of Eq. (2.74) becomes:

$$L(\mathbf{Y}|\mathbf{Z}, \boldsymbol{\theta}) = \mathbf{Y}'^T \mathbf{R}_{\mathbf{Y}'\mathbf{Y}'|\boldsymbol{\theta}}^{-1} \mathbf{Y}' + (\boldsymbol{\beta} - \boldsymbol{\beta}^*)^T \mathbf{R}_{\boldsymbol{\beta}\boldsymbol{\beta}}^{-1} (\boldsymbol{\beta} - \boldsymbol{\beta}^*) + (\mathbf{Z} - \mathbf{H}\mathbf{Y})^T \mathbf{R}_{\mathbf{Z}\mathbf{Z}}^{-1} (\mathbf{Z} - \mathbf{H}\mathbf{Y}) + \text{const.}, \quad (4.22)$$

Since I want to estimate the fields of both transmissivity and storativity, \mathbf{Y} becomes an aggregated vector containing the discrete values of transmissivity and storativity. Correspondingly, $\mathbf{R}_{\mathbf{Y}'\mathbf{Y}'|\boldsymbol{\theta}}$ of the prior covariance matrix consists of four blocks representing the discretized auto-covariance functions of log-transmissivity and log-storativity as well as the discretized cross-covariance function:

$$\mathbf{R}_{\mathbf{Y}'\mathbf{Y}'|\boldsymbol{\theta}} = \begin{bmatrix} \mathbf{R}_{\ln T \ln T|\boldsymbol{\theta}} & \mathbf{R}_{\ln T \ln S|\boldsymbol{\theta}} \\ \mathbf{R}_{\ln T \ln S|\boldsymbol{\theta}}^T & \mathbf{R}_{\ln S \ln S|\boldsymbol{\theta}} \end{bmatrix}, \quad (4.23)$$

in which $\mathbf{R}_{\ln T \ln T|\boldsymbol{\theta}}$ is the auto-covariance matrix of $\ln T$ for given geostatistical parameters $\boldsymbol{\theta}$, $\mathbf{R}_{\ln S \ln S|\boldsymbol{\theta}}$ denotes the auto-covariance matrix of $\ln S$, and $\mathbf{R}_{\ln T \ln S|\boldsymbol{\theta}}$ is the cross-covariance matrix of $\ln T$ and $\ln S$.

The optimal values of the hydraulic parameter field is identified by applying Eqs. (2.75 & 4.22). Since the functional relation between the data and the hydraulic parameters is linear, only a single iteration step is needed and the posterior covariance matrix $\mathbf{R}_{\mathbf{Y}\mathbf{Y}|\mathbf{Z}}$ becomes exact. It may be worth noting that the simple structure of \mathbf{H} does not require computing matrix-matrix products explicitly. $\mathbf{H}\mathbf{R}_{\mathbf{Y}'\mathbf{Y}'|\boldsymbol{\theta}}\mathbf{H}^T$ is the autocovariance matrix of \mathbf{Y} evaluated only for the elements of \mathbf{Y} for which measurements exist. Also, because the relationship between measurements and estimated parameters is linear, the most likely value $\hat{\mathbf{Y}}$ is identical to the expected value of the conditional distribution. Figure 4.3 shows the fields of $\ln T$ and $\ln S$ and their corresponding standard deviations of estimation.

The estimated prior variance of $\ln T$ is very small, namely 0.01, indicating an almost uniform distribution of transmissivity. In comparison, the estimated prior variance of $\ln S$ is higher, namely 0.24. As listed in Table 4.1, the total variances of measurements of $\ln T$ and $\ln S$ are fairly small, while the associated "measurement" errors are relatively large. As explained in Section 4.2.1, the pseudo-local values are obtained by averaging all measurements in which a particular well is involved either as pumping well in one test or monitoring well in another test. Obviously, the variability between measurements, involving the same points, is larger than the variability between the averages obtained at different points. Thus, using the results of type-curve analysis as point-like values is not permitted.

The relatively large estimated variance of $\ln S$ and small variance of $\ln T$ in my study reflects the findings of other studies [Meier et al., 1998; Sánchez-Vila et al., 1999; Leven and Dietrich, 2006], which were based on numerical simulations only. In these studies, a small variability of $\ln T$ and high variability of $\ln S$ were found by type-curve analysis despite using uniform storativity values in the simulations. In general, the variance of storativity in natural systems is thought to be relatively small [e.g., Freeze, 1975; Meier et al., 1998]. Under confined conditions, compressibilities of rock, water, and the pore space determine the storativity. The contributions of the rock and water compressibilities are considered to be small at all local scales [e.g., Meier et al., 1998]. Under phreatic conditions, the storativity becomes the porosity, which varies only within a small range [e.g., Meier et al., 1998; Vesselinov et al., 2001a;b]. That is, I believe that the estimate of the variance of $\ln S$ is biased. The bias may be caused by the inconsistent assumption of homogeneity in the conventional pumping-test analysis. It is worth analyzing whether the bias disappears when I apply the geostatistical inverse approach, in which the hydraulic parameter fields are assumed spatially variable in all stages of the estimation procedure.

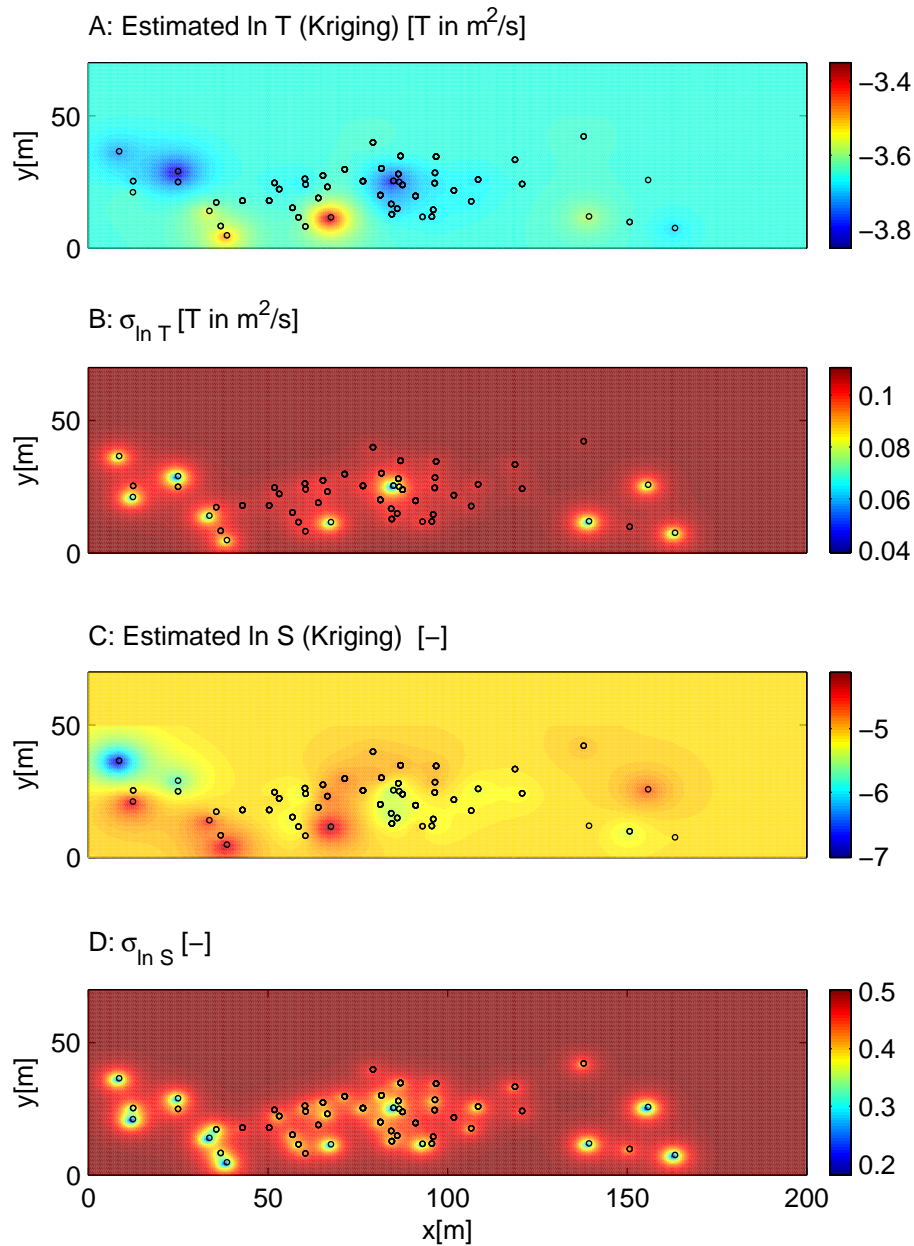


Figure 4.3: Interpolated fields of $\ln T$, $\ln S$ and their corresponding standard derivations of estimation using the values of conventional type-curve approach as pseudo-local values. Circles are the well locations of pumping tests.

4.2.3 Quasi-Linear Geostatistical Inversion of Temporal Moments

In contrast to Section 4.2.2 of this Chapter, I cannot directly derive the geostatistical parameters θ from the computed measurements of m_0 and m_1 , because

the functional relation between the temporal moments and hydraulic parameters is nonlinear. The estimation of geostatistical parameters depends on the current estimates of $\ln T$ and $\ln S$. I have to start with the estimation of $\ln T$ and $\ln S$. To do that, I need initial values of related geostatistical parameters. For the initial value of the correlation length, I take the values estimated in Section 4.2.2. Because I expect more variations in the estimate of $\ln T$ with the geostatistical inverse approach, I take unity as the initial value of the prior variance $\sigma_{\ln T}^2$, a much higher value than the one estimated from the pseudo-local values in Section 4.2.2. As the initial value of the prior variance of $\ln S$, I take the value estimated in Section 4.2.2.

I use the same grid resolution as in Section 4.2.2. To reduce the influence of boundary conditions, I enlarge the domain on each side by 50 meters. Zero drawdown is assumed on the boundaries of the enlarged domain. Following the approaches described in Section 2.7 of Chapter 2, I start the quasi-linear geostatistical inversion of temporal moments with the large-scale pumping test, and use the resulting estimates as the initial guess for analyzing the small-scale pumping tests. The simulated moments of the inverse approached are solved by the corresponding moment-generating equation Eq. (2.28). Here, the Finite Element method with bilinear elements were applied to find the solutions of the partial differential equations. I account for the small-scale pumping tests in a sequential way, beginning with a single small-scale pumping test. Once the optimal parameter set is obtained, I add new pumping-test data to the inversion and estimate the hydraulic parameters using the data of all pumping tests accounted for at the current stage. The estimate from the previous sequential step serve as initial guess for the following estimation. I keep adding new pumping tests until all available tests are used. This successive addition of new measurements stabilizes the inverse procedure. The approach differs from the sequential successive linear estimator (SSLE) developed by Yeh et al. [1996] in the way how information is propagated from one sequential step to the next. While Yeh et al. [1996] take the estimate and approximated conditional covariance matrix as prior mean and covariance in the next step, I consider the previous estimate only as initial

guess. As prior values, I always start from the unconditional distribution, which I then condition on all data accounted for so far. This approach has the advantage that I do not have to perform expensive matrix-matrix multiplications of conditional covariance matrices.

After obtaining the most likely distribution of $\ln T$ and $\ln S$ for all pumping tests based on the initial guess of θ , I start alternating the estimation of the geostatistical and hydraulic parameters. In the alternating procedure, I use only the measurements of temporal moments of the small-scale pumping tests.

It is worth mentioning that the inversion with the Karhunen-Loève(KL) expansion is not applied in the estimations with the measurements of temporal moments of drawdown. Here, I use the geostatistical inversion with the full prior covariance matrix. The major consideration is that the exponential form of the correlation function needs a large number of KL terms in the KL expansion. The performance analysis in Chapter 3 shows that the inversion with the KL expansion is outperformed by the inference with the full prior covariance matrix for such cases.

4.2.3.1 Impact of Measurement Error on the Estimation of Geostatistical Parameters

The measurement error σ_{s_Δ} of Eqs.(4.15)-(4.17) influences the spatial variability of the estimated hydraulic parameter fields. In the following, I take the estimation of the geostatistical parameters as an example to illustrate this influence. Following the sequential and alternating inversion procedure described in Section 2.9, I estimate $\hat{\sigma}_{\ln T}^2$, $\hat{\sigma}_{\ln S}^2$ and λ . Figure 4.4(a) shows the resulting correlation length λ as function of different values of σ_{s_Δ} . With increasing measurement error, I obtain an increasing value of λ , which smoothes the estimates of hydraulic parameters. The estimation of the correlation length is more vulnerable to the change of measurement error than the ones of the prior variances. For the measurement errors used, the estimated prior variances do not show significant changes. Therefore, I do not show the estimation results of $\hat{\sigma}_{\ln T}$ and

$\hat{\sigma}_{\ln S}$. Meanwhile, I calculate the values of the objective function according to Eq. (2.70), which decreases with increasing σ_{s_Δ} . The latter is to be expected because increasing σ_{s_Δ} implies that I trust the measurements less, and therefore an identical misfit between measured and simulated moments results in a smaller value of the objective function.

The influence of the measurement error on the estimation of prior variances becomes clear if I fix the correlation length λ . I take the estimated correlation length in Section 4.2.2 as fixed value of λ . Figure 4.4(b) displays the resulting $\hat{\sigma}_{\ln T}^2$ and $\hat{\sigma}_{\ln S}^2$ as function of the different values of σ_{s_Δ} . The prior variances decrease when σ_{s_Δ} increases, which smoothes the estimated fields of hydraulic parameters.

If the measurement error reflects the real uncertainty of the model, the value of the objective function should follow a χ^2 distribution with $2n_m$ degrees of freedom, where n_m is the number of temporal moment pairs. In our current studies, I have 169 pairs of measurements of temporal moments. In general the 95% confidence interval is used, which implies an interval between 320.11 and 390.82 for our case studies. Since large measurement error will smooth the estimated fields, it is preferable to choose a small measurement error within all acceptable ones. In the following, I have chosen $1.15mm$ as our measurement error σ_{s_Δ} .

In the illustrated examples in Figure 4.4, the estimated values of the prior variance of $\ln S$ are larger than the estimated values of the prior variance of $\ln T$. As I have discussed previously, the variance of $\ln S$ in natural confined system is thought to be small [e.g., Meier et al., 1998]. That is, I believe that the estimated variability of $\ln S$ is biased, like in the conventional pumping test analysis. Although the geostatistical inverse approach is consistent in the sense that the estimated variability of the hydraulic parameters is accounted for in all stages of the estimation procedure, the results of the storativity distribution appear not very reliable.

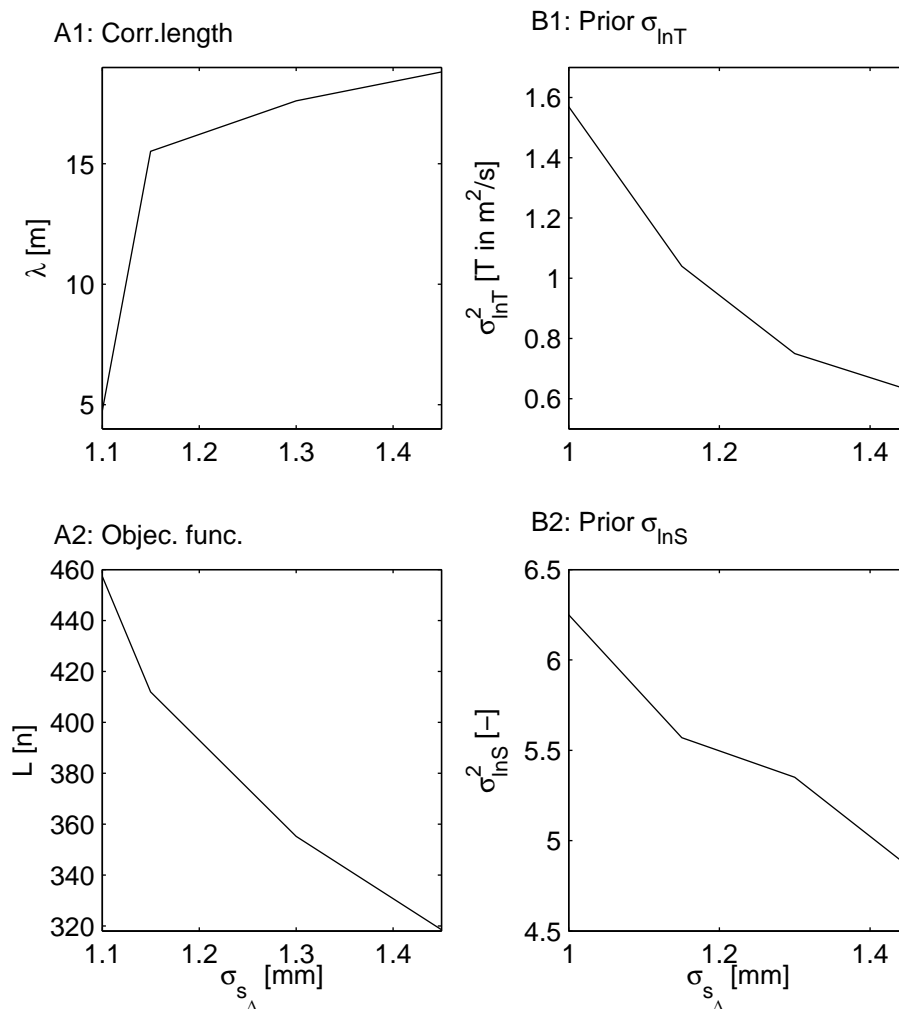


Figure 4.4: Influence of the measurement error on the inversion results. The horizontal axes are the measurement error used in the inverse procedure. A: estimation of geostatistical parameters with varying correlation length; A1: influence on the estimated correlation length; A2: influence on the value of objective function. B: estimation of geostatistical parameters with fixed correlation length; B1: influence on the estimated prior variance of $\ln T$; B2: influence on the estimated prior variance of $\ln S$.

4.2.3.2 Estimation with Uniform Storativity

Presuming that the variance of $\ln S$ is relatively small in nature, I now restrict the analysis to the case of a uniform value of storativity. Then, the prior variance of storativity and the cross-correlation between $\ln T$ and $\ln S$ become zeros.

To make the estimate of $\ln T$ more comparable with that in Section 4.2.2, I fix the correlation length using the value estimated from the pseudo-local values. Following the procedure as described previously, I estimate the spatial $\ln T$ distribution and, as remaining geostatistical parameter, its prior variance $\hat{\sigma}_{\ln T}^2$ given a uniform field of $\ln S$. The mean values of $\ln S$ and $\ln T$ are estimated as well.

As listed in Table 4.1, the estimated prior variance $\hat{\sigma}_{\ln T}^2$ of $\ln T$ for a uniform value of $\ln S$ is 1.57, and S is 0.006. These values are for a measurement error σ_{s_Δ} of 1.15 mm. Figure 4.5 shows the estimate of $\ln T$ -field and the corresponding standard deviation of estimation. In sub-figure 4.5-C, I plot the kriged $\ln T$ field of Section 4.2.2 in the same color scale as for the $\ln T$ distribution estimated in this section. Applying the geostatistical inverse approach, the estimated $\ln T$ field reveals more structure than interpolating the results of the pseudo-local values obtained by type-curve analysis. The estimated prior variance $\hat{\sigma}_{\ln T}^2$ is much higher than the one from the pseudo-local values. The improvement in revealing the structure of the $\ln T$ field is caused by the consistent assumption of heterogeneity in the geostatistical inverse approach.

The validity of the estimated fields is tested by analyzing the orthonormal residuals [Kitanidis, 1991]. If the model is correct, the sum of squares of orthonormal residuals of the measurements follows a χ^2 distribution. In my application, this value is 380.02, which is within the 95% confidence interval [320.11 – 390.82].

4.2.4 Comparison of Estimates

In this section, I compare the results from kriging of pseudo-local values (Section 4.2.2) to those from geostatistical inversion (Section 4.2.3.2). The estimated average properties, the variations of the estimated fields, and the uncertainties of the estimations are investigated.

I compute the mean values of the estimated fields of $\ln T$ and $\ln S$ from kriging and inversion. Table 4.1 lists these values. The mean values of $\ln T$ and $\ln S$ obtained by the conventional approach are almost identical to the ones of geosta-

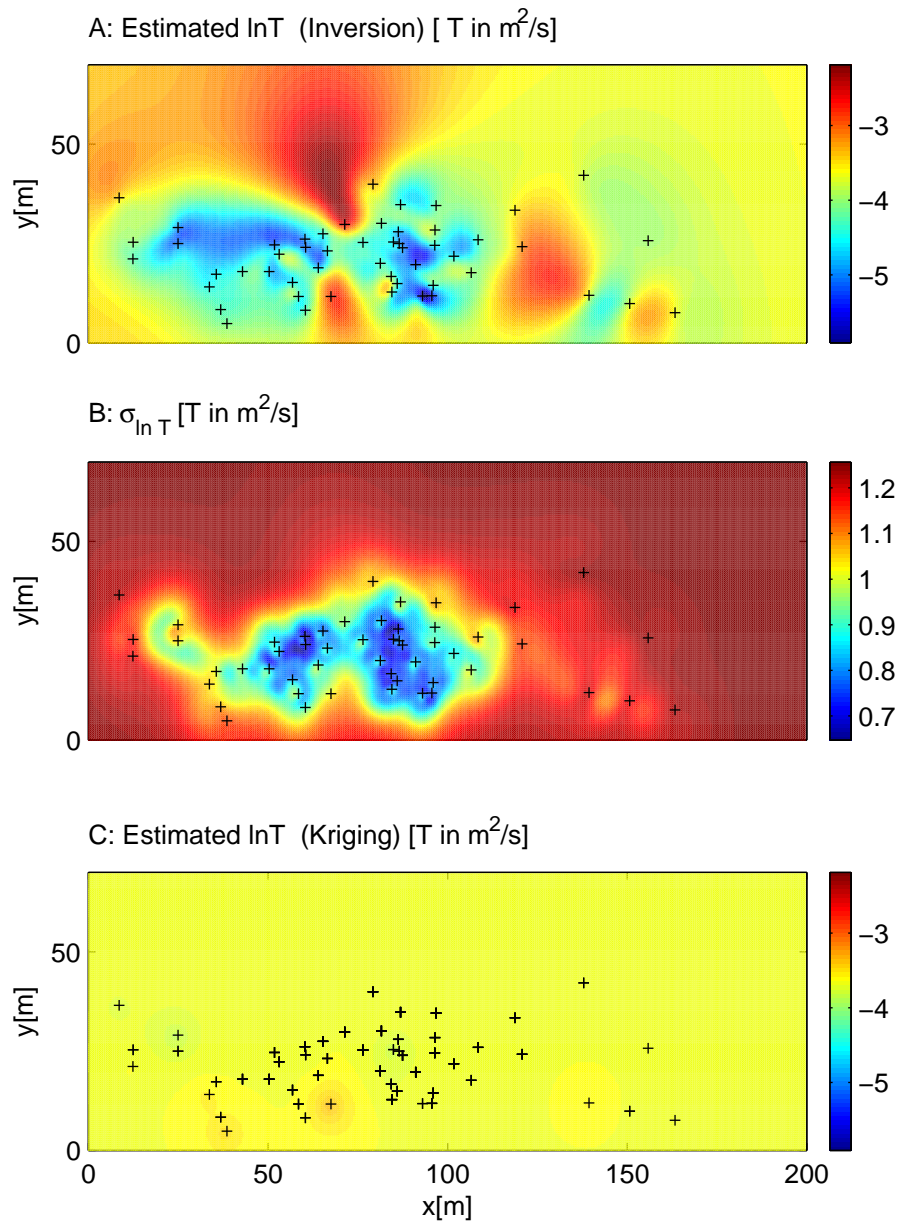


Figure 4.5: A: the most likely estimate of $\ln T$ from geostatistical inversion of the two-dimensional application; B: corresponding standard deviations of estimation; C: kriged $\ln T$ field based on pseudo-local values. Crosses are the well locations of all available pumping tests. The color scales for the two $\ln T$ fields are identical.

tistical inversion. That is, in my application conventional type-curve analysis of pumping tests leads to reliable estimates of the average properties. This is somehow consistent with the underlying assumption of uniformity in the type-curve

analysis.

I calculate the variances of the estimated $\ln T$ field for both kriged and inversed results. Table 4.1 lists the resulting variances. The variance of the resolved inversed $\ln T$ field is higher than the one obtained by kriging. Again, this is consistent with the underlying conceptual assumptions. In geostatistical inversion, I assume that $\ln T$ varies in space, and I try to resolve the fraction of heterogeneity that can unambiguously be identified from the data. In type-curve analysis, I start with the assumption of uniformity, but obtain results varying with the combination of pumping and monitoring wells, which is similar to the results of cross-hole pneumatic injection tests of Illman and Neuman [2003].

I may examine the estimated $\ln T$ values at the points of head measurements. Figure 4.6 shows a comparison of these values for the two types of analysis. The circles stand for the values obtained by geostatistical inversion. The error bars indicate the most likely estimate of $\ln T$ of the geostatistical inversion plus and minus one corresponding standard deviation of the estimate. The crosses denote the pseudo-local values obtained by the conventional method. With very few exceptions, the calculated pseudo-local values are within the acceptable confidence interval.

To quantify the difference between the two $\ln T$ fields throughout the domain, I compute a normalized root mean square error (NRMSE):

$$\text{NRMSE} = \sqrt{\frac{1}{n_e} \sum_{i=1}^{n_e} \frac{(p_i^{inv} - p_i^{kri})^2}{\sigma_{\ln T, c}^2}}, \quad (4.24)$$

where p_i is the estimated $\ln T$ value in element i , the index *inv* stands for the estimate of inversion, the index *kri* for that of interpolated pseudo-local values, and $\sigma_{\ln T, c}^2$ is the estimation variance of $\ln T$ in the inverse method. The value 0.5984 of NRMSE indicates that the values from the conventional approach can produce reasonable fields of hydraulic parameters, although most of the spatial variability is missing.

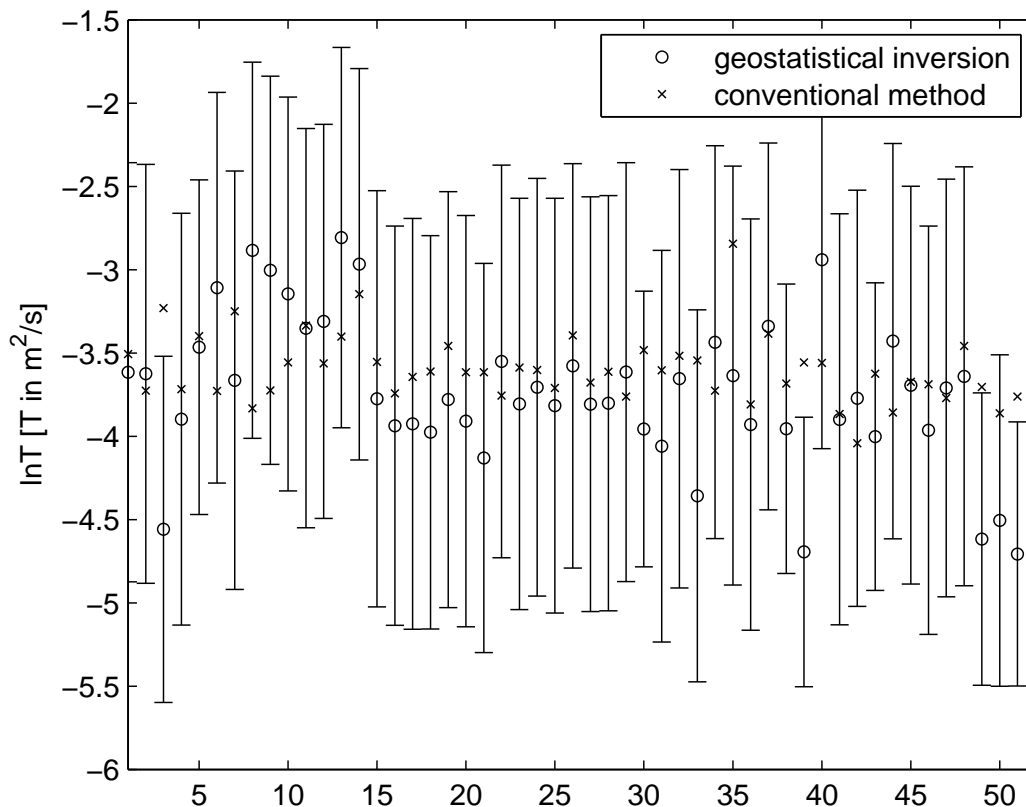


Figure 4.6: $\ln T$ at locations of head measurements. Circles indicate the estimated $\ln T$ values of the geostatistical inverse approach. Error bars correspond to \pm one standard deviation of estimation. Crosses stand for the calculated pseudo-local values of $\ln T$ obtained from the conventional method.

4.2.5 Summary

In this section, I have applied the geostatistical inverse approach to estimate the fields of transmissivity and storativity. The tomographic pumping tests conducted at the test site Krauthausen, Germany were used. In the inversion, I successively added new measurements to stabilize the inverse procedure. The inverted results were compared to the kriged fields of the values obtained by the conventional type-curve method.

Concerning the estimate of transmissivity $\ln T$, the geostatistical inverse approach obtains more structures in the estimated $\ln T$ field than the conventional approach and the variance of the resolved $\ln T$ field in the inversion is higher

than their counterparts using the conventional approach. The results show that the conventional approach provides good estimates of the mean hydraulic parameters, but fails to reproduce the spatial variability of the information. This indicates that kriging $\ln T$ values obtained by type-curve analysis may be acceptable in cases where detailed knowledge about the variability of the parameter fields is not required.

Regarding storativity, both approaches show a high value of estimated variance. In both estimations, I do not have prior information of the corresponding geostatistical parameters and they are purely inferred from measurements. Because variability of all terms making up storativity is small, the estimated high variance of storativity is conjectured to be biased. The measurements are not informative with respect to the estimation of the prior variance of storativity. I believe that this is an effect of aliasing. The estimated distribution of transmissivity is smoother than the real field. The unresolved variability, particular at small scales, has a large effect on the simulated first temporal moments, representing the characteristic time of drawdown, than the zeroth temporal moments, representing final drawdown. Given a smooth estimate of transmissivity, the inverse approach attributes the derived variability in first temporal moments to the variability of storativity. In the estimation, I assumed a two-dimensional aquifer. The unresolved vertical variability may also be a particular cause for the unrealistic results. Dealing with field data, I cannot exclude that conceptual uncertainties (e.g. regarding the validity of treating the system as a confined formation) may contribute to biased results.

It may be worth noting that - to my knowledge - no reliable information about the variability of storativity exists. *Meier et al.* [1998] among others conjectured that the variability should be small because of the small variability of the quantities making up storativity. Experimental data on the variability of $\ln S$, however, hardly exists. For the cases where experimental data of storativity are available, such as the joint estimation of Hendricks Franssen et al. [1999], the amount of measurements storativity is limited and cannot be representative for the whole field.

In this study, I have exclusively analyzed pumping test data, trying to estimate both hydraulic parameter fields and corresponding geostatistical parameters. I could show that the estimation of the geostatistical parameters depends on the uncertainty of the measured data. If I trust the measurements less, I obtain a larger correlation length and small variances, which smooth the estimated fields.

4.3 Three-Dimensional Estimation

In the two-dimensional field application in Section 4.2, a high variance of storativity is obtained and the high variance is believed to be biased. Although the two-dimensional assumption is consistent with data obtained in fully screened wells, the unresolved vertical variability may be a particular cause for the presumed bias in estimating the variability of storativity. Considering a three-dimensional inversion may help to reduce the aliasing effect.

Estimating three-dimensional structures requires that dependent supporting measurements, or at least joint data of different types of data, reflect three-dimensional information of aquifers. To my knowledge, the reliable estimation of storativity is mainly based on pumping tests. The pumping tests at the test site Krauthausen were conducted in fully screened wells. The measurements are depth-averaged and reflect only horizontal depth-averaged features of aquifers. This implies that the measurements of pumping tests, without considering other data containing vertical distribution of specific storage coefficient, are not suitable for estimating a three-dimensional field of specific storage coefficient. Although flowmeter data contain vertical distributions of aquifer features, these measurements reflect only the properties of hydraulic conductivity and do not contain vertical information of specific storage coefficient. Based on these considerations, I decide to only estimate a three-dimensional field of hydraulic conductivity by jointly considering the data of pumping and flowmeter tests. With this decision, I am no more able to test the hypothesis that a three-dimensional inversion may reduce the aliasing effect in estimating storativity. But it is still valuable to test the performance of the inverse approach in three-dimensional setup with a large

Table 4.1: Field and grid information of the two-dimensional application, prior and posterior information of hydraulic parameter fields in Section 4.2.2 and 4.2.3.2, and the results of comparison in Section 4.2.4.

Variable	Description	Value
<i>Field Domain and Grid Information</i>		
L_1	Domain width [m]	70
L_2	Domain length [m]	200
Δx_1	Grid spacing in x_1 [m]	0.5
Δx_2	Grid spacing in x_2 [m]	0.5
<i>Prior information about the mean of the fields</i>		
$\beta_{\ln T}^*$	Prior mean of trend coeff. of $\ln T$	-3.8
$\sigma_{\beta_{\ln T}^*}^2$	Uncertainty of $\beta_{\ln T}^*$	5.3
$\beta_{\ln S}^*$	Prior mean of trend coeff. of $\ln S$	-6.0
$\sigma_{\beta_{\ln S}^*}^2$	Uncertainty of $\beta_{\ln S}^*$	5.3
<i>Results of curve-fitting in Section 4.2.2</i>		
$\sigma_{\ln T, m}^2$	Variance of calculated $\ln T$ at wells	0.0349
$\sigma_{\ln S, m}^2$	Variance of calculated $\ln S$ at wells	0.6590
$\bar{\sigma}_{\ln T}$	Mean measurement error of $\ln T$	0.3288
$\bar{\sigma}_{\ln S}$	Mean measurement error of $\ln S$	0.9498
<i>Estimated geostatistical parameters in Section 4.2.2</i>		
$\dot{\sigma}_{\ln T}^2$	Estimated prior variance of $\ln T$ in Sec. 4.2.2	0.01
$FV_{\dot{\sigma}_{\ln T}^2}$	Factor of variation of $\dot{\sigma}_{\ln T}^2$	2.2
$\dot{\sigma}_{\ln S}^2$	Estimated prior variance of $\ln S$ in Sec. 4.2.2	0.24
$FV_{\dot{\sigma}_{\ln S}^2}$	Factor of variation of $\dot{\sigma}_{\ln S}^2$	1.62
$\dot{C}_{\ln T \ln S}$	Estimated prior cross-corr. coeff. between $\ln T$ and $\ln S$	0.35
$R_{\dot{C}_{\ln T \ln S}}$	Estimation variance of $\dot{C}_{\ln T \ln S}$	0.49
λ	Correlation length of covariance function [m]	5.21
FV_{λ}	Factor of variation of λ	2.46
<i>Sum of squares of orthonormal residuals r_n in Sec. 4.2.3.1</i>		
$\chi_{r_n}^2$	λ estimated $s_\delta = 1.15mm$	577.49
$\chi_{r_n}^2$	λ fixed $s_\delta = 1.15mm$	403.13
<i>Results in Section 4.2.3.2</i>		
$\dot{\sigma}_{\ln T}^2$	Estimated prior variance of $\ln T$	1.57
$FV_{\dot{\sigma}_{\ln T}^2}$	Factor of variation of $\dot{\sigma}_{\ln T}^2$	0.14
L	Value of objective function (Eq. 2.74)	380.04
$\chi_{r_n}^2$	Sum of squares of r_n	380.02
<i>Results of Comparison in Section 4.2.4</i>		
T_g	Geom. mean of est. $\ln T$ (Sec. 4.2.2)	-3.61
	Geom. mean of est. $\ln T$ (Sec. 4.2.3.2)	-3.65
S_g	Geom. mean of est. $\ln S$ (Sec. 4.2.2)	-5.81
	Geom. mean of est. $\ln S$ (Sec. 4.2.3.2)	-5.12
$\sigma_{\ln T, c}^2$	Variance of est. $\ln T$ (Sec. 4.2.2)	0.0004
	Variance of est. $\ln T$ (Sec. 4.2.3.2)	0.26
NRMSE	Normalized root mean square error (Eq. 4.24)	0.5984

number of unknowns. In the three-dimensional estimation of hydraulic conductivity³, I discretize the domain with about one million of unknowns. By doing such a performance test on large scales, potential problems can be identified, which could be used for improving the inverse approach in other applications.

Flowmeter data contain only relative values of hydraulic conductivity. In conventional analysis of flowmeter tests, the relative values must be converted to absolute ones [Javandel and Witherspoon, 1969]. For such purpose, the depth-averaged values of hydraulic conductivity at wells need to be known. To achieve these values, one has to rely on other tests such as slug tests or small-scale pumping tests. However, the converting will be difficult for wells, for which unfortunately extra tests are not available. If a measurement of the depth-averaged hydraulic conductivity at a particular well is missing, one may try to estimate it from values obtained nearby, e.g., from slug tests in different wells [e.g., Chen et al., 2001]. These estimated average values are then used to convert the relative hydraulic conductivities to absolute values.

Fienen et al. [2004] analyzed flowmeter tests using a geostatistical inverse method. Similar to conventional approaches, they need depth-averaged values of K at well locations. The depth-averaged values were considered as a known prior in the inference, which is an inconsistent requirement, because the mean value itself should be an outcome of the inversion. In some applications of geostatistical inversion, hydraulic conductivity values obtained by flowmeter tests are considered as direct measurements of local hydraulic conductivity [e.g., Rehfeldt et al., 1992; Chen et al., 2001]. To the best of my knowledge, these measurements are considered as independent values in the cited studies. The K estimates derived from flowmeter tests, however, are correlated, which needs to be accounted for in conditioning. In my thesis, I use discharge profiles of flowmeter tests as my data. By doing this, I do not need to convert the profiles to absolute hydraulic conductivity. Since the flowmeter data in a well are correlated, I fully consider their correlation in the inversion.

I organize this section as follows: First I demonstrate the concept of discharge

³This three-dimensional estimation study has been published by Li et al. [2008]

ratios. I will illustrate that discharge ratios and their sensitivities with respect to log hydraulic conductivity do not depend on the depth-average values at the well locations. Next, I show the numerical implementation and results. Here, I discuss the detailed inference procedure and present the final estimate and the corresponding estimation variance.

4.3.1 Discharge Ratios as Data of Flowmeter Tests

In this section, I introduce discharge ratios for flowmeter data and derive their sensitivities with respect to log hydraulic conductivity.

In the following, the ratio η_i (Eq. (4.2)) of the measured discharge in the i -th increment to the total discharge is denoted as discharge ratio. The vector of discharge ratios $\boldsymbol{\eta}$ does not explicitly depend on the depth-averaged value of hydraulic conductivity at the well location. Per flowmeter test, one vector $\boldsymbol{\eta}$ of discharge ratios is observed. Because $\boldsymbol{\eta}$ is a function of the differences of discharge rates between increments, the elements of $\boldsymbol{\eta}$ are correlated. I have to consider the correlation when defining the measurement error for $\boldsymbol{\eta}$.

For a particular flowmeter test, the sensitivity H_{ij} of the discharge ratio η_i with respect to the logarithm of hydraulic conductivity in cell j is zero everywhere except for the locations in the direct vicinity of the borehole where the test is conducted. I derive the corresponding H_{ij} based on Eq. (4.2) and (4.3):

$$\begin{aligned}
 H_{ij} &= \frac{\partial \eta_i}{\partial \ln K_j}, \\
 &= \frac{\frac{\partial K_i}{\partial \ln K_j} \bar{K} - K_i \frac{\partial \bar{K}}{\partial \ln K_j}}{\bar{K}^2}, \\
 &= \frac{\delta_{ij} K_i \bar{K} - K_i \frac{\partial \bar{K}}{\partial K_j} K_j}{\bar{K}^2}, \\
 &= \delta_{ij} \eta_i - \eta_i \frac{\Delta z_j}{b} \eta_j, \quad i, j = 1 \dots m_\eta,
 \end{aligned} \tag{4.25}$$

in which δ_{ij} is the Dirac delta function, which is one if $i = j$ and zero otherwise. As shown, the sensitivity of η with respect to the logarithm of hydraulic conductivity is not a function of the absolute hydraulic conductivity at the well location.

I compute the measurement error $\sigma_{\eta_i}^2$ of η_i through error propagation:

$$\sigma_{\eta_i}^2 = \frac{\sigma_{Q_i}^2 + \sigma_{Q_{i-1}}^2}{Q_p^2} + \frac{\eta_i^2}{Q_p^2} \sigma_{Q_p}^2, \quad (4.26)$$

in which $\sigma_{Q_i}^2$ is the variance of Q -measurements at the i -th increment, $\sigma_{Q_p}^2$ stands for the variance of the total discharge measurement, and I assume that the measurement errors between Q_i and Q_{i-1} are not correlated. The cross-correlation between the data of η is given by:

$$C_{\eta_i \eta_j} = \frac{\eta_i \eta_j}{Q_p^2} \sigma_{Q_p}^2 - \frac{\sigma_{Q_i}^2}{Q_p^2} \delta_{j,i+1} - \frac{\sigma_{Q_{i-1}}^2}{Q_p^2} \delta_{j,i-1}. \quad (4.27)$$

For my joint analysis, \mathbf{Z} is an aggregated vector:

$$\mathbf{Z} = \begin{bmatrix} \mathbf{s} & \boldsymbol{\eta} \end{bmatrix}^T, \quad (4.28)$$

in which \mathbf{s} denotes the measurements of steady-state drawdown of the small-scale pumping tests. In the inference, I compute the simulated drawdowns and their adjoint-state variables using the Finite Element Method on a regular grid. Based on the current hydraulic conductivity field, model outputs of the discharge ratios are simulated through Eqs. (4.2) and (4.3). The matrix of measurement error $\mathbf{R}_{\mathbf{ZZ}}$ is made of:

$$\mathbf{R}_{\mathbf{ZZ}} = \begin{bmatrix} \mathbf{R}_{\mathbf{ss}} & \mathbf{0} \\ \mathbf{0} & \mathbf{R}_{\boldsymbol{\eta}\boldsymbol{\eta}} \end{bmatrix}, \quad (4.29)$$

in which $\mathbf{R}_{\mathbf{ss}}$ is the matrix of measurement error of drawdowns and $\mathbf{R}_{\boldsymbol{\eta}\boldsymbol{\eta}}$ of discharge ratios. I compute $\mathbf{R}_{\boldsymbol{\eta}\boldsymbol{\eta}}$ using Eqs.(4.26) and (4.27). Here, matrix \mathbf{H} is

an aggregated matrix as well:

$$\mathbf{H} = \begin{bmatrix} \mathbf{H}^s \\ \mathbf{H}^\eta \end{bmatrix}, \quad (4.30)$$

where \mathbf{H}^s denotes the sensitivity matrix of drawdown with respect to log-hydraulic conductivity and \mathbf{H}^η the sensitivity matrix of discharge ratios given by Eq. (4.25).

4.3.2 Numerical Implementation and Results

I discretize the field on an orthogonal structured grid. The field dimensions and grid spacing used in the model are listed in Table 4.2. From the two-dimensional field study and preliminary investigation of the flowmeter data, I obtain the geostatistical parameters (Table 4.2) of log conductivity at the site. These parameters indicate that the field of hydraulic conductivity shows moderate heterogeneity with a strong horizontal to vertical anisotropy. State variables such as drawdown are simulated using the Finite Element Method. Here, the steady-state groundwater flow equation (Eq. (2.10) but without the storage term) with short-cut boundaries at wells were applied. The sensitivities of drawdown with respect to log conductivity are computed by the efficient adjoint-state method [Sun and Yeh, 1990]. In principle, one prefers to use grids allowing regional refinements around wells for pumping tests, rather than a regular grid. However, for unstructured grids, the efficient FFT methods for the evaluation of the covariance matrix [Nowak et al., 2003] will fail. For my application with 1.1 millions of unknowns, the evaluation of the covariance matrix on unstructured grids is computationally prohibitive. Although the application of the Karhunen-Loève expansion to approximate the covariance function enables using an unstructured grid with a large number of unknowns, previous two-dimensional studies (Chapter 3) have shown that the results on a regular grid are very close to the values on an unstructured one [Li and Cirpka, 2006]. Based on these considerations, I apply a regular grid for my inverse model.

Table 4.2: Geometric and geostatistical parameters used in the joint inversion

Variable	Description	Value
<i>Field Domain and Grid Information</i>		
L_1	Domain width [m]	70
L_2	Domain length [m]	200
L_3	Domain length [m]	8
Δx_1	Grid spacing in x_1 [m]	1
Δx_2	Grid spacing in x_2 [m]	1
Δx_3	Grid spacing in x_3 [m]	0.1
<i>Geostatistical Parameters</i>		
σ^2	prior variance of $\log_{10} K$ [K in m/s]	0.32
β^*	prior mean of $\log_{10} K$ [K in m/s]	-2.8
λ_1	correlation length in x_1 direction [m]	5.3
λ_2	correlation length in x_2 direction [m]	5.3
λ_3	correlation length in x_3 direction [m]	0.23

Since I use drawdown in my inversion, the influence of ambient flow is eliminated. In small-scale pumping tests, I did not observe signals of drawdown on the horizontal edges of the field, because the field dimension is much larger than the radius of influence of the small-scale pumping tests. Based on these observations, I apply zero-drawdown boundary conditions on the boundaries forming vertical faces and no-flux boundary conditions on the top and bottom of the aquifer. The drawdown during the small-scale pumping tests was considerably smaller than the water-saturated thickness of the aquifer. Hence, it is permissible to analyze the steady-state pumping data assuming confined conditions.

In a flowmeter test, the sensitivity of incremental flux Q_i with respect to log-hydraulic conductivity is focused and decreases dramatically with increasing distance from the measurement location. The sensitivity approximately scales with $1/r^2$, where r is the distance to the measurement location. If near-well anomalies are not in the direct vicinity of the operating well, they hardly influence the flowmeter measurements. In this model, I apply a resolution of one meter in the horizontal directions. One single column of elements at the well location could capture most information of the flowmeter tests.

In my inverse procedure, I account for the small-scale pumping tests and flowmeter tests in a sequential way. Like the procedure in the two-dimensional estimation of Section 4.2, I begin with a single small-scale pumping test and all the flowmeter tests. Once optimal values of hydraulic conductivity are obtained, I add further pumping-test data to the joint inversion, using the estimate from the previous step as initial guess for the following estimate. In each of these steps, all flowmeter data and an increasing number of pumping-test data are jointly inverted. I repeatedly add pumping-test data until all are used. In total, 175 measurements of drawdown and 808 observations of flowmeter data are considered.

The CPU time to estimate the approximately 1.1 million log-conductivity values was around 50 hours on a 3GHz dual core PC operating under Linux. Figure 4.7 displays the resulting fields of log-conductivity and its posterior uncertainty. Here, I select three vertical cross-sections cutting through wells. Figure 4.7a shows log-hydraulic conductivity after joint inversion of pumping-test and flowmeter data. The contour lines on the bottom describe the distribution of depth-averaged values. Figure 4.7b shows the standard deviation of estimation. Again, the contour lines display the corresponding depth-averaged values. In Figure 4.7, the gray vertical lines and the crosses indicate the locations of wells used for pumping tests. And the black vertical lines and the circles are the well locations in flowmeter tests.

In Figure 4.7a, one clearly sees that the three-dimensional structure of hydraulic conductivity can only be revealed in the vicinity of wells where flowmeter tests were performed. In regions where only pumping test data exist, the estimated log-conductivity field becomes vertically uniform. Figure 4.7b shows that the remaining uncertainty of the estimated log-hydraulic conductivity field decreases considerably near the wells used for flowmeter tests. That is, by adding flowmeter data to the inversion of pumping tests, the remaining uncertainty of hydraulic conductivity is reduced while vertical resolution is gained. I examine the variability of the obtained hydraulic conductivity near the wells used in flowmeter tests. For this purpose, I compute the variance of $\log_{10} K$ for all elements that

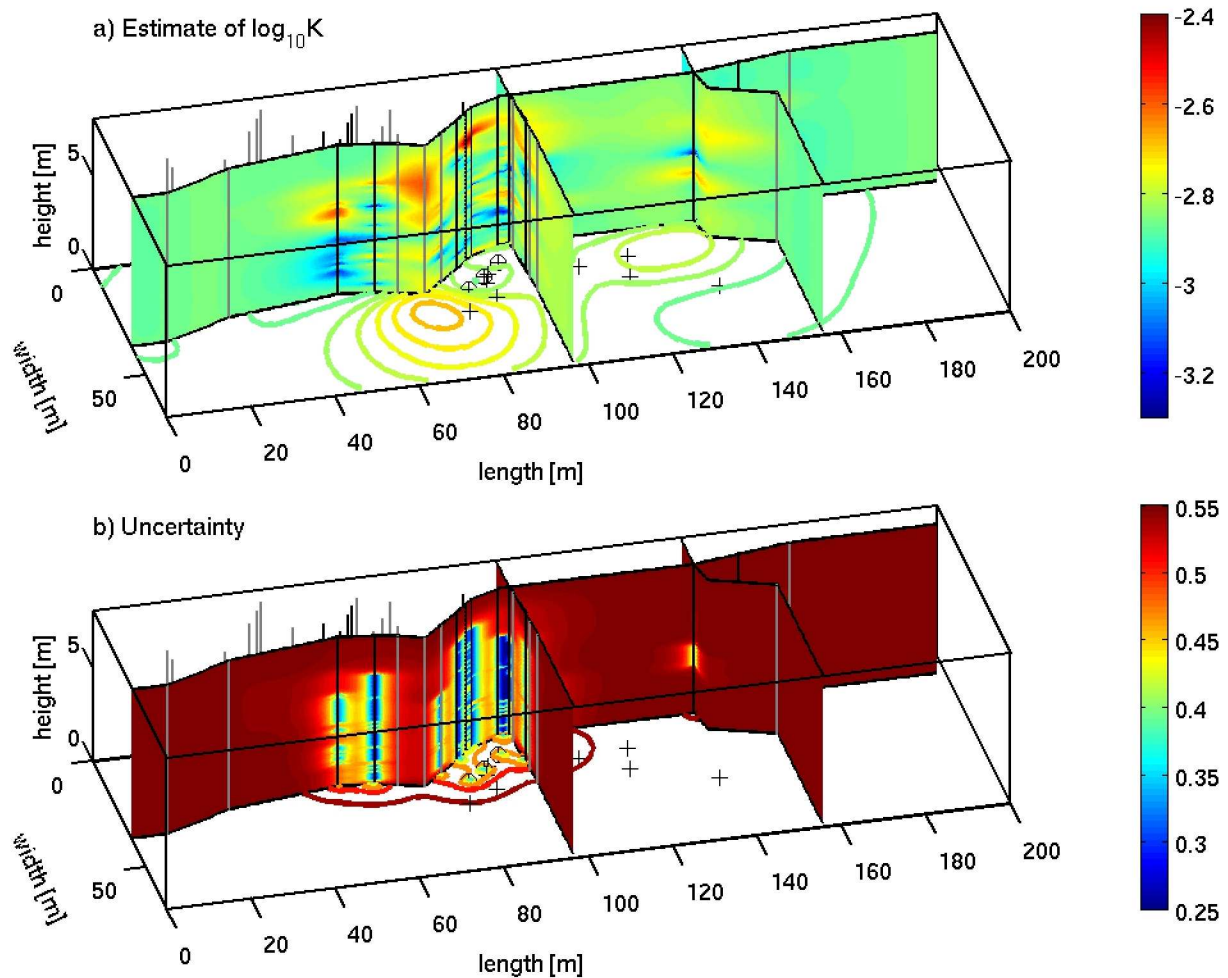


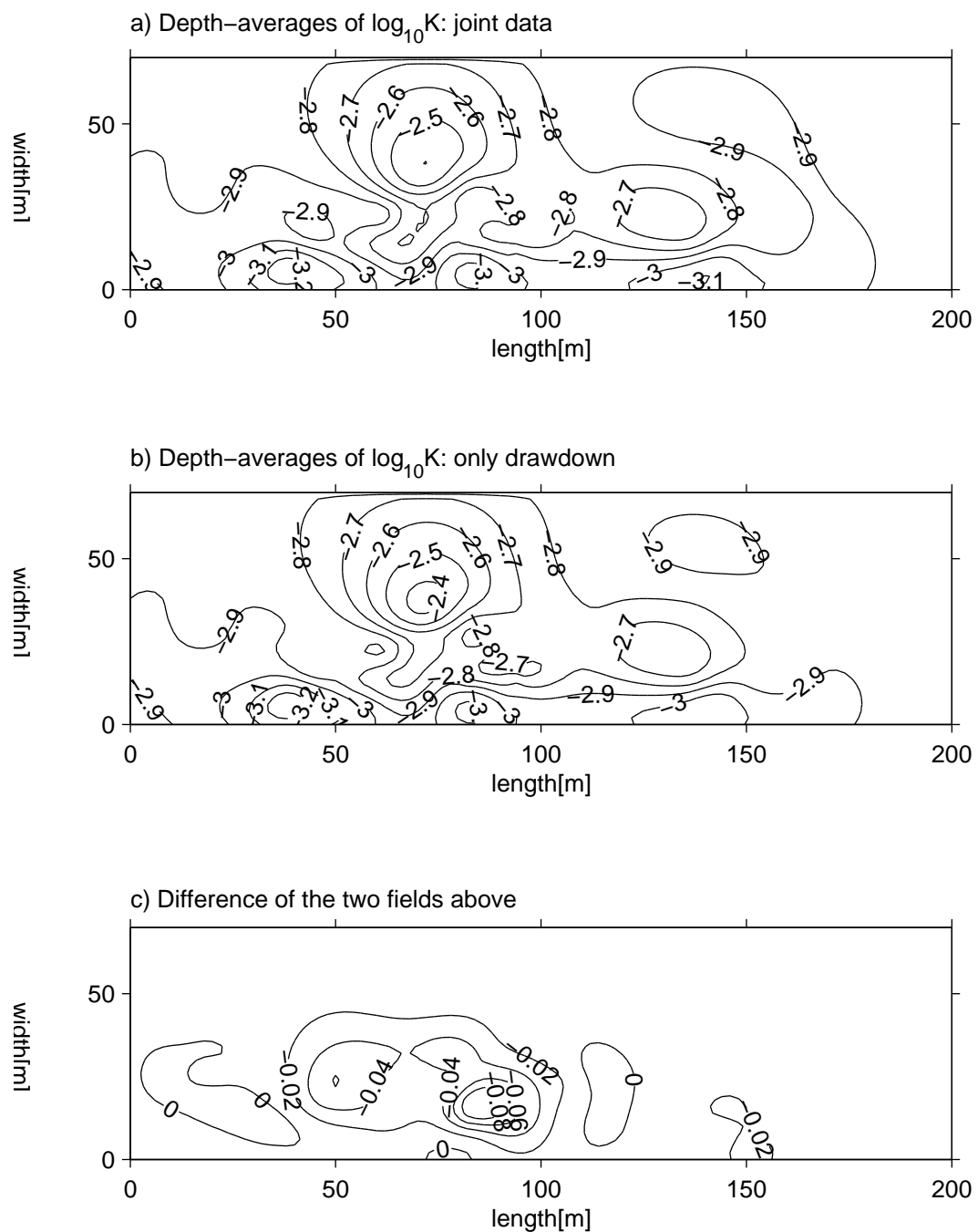
Figure 4.7: Results of joint geostatistical inversion of flowmeter and pumping-test data. Sub-figure a) is the estimate of $\log_{10}K$ with joint data of flowmeter and pumping tests; sub-figure b) displays the standard deviation of estimation of $\log_{10}K$ with joint data. Vertical black solid lines and the circles are the locations of the wells in flowmeter tests; and the vertical gray lines and the crosses indicate the positions of the wells used in multiple pumping tests. Contour lines display the corresponding depth-averaged values.

are less than one correlation length away from such wells. The resulting variance is 0.06, which is considerably higher than 0.03, the variance of the entire estimated field. This confirms that resolution in the inversion is gained by adding flowmeter data to the pumping-test data.

In Figure 4.8, I plot the fields of depth-averaged log-conductivities inferred from

joint inversion of flowmeter and pumping-test data in comparison to the estimate derived from drawdown only. The patterns of depth-averaged log-conductivity are almost identical in both cases. Figure 4.8c displays the difference of the two fields. The root mean square of the difference between the two fields is 0.086, indicating that the drawdown data provide a good estimate of the depth-averaged properties. In my test case, flowmeter data affect almost only vertical fluctuations of log-conductivity in the inversion. These vertical fluctuations in turn hardly affect the simulated drawdown in the fully penetrated wells, so that, in my application, the depth-averaged conductivity could be inferred from pumping-test data alone.

The validity of the estimate can be statistically tested by considering the orthonormal residuals [Kitanidis, 1991]. The sum of the squared orthonormal residuals should follow a χ^2 distribution with n_m degrees of freedom, where n_m is the number of measurements. For my test, the sum is 1056 which is within the 95% confidence interval for statistical validation, however, does not guarantee that the obtained estimate is sufficient for detailed predictive modeling. As is seen in Figure 4.7a, the three-dimensional structure of the subsurface is revealed only in the direct vicinity of wells used in flowmeter tests. Eliminating a flowmeter test from my data base would result in an estimate lacking vertical resolution at the corresponding well. Because the associated estimation variance would also increase, measured flowmeter data at a well not included in the estimation would most likely remain within the predicted uncertainty bounds. That is, statistical cross-validation is possible, but there are no redundant measurements. Any estimate with a reduced data set will result in deteriorated identification of subsurface structure. This makes validation beyond statistical tests difficult. At the field site, tracer tests have been performed. These data could be used for additional verification. A detailed analysis, whether the number of flowmeter tests performed at the site is already sufficient to predict the tracer test, however, is beyond the scope of the present study.



4.3.3 Summary

I have applied the Quasi-Linear Geostatistical Inverse Approach to estimate a three-dimensional field of hydraulic conductivities with about one million unknowns. With the help of efficient spectral methods of computing large matrix-matrix products and adjoint-state method of computing sensitivity matrices, I obtained the three-dimensional estimate on a personal computer within two days.

The most likely estimate of three-dimensional hydraulic conductivity is obtained by joint inversion of flowmeter and pumping-test data. By integrating flowmeter data to pumping-test analysis, I overcome the disadvantage of providing only depth-averaged aquifer properties when pumping tests are performed using fully screened wells. The resulting estimate shows a significant improvement in identifying three-dimensional structures, especially for the regions where flowmeter tests are available. The uncertainties of the estimates in these regions are significantly decreased. However, for the regions where only pumping tests are available, the estimates become vertically uniform and the uncertainties are high. The inversion of pure drawdown data lacks vertical resolution, but provides a good estimate of the depth-averaged hydraulic conductivity.

Chapter 5

Conclusions and Outlook

5.1 Main Findings

Using the Karhunen-Loève(KL) expansion as parameterization of the spatial log-conductivity fluctuations, I have derived, implemented and successfully applied a geostatistical inverse method for the identification of the spatial log-conductivity distribution from measurements of heads. By periodic embedding, I have made spectral methods accessible to the derivation of the base functions used in the approach. These base functions are continuous in space and can be discretized by any type of grids. Although the numerical derivation of the base functions employs spectral operations, I am not restricted to regular grids in the discretization of the domain. Test cases have shown that the inverse approach with a limited number of KL terms can produce almost identical estimate with the inverse approach applying the full covariance matrix. The inverse approach with the KL expansion appears to be the most efficient method on unstructured grids.

I have implemented the geostatistical inverse approach in estimating two-dimensional fields of transmissivity and storativity with transient drawdown data and inferring a three-dimensional field of hydraulic conductivity given measurements of pumping tests and flowmeter data. For the two-dimensional implementation, I have compared the inversed results with the values obtained by

the conventional type-curve approach. Results show that the geometric means of transmissivity and storativity by both approaches are almost identical. Regarding the estimate of transmissivity, due to more consistent assumptions of the geostatistical inverse approach about the variability of aquifers, the inversed fields show more variations than the interpolated fields that are interpolated by the values obtained from the conventional type-curve approach. The conventional approach may provide acceptable estimates when detailed variability of aquifers is not required. Structures obtained in the inversion are focused in the regions where wells are used for pumping tests. Uncertainties of the estimate are reduced in the areas around wells. With respect to the estimate of storativity, both approaches show unrealistic high value of estimated variance. My estimates are smooth. The unresolved variabilities at small scales may be the major cause of this biased result. In my estimation, the aquifer is assumed two-dimensional. This assumption is consistent with data obtained in fully screened wells. The unresolved vertical variability, however, may also be one cause for the presumed bias in estimating the variance of storativity.

Estimating a three-dimensional field of specific storage coefficient requires necessary measurements that can provide relevant three-dimensional information. Unfortunately, the drawdown measurements at the test site are depth averaged. Without jointly considering other measurements, which contain vertical distributions of specific storage coefficient, the depth-averaged transient drawdown are not suitable for inferring a three-dimensional field of storage coefficient. Based on these considerations, I did not estimate the field of specific storage coefficient in the three-dimensional implementation, but focused on the estimation of hydraulic conductivity.

In the three-dimensional estimation with about one million parameters, I obtain the three-dimensional estimate of hydraulic conductivity and its conditional uncertainty on a standard personal computer within about two days. This performance is made possible mainly by applying the spectral methods of computing large matrix-matrix products and convenient adjoint-state method of computing sensitivity matrices. I overcome the disadvantage of providing only depth-

averaged aquifer properties when pumping tests are performed in fully screened wells. The vertical distributions of hydraulic conductivity are obtained by considering flowmeter data. The resulting estimate shows a significant improvement of identifying three-dimensional structures in the vicinity of the wells used for flowmeter tests. The corresponding uncertainties of the estimate are decreased at the well locations of flowmeter tests. In contrast, in the regions where only pumping tests were conducted, the estimated field becomes vertically uniform. Flowmeter data are related to local hydraulic conductivity values. Thus, in geostatistical inverse models, flowmeter data lead to modifications of the estimated conductivity field up to the distance about one correlation length.

For estimating hydraulic conductivity, transient data of drawdown are not required; the conductivity field is inferred from final steady-state drawdown alone. Transient head measurements would be required in the estimate of specific storage coefficient. Although the flowmeter tests contain information only about hydraulic conductivities, the measured data have the potential to improve the estimate of specific storage coefficient, because the transient drawdown depends on both hydraulic conductivity and specific storage coefficient. Any improvement in estimating hydraulic conductivity will reduce the chance of aliasing unresolved conductivity to storativity, thus leading to more reliable estimate of specific storage coefficient.

5.2 Recommendations

The efficient spectral methods for computing cross-covariance matrices are restricted to regular structured grids and not applicable for unstructured grids. In contrast, parameterization with the KL expansion does not distinguish different discretization schemes. With equivalent numbers of nodes and elements on structured regular grids, the inverse approach with the full covariance matrix outperforms the one with the KL expansion. Since computational effort is one of the major concerns in numerical implementations, one has to make a decision based on the needs of particular cases. I recommend that a performance

analysis can be conducted before implementation. Questions, such as whether the estimate is sensitive to different discretization schemes and grid resolutions, can be answered. The basic principle is that one should apply sufficient fine resolution in numerical studies. With defined grid resolution, one could select regular grids and the inverse approach with the full covariance matrix if the estimate is not sensitive to different grids. But if estimates need grid refinement, namely if they are very sensitive to local grid resolution, one should estimate the fields using the inverse approach with the KL expansion. The parameterization by the KL expansion is highly recommendable for the cases with a smooth covariance function, particularly with large correlation lengths. For such cases, the KL expansion can be truncated after a few terms.

Obtaining reliable estimates of hydrogeological parameters depends not only on a proper inference approach, but also an efficient data-acquisition technique. In the two- and three-dimensional field applications, structures are obtained only in the regions where wells are available. Uncertainties in the regions that are far from the testing wells are high. To identify the spatial structure of the fields, about one measurement per correlation length is required. Traditional hydraulic tests, such as pumping and flowmeter tests, are expensive due to high costs in constructing wells. Other efficient data-acquisition techniques seem necessary. To obtain measurements in a wide range, the recent developed direct-push techniques such as permeameter tests [Butler et al., 2007] can be applied. The measurements of such direct-push tests are very useful for three-dimensional parameter estimation. Because the technique can quickly be performed in a large area at different depths, one can obtain a large number of measurements within a manageable time. In addition, the cost of direct-push is comparably lower than that of constructing conventional wells. As alternative to direct hydraulic observations, one may make use of non-intrusive geophysical monitoring techniques such as electrical resistivity tomography (ERT) applied during salt-tracer tests [Binley et al., 1996; 2002; Slater et al., 2000; Kemna et al., 2002; Vanderborght et al., 2005; Singha and Gorelick, 2005]. It is mandatory, however, that these data are analyzed under full consideration of underlying laws of flow

and transport. Sequential inversion, in which geophysical data have been used for imaging, and these image were subsequently analyzed in hydrogeological context, has failed [Singha and Gorelick, 2005].

The restricted maximum likelihood method by Kitanidis [1995]) of estimating geostatistical parameters such as the variance and the correlation lengths of covariance functions works well only for cases with a small variance. The resulting values of geostatistical parameters for cases with a high variance may be biased. To obtain right geostatistical parameters when the variance is high, one needs to work with conditional realizations that show similar variations as the true fields. For this purpose, the Expectation Maximization(EM) [Dempster et al., 1977] algorithm is suitable. The EM algorithm generates a set of conditional realizations of the hydrogeological parameters given measurements and a current estimate of geostatistical parameters. Then, the conditional realizations are used to optimize the values of geostatistical parameters. With updated geostatistical parameters, a new set of conditional realizations are generated. This procedure continues until the changes of geostatistical parameters are sufficient small.

Various methods of generating conditional realizations exist. The most prominent methods include the approach based on Cholesky decomposition of the conditional covariance matrix [Harvey and Gorelick, 1995a], the method of smallest modification of unconditional realizations [Kitanidis, 1995], the Pilot-Point Method of RamaRao et al. [1995], and the method of Sequential Self-Calibration of Sahuquillo et al. [1992]. Due to its simplicity, the approach with Cholesky decomposition is recommendable when the dimension of the covariance matrix is low. However, when the dimension is high, one has to rely on other approaches. In the method of smallest modification of unconditional realizations, an unconditional realization is corrected by smooth functions, so that measurements are met [Kitanidis, 1995]. This method leads to equations formally identical to the ones of the Quasi-Linear Geostatistical Inverse Approach [Kitanidis, 1995], implying that the accelerating and stabilizing techniques of the latter approach can directly be applied to generate conditional realizations. The computational cost of a conditional realization is equivalent to finding the most likely estimate of the

latter approach. Since this approach is theoretically rigorous, it is highly recommendable. Because of computational efficiency, the Pilot-Point Method of RamaRao et al. [1995] and the method of Sequential Self-Calibration of Sahuquillo et al. [1992] can be good choices.

The most likely estimate of the inverse approach is smooth. When the functional relationship between the measurements and the parameters is linear, this estimate is identical to the mean of conditional realizations. However, for cases with strong nonlinearity, the most likely estimate differs from the conditional mean. In such cases, one may rely on other methods such as the generation of conditional realizations discussed above or inverse approaches with high-order approximations like the Stochastic Moment Analysis Method by Hernandez et al. [2006], which are computationally more demanding than the Quasi-Linear Geostatistical Inverse Approach [Kitanidis, 1995].

The Quasi-Linear Geostatistical Inverse Approach [Kitanidis, 1995] is exclusively tested using Matlab on normal personal computers. It will be of great interest to perform the inverse method also on parallel computers using other advanced computer languages. This may be relevant for large regional groundwater models. It will be very useful to identify the feasibility of the inverse approach for such problems where the topographic setup of the subsurface and interaction with surface water models need to be considered.

The presented inverse approach is a mathematical model that requires strong knowledge of statistics and numerics. The code comes without a user-friendly interface. This implies that the model is used only by a small group of researchers, but not by consultants, regulators or other water-resource managers. To extend the applicability of the model, one needs to encapsulate the inferring kernel in such a way that the users can interact with the kernel but do not need to know the mathematical details. The users eventually obtain their estimates by providing the corresponding field setup and available measurements. The outcomes are easily readable maps of the estimate of the subsurface and the corresponding uncertainty as well.

5.3 Concluding Remarks

With the Quasi-Linear Geostatistical Inverse Approach and its modifications, one can obtain reliable estimates of spatial distributions of hydrogeological parameters on large scales with a reasonable computational effort if a sufficient number of measurements with required support volumes are provided.

5.4 Future Research

In the three-dimensional estimation, I did not estimate the field of specific storage coefficient due to lack of measurements with suitable support volumes. The hypothesis that a three-dimensional inversion may reduce the aliasing effect in estimating storativity has not been tested. In order to verify this presumption, one may conduct a virtual three-dimensional inversion with synthetic data, in which the fields of hydraulic conductivity and specific storage coefficient are generated using the spectral method of Dietrich and Newsam [1993] and hydraulic aquifer tests are numerically performed as the test cases in Chapter 3. Since one has perfect knowledge on the setups of the fields including boundary conditions, the potential causes of erroneous model setup can be eliminated. In such three-dimensional estimation, one can systematically investigate the effect of increased resolved variability of estimated hydrogeological parameters on estimation of geostatistical parameters. By doing this, the hypothesis that the unresolved variabilities may be the major cause of obtaining a high value of estimated storativity can be tested.

Other measurements, such as geophysical/geochemical data and solute concentration, are important indicators of groundwater and aquifer properties. Integrating these data in the inversion can help improve the descriptions of the subsurface. This may also be a research topic of extending the inverse approach.

Bibliography

- M. Bakker, K. Maas, F. Schaars, and J. R. von Asmuth. Analytical modeling of groundwater dynamics with an approximate impulse response function for areal recharge. *Advances Water Resour.*, 30:493–504, 2007.
- S. Barnett. *Matrices Methods and Applications*. Oxford Applied Mathematics and Computing Science Series. Clarendon Press, Oxford, 1990.
- A. F. Bennett. *Inverse Methods in Physical Oceanography*. Cambridge Uni. Press, Cambridge, 1992.
- A. Binley, S. Henry-Poulter, and B. Shaw. Examination of solute transport in an undisturbed soil column using electrical resistance tomography. *Water Resour. Res.*, 32(4):763–769, 1996.
- A. Binley, G. Cassiani, R. Middleton, and P. Winship. Vadose zone flow model parameterisation using cross-borehole radar and resistivity imaging. *J. Hydrol.*, 267(3-4):147–159, 2002.
- G. C. Bohling. Hydraulic tomography in two-dimensional, steady-state groundwater flow. *Eos Trans. AGU*, 74(16), 1993. Spring Meet. Suppl. 141.
- J. J. Butler and W. Z. Liu. Pumping tests in nonuniform aquifers: The radially asymmetric case. *Water Resour. Res.*, 29(2):259–269, 1993.
- J. J. Butler, P. Dietrich, V. Wittig, and T. Christy. Characterizing hydraulic conductivity with the Direct-Push Permeameter. *Ground Water*, 45(4):409–419, 2007.

- J. Carrera and S. P. Neuman. Estimation of aquifer parameters under transient and steady state conditions: 1. maximum likelihood method in incorporating prior information. *Water Resour. Res.*, 22(2):190–210, 1986a.
- J. Carrera and S. P. Neuman. Estimation of aquifer parameters under transient and steady state conditions: 2. uniqueness, stability and solution algorithms. *Water Resour. Res.*, 22(2):211–227, 1986b.
- J. Carrera and S. P. Neuman. Estimation of aquifer parameters under transient and steady state conditions: 3. application to synthetic and field data. *Water Resour. Res.*, 22(2):228–242, 1986c.
- J. S. Chen, S. Hubbard, and Y. Rubin. Estimating the hydraulic conductivity at the South Oyster Site from geophysical tomographic data using Bayesian techniques based on the normal linear regression model. *Water Resour. Res.*, 37(6):1603–1613, 2001.
- O. A. Cirpka and P. K. Kitanidis. Sensitivity of temporal moments calculated by the adjoint-state method and joint inversing of head and tracer data. *Advances Water Resour.*, 24(1):89–103, 2000.
- O. A. Cirpka and W. Nowak. First-order variance of travel time in non-stationary formations. *Water Resour. Res.*, 40(3):W03507, 2004. doi: 10.1029/2003WR002851.
- N. A. C. Cressie. *Statistics for spatial data*. John Wiley & Son, New York, 1991.
- G. Dagan. Stochastic modeling of groundwater flow by unconditional and conditional probabilities, 1. conditional simulation and the direct problem. *Water Resour. Res.*, 18:1571–1585, 1982.
- G. Dagan. *Flow and Transport in Porous Media*. Springer Verlag, New York, 1989.
- G. De Marsily, C. Lavedan, M. Boucher, and Fasanino G. Interpretation of interference tests in a well field using geostatistical techniques to fit the per-

- meability distribution in a reservoir model. In G. Verly, M. David, G. Journel, and A. Marechal, editors, *in Geostatistics for Natural Resources Characterization*, pages 831–849. NATO ASI Ser, Ser C, 1984.
- J. F. Delhomme. Spatial variability and uncertainty in groundwater flow parameters: A geostatistical approach. *Water Resour. Res.*, 15(2):269–280, 1979.
- A. P. Dempster, N. M. Laird, and D. B. Rubin. Maximum likelihood from incomplete data via the em algorithm. *J. Roy. Statist. Soc. Ser. B*, 39:1–38, 1977.
- C. R. Dietrich and G. N. Newsam. A fast exact method for multidimensional Gaussian stochastic simulations. *Water Resour. Res.*, 29(8):2861–2869, 1993.
- M. N. Fienen, P. K. Kitanidis, D. Watson, and P. Jardine. An application of Bayesian inverse methods to vertical deconvolution of hydraulic conductivity in a heterogeneous aquifer at Oak Ridge National Laboratory. *Math. Geol.*, 36(1):101–126, 2004.
- R. A. Freeze. Regionalization of hydrogeologic parameters for use in mathematical models of groundwater flow. *Hydrogeology*, 1972.
- R. A. Freeze. A stochastic-conceptual analysis of one-dimensional groundwater flow in nonuniform homogeneous media. *Water Resour. Res.*, 11(5):725–741, 1975.
- E. O. Frind and G. F. Pinder. Galerkin solution to the inverse problem for aquifer transmissivity. *Water Resour. Res.*, 9(5):1397–1410, 1973.
- R. Ghanem. Scales of fluctuation and the propagation of uncertainty in random porous media. *Water Resour. Res.*, 34(9):2123–2136, 1998.
- R. Ghanem and P. D. Spanos. *Stochastic Finite Element: A Spectral Approach*. Springer-Verlag, New York, 1991.

- J. W. Gibbs. *Elementary Principles in Statistical Mechanics*. Yale University Press, Yale, 1902.
- J. J. Gómez-Hernández and X. H. Wen. To be or not to be multi-Gaussian? A reflection on stochastic hydrogeology. *Advances Water Resour.*, 21(1):47–61, 1998.
- J. J. Gómez-Hernández, A. Sahuquillo, and J. E. Capilla. Stochastic simulation of transmissivity field conditional to both transmissivity and piezometric data. 1. theory. *J. Hydrology*, 203:162–174, 1997.
- J. Gottlieb and P. Dietrich. Identification of the permeability distribution in soil by hydraulic tomography. *Inverse Problems*, 11(2):353–360, 1995.
- R. M. Gray. On the asymptotic eigenvalue distribution of toeplitz matrices. *IEEE Trans. Infom. Theory*, 18(6):725–730, 1972.
- C. F. Harvey and S. M. Gorelick. Mapping hydraulic conductivity: Sequential conditioning with measurements of solute arrival time, hydraulic head, and local conductivity. *Water Resour. Res.*, 31(7):1615–1626, 1995a.
- C. F. Harvey and S. M. Gorelick. Temporal moment-generating equations: modeling transport and mass-transfer in heterogeneous aquifers. *Water Resour. Res.*, 31(8):1895–1911, 1995b.
- H. J. Hendricks Franssen, J. J. Gomez-Hernandez, J. E. Capilla, and A. Sahuquillo. Joint simulation of transmissivity and storativity fields conditional to steady-state and transient hydraulic head data. *Advances Water Resour.*, 23(1):1–13, 1999.
- A. F. Hernandez, S. P. Neuman, A. Guadagnini, and J. Carrera. Inverse stochastic moment analysis of steady flow in randomly heterogeneous media. *Water Resour. Res.*, 42:W05425, 2006. doi: 10.1029/2005WR004449.
- M. R. Hestenes and E. Stiefel. Methods of conjugate gradients for solving linear systems. *J. Res. Nat. Bur. Standards*, 49(6):409–436, 1952.

- W. A. Illman and P. S. Neuman. Steady-state analysis of cross-hole pneumatic injection tests in unsaturated fractured tuff. *J. Hydrol.*, 281:36–54, 2003.
- A. I. James, W. D. Graham, K. Hatfield, P. S. C. Rao, and M. D. Annable. Optimal estimation of residual non-aqueous phase liquid saturations using partitioning tracer concentration data. *Water Resour. Res.*, 33(12):2621–2636, 1997.
- I. Javandel and P. A. Witherspoon. A method of analyzing transient fluid flow in multilayered aquifer. *Water Resour. Res.*, 5:856–869, 1969.
- A. J. Journel and C. J. Huijbregts. *Mining Geostatistics*. Academic Press, London, 1978.
- A. Kemna, J. Vanderborght, B. Kulesa, and H. Vereecken. Imaging and characterisation of subsurface solute transport using electrical resistivity tomography (ERT) and equivalent transport models. *J. Hydrol.*, 267(3-4):125–146, 2002.
- P. K. Kitanidis. Orthonormal residuals in geostatistics: model criticism and parameter estimation. *Math. Geol.*, 23(5):741–758, 1991.
- P. K. Kitanidis. Quasi-linear geostatistical theory for inversing. *Water Resour. Res.*, 31(10):2411–2419, 1995.
- P. K. Kitanidis. Generalized covariance functions associated with the laplace equation and their use in interpolation and inverse problems. *Water Resour. Res.*, 33(5):1361–1367, 1999.
- P. K. Kitanidis and E. G. Vomvoris. A geostatistical approach to the inverse problem in groundwater modeling (steady state) and one-dimensional simulations. *Water Resour. Res.*, 19(3):677–690, 1983.
- F. Lamertz. Messung räumlicher Variabilität hydraulischer Parameter unter Anwendung von Pumpversuchen. Master's thesis, Geowissenschaften und Geographie, RWTH Aachen, 2001.

- C. Leven and P. Dietrich. What information can we get from pumping tests? - comparing pumping test configurations using sensitivity coefficients. *J. Hydrol.*, 319:199–215, 2006. doi: 10.1016/j.jhydrol.2005.06.030.
- K. Levenberg. A method for the solution of certain nonlinear problems in least squares. *Quart. Appl. Math.*, 2:164–168, 1944.
- W. Li and O. A. Cirpka. Efficient geostatistical inverse method for structural and unstructural grids. *Water Resour. Res.*, 42, 2006. doi: 10.1029/2005WR004668.
- W. Li, W. Nowak, and O. A. Cirpka. Geostatistical inverse modeling of transient pumping tests using temporal moments of drawdown. *Water Resour. Res.*, 41, 2005. doi: 10.1029/2004WR003874.
- W. Li, A. Englert, O. A. Cirpka, J. Vanderborght, and H. Vereecken. Two-dimensional characterization of hydraulic heterogeneity by multiple pumping tests. *Water Resour. Res.*, 43(4):W04433, 2007. doi: 10.1029/2006WR005333.
- W. Li, A. Englert, O. A. Cirpka, and J. Vanderborght. Three-dimensional geostatistical inversion of flowmeter and pumping test data. *Ground Water*, 46(2), 2008. doi: 10.1111/j.1745-6584.2007.00419.x.
- X. Liu, W.A. Illman, A.J. Craig, J. Zhu, and T.-C.J. Yeh. Laboratory sandbox validation of transient hydraulic tomography. *Water Resour. Res.*, 43:W05404, 2007. doi: 10.1029/2006WR005144.
- M. Loève. *Probability Theory*. Springer-Verlag, New York, 4 edition, 1977.
- D. W. Marquardt. An algorithm for least squares estimation of non-linear parameters. *J. Soc. Indust. Appl. Math.*, 11:431–441, 1963.
- G. Matheron. *The theory of regionalized variables and its applications*. Ecole de Mines, Fontainbleau, France, 1971.

- D. McLaughlin and L. R. Townley. A reassessment of the groundwater inverse problem. *Water Resour. Res.*, 32(5):1131–1161, 1996.
- P. M. Meier, J. Carrera, and X. Sánchez-Vila. An evaluation of Jacob's method for the interpolation of pumping tests in heterogeneous formations. *Water Resour. Res.*, 34(5):1011–1025, 1998.
- A. Möller. Analyse der räumlichen Heterogenität der Permeabilität eines quartären Grundwasserleiters auf der Basis von vertikal aufgelösten Kleinpumpversuchen. Master's thesis, Geologisches Institut, Universität Bonn und ICG-IV, Forschungszentrum, Jülich, 2003.
- A. M. Mood, F. A. Graybill, and D. C. Boes. *Introduction to the theory of statistics*. McGraw-Hill, New York, 1963.
- S. P. Neuman. Stochastic continuum representation of fractured rock permeability as an alternative to the REV and fracture network concepts. In *Rock Mechanics: Proceedings of the 28th US Symposium*, pages 553–561, A. A. Balkema, Rotterdam, 1987.
- S. P. Neuman and S. Yakowitz. A statistical approach to the inverse problem of aquifer hydrology, 1, theory. *Water Resour. Res.*, 15(4):845–860, 1979.
- W. Nowak. *Geostatistical methods for the identification of flow and transport parameters in the subsurface*. PhD thesis, Institut für Wasserbau, Universität Stuttgart, 2004.
- W. Nowak and O. A. Cirpka. A modified Levenberg-Marquardt algorithm for quasi-linear inversion. *Advances Water Resour.*, 27(7):735–750, 2004.
- W. Nowak and O. A. Cirpka. Geostatistical inference of hydraulic conductivity and dispersivities from hydraulic heads and tracer data. *Water Resour. Res.*, 42(8):W08416, 2006. doi: 10.1029/2005WR004832.

- W. Nowak, S. Tenkleve, and O. A. Cirpka. Efficient computation of linearized cross-covariance and auto-covariance matrices of interdependent quantities. *Math. Geol.*, 35(1):53–66, 2003. doi: 101023/A:1022365112368.
- W. H. Press, B. P. Flannery, S. A. Teukolsky, and W. T. Vetterling. *Numerical Recipes: The Art of Scientific Computing*. Cambridge University Press, Cambridge, 2nd edition, 1992.
- B. S. RamaRao, A. M. LeVenue, G. deMarsily, and M. G. Marietta. Pilot point methodology for automated calibration of an ensemble of conditionally simulated transmissivity fields. 1. theory and computational experiments. *Water Resour. Res.*, 31(3):475–493, 1995.
- K. R. Rehfeldt, J. M. Boggs, and L. W. Gelhar. Field study of dispersion in a heterogeneous aquifer: 3. geostatistical analysis of hydraulic conductivity. *Water Resour. Res.*, 28(12):3309–3324, 1992.
- Y. Rubin. *Applied Stochastic Hydrogeology*. Oxford University Press, New York, 2003.
- A. Sahuquillo, J. E. Capilla, J. J. Gómez-Hernández, and J. Andreu. Conditional simulation of transmissivity fields honoring piezometric data. In W. R. Blain and E. Carrera, editors, *Hydraulic Engineering Software IV, Fluid Flow Modeling*, volume 2. Elsevier, New York, 1992.
- X. Sánchez-Vila, P. M. Meier, and J. Carrera. Pumping tests in heterogeneous aquifers: an analytical study of what can be obtained from their interpretation using Jacob’s method. *Water Resour. Res.*, 35(4):943–952, 1999.
- K. Singha and S. M. Gorelick. Saline tracer visualized with three-dimensional electrical resistivity tomography: Field-scale spatial moment analysis. *Water Resour. Res.*, 41(5):W05023, 2005. doi: 10.1029/2004WR003460.
- L. Slater, A. M. Binley, W. Daily, and R. Johnson. Cross-hole electrical imaging of a controlled saline tracer injection. *J. Appl. Geophys.*, 44(2-3):85–102, 2000.

- S. Straface, T.-C.J. Yeh, J. Zhu, S. Troisi, and C. H. Lee. Sequential aquifer tests at a well field, montalto uffugo scalo, italy. *Water Resour. Res.*, 43(12): W07432, 2007. doi: 10.1029/2006WR005287.
- S. Strebelle. Conditional somulation of complex geological structures using multiple-point geostatistics. *Math. Geol.*, 34(1):1–22, 2002.
- N. Z. Sun. *Inverse problems in groundwater modeling*. Kulwer Academic Publisher, Norwell Mass., 1994.
- N. Z. Sun and W. W. G. Yeh. Coupled inverse problems in groundwater modeling. 1. sensitivity analysis and parameter identification. *Water Resour. Res.*, 26(10):2507–2525, 1990.
- C. Theis. Relation between the lowering of the piezometric surface and the rate and duration of discharge of a well using groundwater storage. *Trans. Am, Geophys. Union*, (2):519–524, 1936.
- J. R. Valstar, D. B. McLaughlin, C. B. te Stroet, and F. C. van Geer. A representer-based inverse method for groundwater flow and transport applications. *Water Resour. Res.*, 40:W05116, 2004. doi: 10.1029/2003WR002922.
- J. Vanderborght and H. Vereecken. Analyses of locally measured bromide breakthrough curves from a natural gradient tracer experiment at krauthausen. *J. Contam. Hydrol.*, 48:23–43, 2001.
- J. Vanderborght, A. Kemna, H. Hardelauf, and H. Vereecken. Potential of electrical resistivity tomography to infer aquifer transport characteristics from tracer studies: A synthetic case study. *Water Resour. Res.*, 41(6):W06013, 2005. doi: 10.1029/2004WR003774.
- H. Vereecken, U. Jaekel, O. Esser, and O. Nitzsche. Solute transport analysis of bromide, uranin LiCl using breakthrough curves from aquifer sediment. *J. Contam. Hydrol.*, 39:7–34, 1999.

- H. Vereecken, U. Döring, H. Hardelauf, U. Jaekel, U. Hashagen, O. Neuendorf, H. Schwarze, and R. Seidemann. Analysis of solute transport in heterogeneous aquifer: The Krauthausen field experiment. *J. Contam. Hydrol.*, 45: 329–358, 2000.
- V. V. Vesselinov, S. P. Neuman, and W. A. Illman. Three-dimensional numerical inversion of pneumatic cross-hole tests in unsaturated fractured tuff. 1. methodology and borehole effects. *Water Resour. Res.*, 37(12):3001–3017, 2001a.
- V. V. Vesselinov, S. P. Neuman, and W. A. Illman. Three-dimensional numerical inversion of pneumatic cross-hole tests in unsaturated fractured tuff. 2. equivalent parameters, high resolution stochastic imaging and scale effects. *Water Resour. Res.*, 37(12):3019–3041, 2001b.
- T.-C. J. Yeh and S. Liu. Hydraulic tomography: Development of a new aquifer test method. *Water Resour. Res.*, 36(8):2095–2105, 2000.
- T.-C. J. Yeh, M. Jin, and S. Hanna. An iterative stochastic inverse method: Conditional effective transmissivity and hydraulic head fields. *Water Resour. Res.*, 32(1):85–92, 1996.
- W. W.-G. Yeh. Review of parameter identification procedures in groundwater hydrology: The inverse problem. *Water Resour. Res.*, 22(2):95–108, 1986.
- W. W.-G. Yeh and Y. S. Yoon. Aquifer parameter identification with optimum dimension in parameterization. *Water Resour. Res.*, 17(3):664–672, 1981.
- D. Zhang and Z. Lu. An efficient, high-order perturbation approach for flow in random porous media via Karhunen-Loève and polynomial expansions. *J. Comput. Phys.*, 194:773–794, 2004.
- J. Zhang and T.-C. J. Yeh. An iterative geostatistical inverse method for steady flow in the vadose zone. *Water Resour. Res.*, 33(1):63–71, 1997.

- J. Zhu and T.-C. J. Yeh. Characterization of aquifer heterogeneity using transient hydraulic tomography. *Water Resour. Res.*, 41:W07028, 2005. doi: 10.1029/2004WR003790.
- J. Zhu and T.-C. J. Yeh. Analysis of hydraulic tomography using temporal moments of drawdown recovery data. *Water Resour. Res.*, 42:W02403, 2006. doi: 10.1029/2005WR004309.
- D. A. Zimmerman, G. de Marsily, C. A. Gotway, M. G. Marietta, C. L. Axness, R. L. Beauheim, R. L. Bras, J. Carrera, G. Dagan, P. B. Davies, D. P. Gallegos, A. Galli, J. Gomez-Hernandez, P. Grindrod, A. L. Gutjahr, P. K. Kitanidis, A. M. Lavenue, D. McLaughlin, S. P. Neuman, B. S. RamaRao, C. Ravenne, and Y. Rubin. A comparison of seven geostatistically based inverse approaches to estimate transmissivities for modeling advective transport by groundwater flow. *Water Resour. Res.*, 34(6):1373–1413, 1998.
- D. L. Zimmerman. Computationally exploitable structure of covariance matrices and generalized covariance matrices in spatial models. *J. Statis. Comp. Simul.*, 34(6):1373–1413, 1998.